1-1-2013

Histone Deacetylase 1: Mutagenesis And Small Molecule Studies

Magdalene Wambua
Wayne State University,

HUMAN HISTONE DEACETYLASE 1: MUTAGENESIS AND SMALL MOLECULE STUDIES.

by

MAGDALENE KAMANTHE WAMBUA

DISSERTATION

Submitted to the Graduate School

of Wayne State University,

Detroit, Michigan

in partial fulfillment of the requirements

for the degree of

DOCTOR OF PHILOSOPY

2013

MAJOR: CHEMISTRY (Biochemistry)

Approved by:

_____

Advisor Date

_____

_____

_____

_____

ACKNOWDLEDGEMENT

I would like to thank Dr. Mary Kay H. Pflum. Thanks A LOT!

.

TABLE OF CONTENTS

LIST OF TABLES

LIST OF FIGURES

Chapter 1

Introduction

1.1 The nucleosome and epigenetics

Epigenetics describes the heritable phenotypic changes in an organism that do not arise from changes in the DNA base sequence. DNA is the genetic bank house in the cell, storing an immense amount of genetic instruction that allows cells to maintain many biological functions. The patterns of genetic inheritance are, therefore, dependent on the information contained in DNA, as well as any epigenetic marks.

The human genome contains three billion base pairs, which encode approximately 30,000 to 40,000 genes. To allow for efficient storage of this enormous size in a cell, approximately 146 base pairs of DNA are wrapped around an octameric structure consisting of two copies each of the histone proteins H2A, H2B, H3 & H4 to form the nucleosome [1]. The nucleosome therefore is the simplest unit of DNA storage in a cell. Linker histones (H1) associating with approximately 10-60bp of DNA further package the nucleosomal structure into chromatin fibers (Figure 1.1). Chromatin fibers further condense into chromosomes. This nucleoprotein structure consisting of DNA, histone proteins and the linker histones limit the accessibility of DNA.

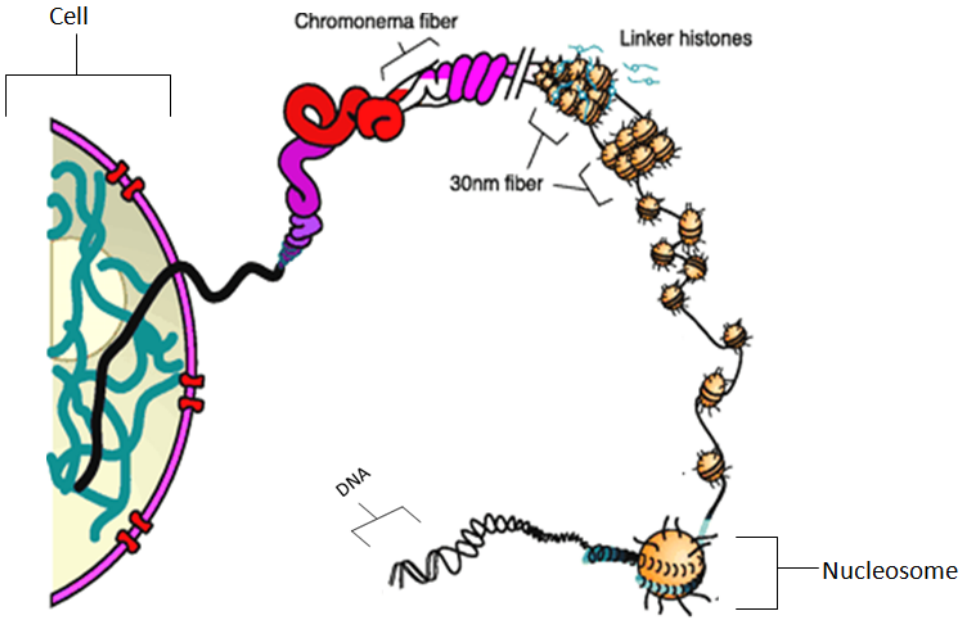

Figure 1.1: Duplex DNA is assembled into chromatin fibers. DNA is coiled around histone proteins forming the nucleosome. Consecutive nucleosomes are linked via linker histones (H1) and short pieces of DNA which further condense into approximately 30 nM chromatin fibers. More compacting of chromatin fibers forms the chromatids, which are paired and stored in the cell as the genetic material. *Reproduced with permission from FEBS Letters, 579 (2005) 895-898.*

A high resolution crystal structure (2.8 Å) of the nucleosome was reported by Luger *et al.* in 1997. The nucleosomal structure has a disc-like shape, consisting of 1.65 turns of left-handed superhelical DNA with 145 DNA base pairs wound around a core nucleosome structure (Figure 1.2). This structure revealed that, whereas the C-terminal regions of the histone proteins bind to DNA and form the nucleosome core, the N-terminal regions are unstructured and are not involved in formation or stability of the nucleosome core but are critical for chromatin condensation. Further, the N-terminal tails are rich in basic amino acids. Subsequent studies later showed that histones are subject to a number of covalent post-translational modifications [2].

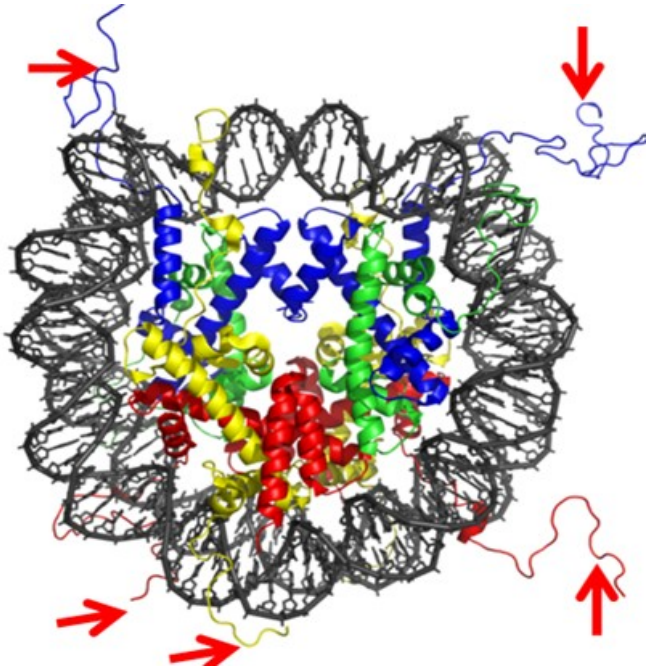

Figure 1.2: Crystal structure of a nucleosome. The duplex DNA (grey) is wrapped around an octamer of histone proteins (blue: H3; green: H4; yellow: H2A; and red: H2B). N-terminal lysine-rich tails on histones are shown by the red arrows *(Luger et al Nature 1997 389, 251-260). Reproduced with permission from FEBS Let., 579 (2005) 895-898.*

To maintain proper functioning in a tissue specific manner, cells have to express gene products on demand. The central dogma of molecular biology dictates that DNA can act as a template to make a replica DNA daughter molecule or RNA transcript. RNA biosynthesized this way is typically further translated into proteins by the ribosome. In addition, for replication, the DNA daughter molecule is transferred to a new cell, allowing passage and continuity of genetic information. In addition to replication and transcription, gene recombination, repair, and mitotic condensation involve chromosomally bound DNA. The question arises: How does chromosomally bound DNA become available for any of these processes to occur? Cells have to modulate chromatin structure in order to allow for the accurate execution of these processes for proper cell functioning. Remodeling of chromatin structure involves a variety of mechanisms.

1.2 Epigenetics: Histone modifications, chromatic remodeling and DNA marks

Post-translational modifications on histones modify the nucleosomal physical structure for DNA accessibility. Covalent modifications on the DNA and N-terminal histone tails are central to

epigenetic gene regulation. In contrast to the DNA, which is mainly methylated on cystosine bases, histone modifications are varied [3, 4]. Key modifications include phosphorylation, acetylation methylation, ubuquitination, sumoylation, citrulination and ribosylation [3]. Lysine and arginine residues can be mono-, di- or trimethylated; all of which add complexity to histone modification patterns. Combinations of these histone modifications can give rise to a specific histone code that dictates the transcriptional status of associated genes [3]. For instance combinations of acetylations of H4 K8 and H3 K14, together with phosphorylation of S10 on H3, gives rise actively transcribed genes [3]. Besides histone modifications, other epigenetic marks involve modifications on the DNA itself, chromatin remodeling and non-coding RNAs [5]. ATP-dependent chromatin remodeling complexes such as the SWI/SNF (SWItch/Sucrose NonFermantable), ISWI (imitation switch) and CHD (chromodomain helicase DNA-binding) families of remodelers, are recruited by some histone modifications and eject or move nucleosomes allowing DNA access [6]. Importantly, a link between histone modifications and DNA methylation has been reported. Specifically, DNA methylation on CpG islands leads to transcriptional repression, which is attributed to the recruitment of histone modifiers to promoter regions by the methyl- CpG-binding protein 2, MeCP2 [4].

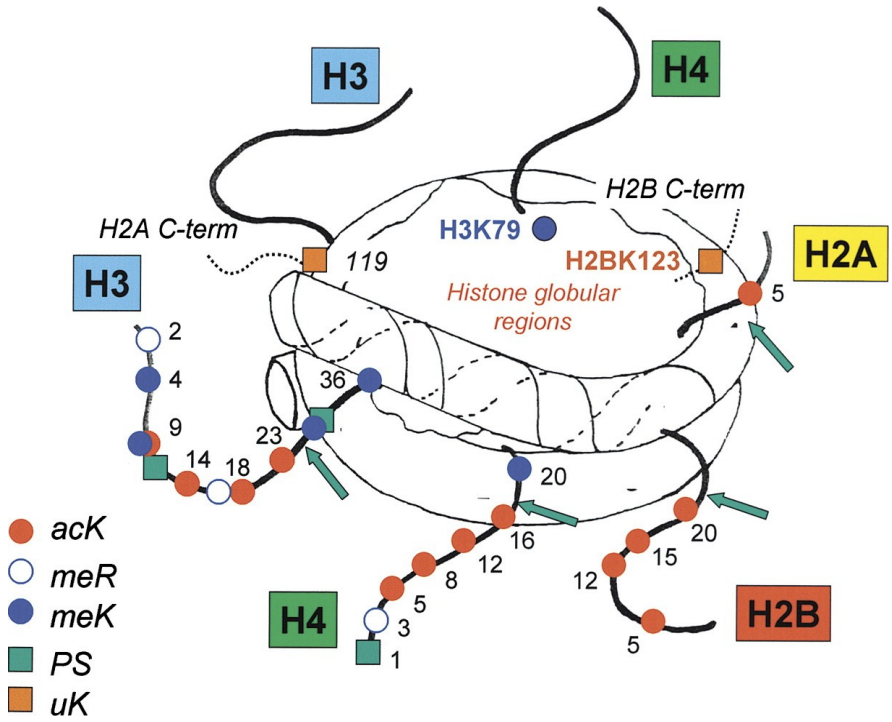

Figure 1.3: Common histone modifications [3]. Schematic representing the nucleosome core with common post-translantional histone modifications, including: acetyl lysine (acK), methyl-arginine (meR), methyl lysine (meK), phosphoserine (PS), and ubiquitinated lysine (uK). Post-translational modifications are represented by colored shapes (legend in bottom left corner). *Reproduced with permission from Curr. Bio., 2004, 14 (14), 546-51.*

1.3 Histone acetylation and deacetylation

Histone acetylation is the most abundant and well studied post-translational modification on histones. Two classes of enzymes, histone acetyl transferase (HAT) and histone deacetylases (HDAC), mediate the balance between the acetylated and deacetylated states. Acetylation has a prominent role in disease states and several small molecules have been created that target both histone enzymes.

HATs use the cofactor acetyl-coenzyme A to transfer an acetyl-group to the ε-amino group of specific lysine residues on histone proteins (Figure 1.4). The removal of the acetyl group is catalyzed by HDACs (Figure 1.4). Acetylation neutralizes the positive charge on the DNA backbone to loosely bind to the nucleosomal structure, which results in the open chromatin form

that is generally associated with actively transcribed genes in euchromatin. Removal of the acetyl group by HDACs results in positively charged lysine residues capable of ionic bonding with the back to the negatively charged phosphates on DNA. Deacetylated histones bind tightly to DNA, making DNA inaccessible to transcription factors and promoting the heterochromatin form (Figure 1.5).

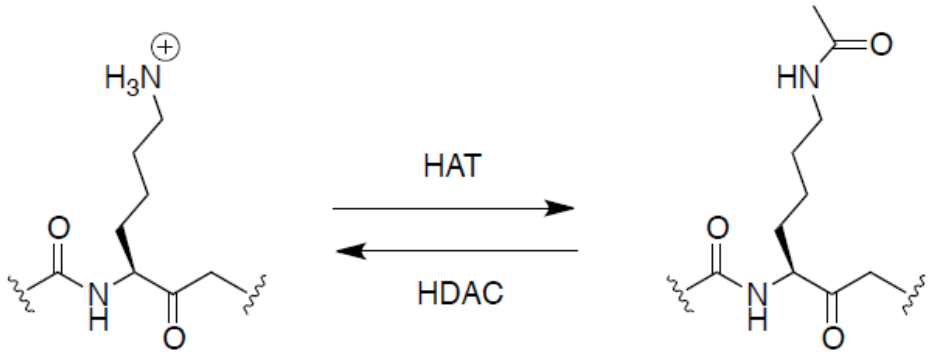

Scheme 1.1: Acetylation and deacetylation of the ε-amino group on histone proteins. Histone acetyl transferase (HAT) enzymes catalyze the transfer of an acetyl group from the co-factor acetyl-CoA to lysine residues resulting in a neutral acetyl-lysine. The removal of the acetyl group is catalyzed by histone deacetylases (HDAC). Deacetylation results in a cationic lysine residue capable of forming ionic interaction with the anionic phosphate backbone on the DNA. Acetylation and deacetylation are reversible processes and the key enzymes involved are HATs and HDACs.

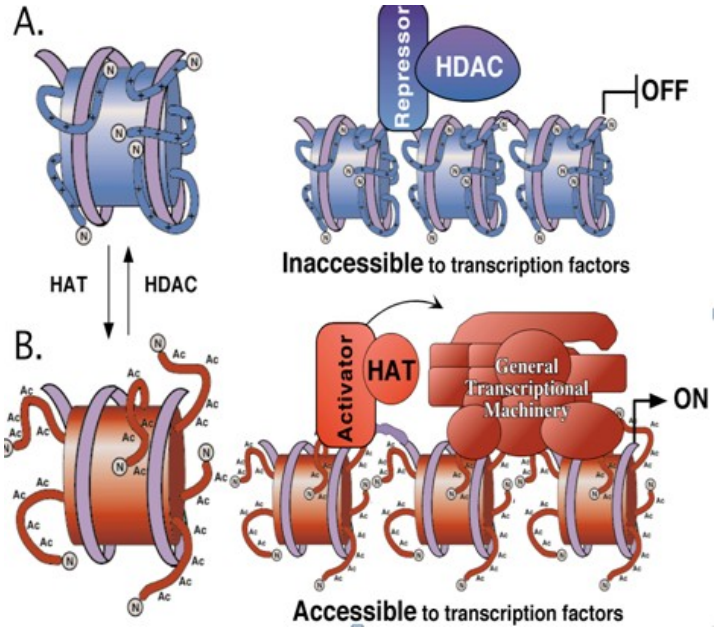

Figure 1.4: Effect of acetylation and deacetylation of nucleosome on gene transcription. (A). Acetylation of histones by histone acetyltransfarases (HAT) makes DNA accessible to transcription factors and gene transcription is on (B). Removal of the acetyl group makes DNA inaccessible to transcription factors (A) and gene transcription is off. (Picture credit Dr. Pflum)

1.4: Histone deacetylases: Classes, structure and mechanism

1.4.1: Classes of HDAC proteins

Eighteen human HDAC proteins are known to date; these are classified into four main classes on the basis of size, enzymatic mechanism and sequence homology to yeast proteins. Class I HDAC proteins are relatively small, ranging from 49-55 kDa and are homologous to the yeast Rpd3 (Reduced potassium dependence 3). Class I includes HDAC1, HDAC2, HDAC3 and HDAC8 (Figure 1.5) [7] [8] [9]. The class I HDAC proteins have a metal dependent mechanism, which will be discussed in detail in section 1.4.2. The class I HDAC proteins are mainly nuclear and are ubiquitously expressed in many cell types, which is in agreement with their role in cell cycle regulation in various tissues [7] [10] [11].

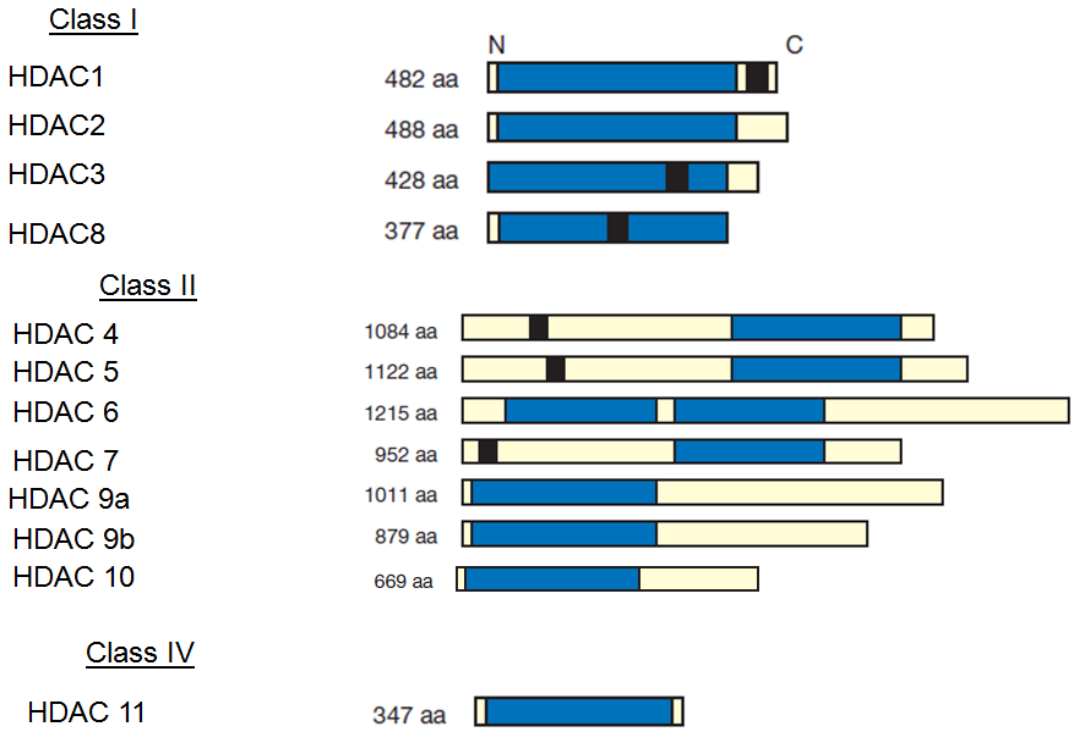

Figure 1.5: Summary in length of HDAC classes. Class I HDACs 1-3 and 8 range from 377-448 amino acids. Class II HDACs: 4-7and 9-10 have 669 to 1122 amino acids. The class IV HDAC11 is 347 amino acids long. Bars depict the length of the protein. The catalytic domains are shown in blue. Black depicts a nuclear localization domain, N, N-terminus, C, and C-terminus.

HDAC4, HDAC5, HDAC6, HDAC7, HDAC9 and HDAC10 belong to the class II subfamily and have sequence homology to the yeast HdaI (Histone deacetylase 1) protein and are much bigger in size (80-131 kDa) than class I [12-15]. Unlike the other class II isoforms, HDAC6 has two active sites on its N-terminal and C-terminus regions, which can be attributed to an in-shift gene duplication event [12]. Further, the N-terminus active site is dispensable in HDAC6. On the other hand, HDAC9 and HDAC10 have two splice variants, which possess deacetylase activities at comparable levels [15]. The rest of the class II isoforms, HDAC4, HDAC5 and HDAC7, have a single active site on their C-terminal domains. In contrast to the class I HDACs, which are mainly nuclear and ubiquitously expressed in several cell types, the class II HDACs can shuttle from the nucleus to the cytoplasm in response to a specific cell signal, for instance to participate in metabolic events [16].

The class IV deacetylase, HDAC11, is a 39 kDa protein and is the only class IV member. Similar to class I HDACs, HDAC11 has a single active site and is mainly nuclear, but it is thought to have diverged in evolution much earlier from the other HDAC proteins [17]. Despite these similarities, HDAC11 is expressed in a tissue specific manner with higher levels seen in the brain, heart, skeletal muscle and kidneys, suggesting a tissue specific function [17].

Class III HDAC proteins are the sirtuins and are homologous to the yeast Sir2 (Silent information regulator) proteins and include Sirt1, 2, 3, 4, 5, 6 and 7. Whereas class I, II and IV display a similar metal-dependent enzymatic mechanism, class III HDACs require NAD+ for catalysis. In this dissertation the sirtuins will not be further discussed because they have a different enzymatic mechanism distinct from the other classes and are insensitive to the HDAC inhibitors of interest in the Pflum lab.

Due to the similarities in catalytic mechanisms among classes I, II and IV HDACs, most HDAC inhibitors (HDACi) display pan inhibition towards these enzymes with only a few being selective [18, 19]. This topic will be discussed in details in Section 1.6. Additionally, whereas class I and II HDACs bind to the mSin3A, RbAp48, N-CoR co-repressors *in vivo*, HDAC11 does not associate with these complexes, suggesting that HDAC11 is distinct from the rest of the metal-dependent HDAC proteins [17]. Importantly, the function(s) of the metal-dependent HDACs is poorly understood, a current problem in cancer treatment, as will be discussed in section 1.5.

1.4.2: HDAC structure and catalytic mechanism

As discussed in section 1.4.1, Classes I, II and IV HDAC proteins have a similar metal-dependent catalytic mechanism. The crystal structures of a histone deacetylase like protein (HDLP) from a thermophilic bacterium *Aquifex aeolicus,* which displays 35.2% sequence homology to HDAC1, has been used as a model to study class I HDAC proteins. The

crystallographic structure of HDLP resolved at 2.1 Å in complex with the HDAC inhibitors suberoylanilide hydroxamic acid (SAHA, Zolinza) and Trichostatin A (TSA), was reported in 1999 (Figure 1.6) [20].

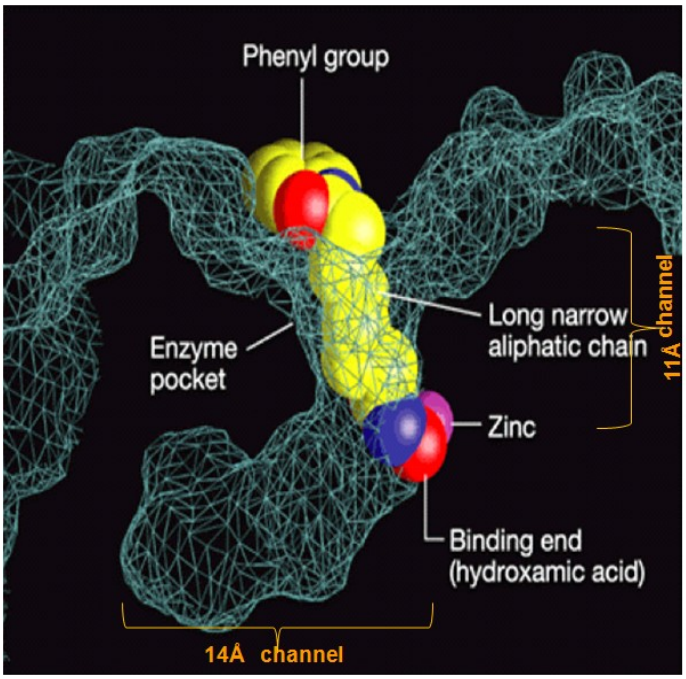

Figure 1.6: Crystal structure of the HDAC-like bacterial homolog (HDLP) in complex with the HDAC inhibitor SAHA [20]. The phenyl capping group of SAHA projects towards the solvent exposed region. The hydrophobic linker chain of SAHA is accommodated in the 11 Å channel (also known as the enzyme pocket). The hydroxamic metal binding group of SAHA is at the bottom of this channel. The 14 Å channel is located on the other side of the catalytic zinc metal ion. *Reproduced with permission from Nat., 1999, 401 (6749), 188-93.*

The HDLP structure revealed that the active site contains a hydrophobic, 11 Å channel that interacts with the long hydrophobic linker chain in TSA and SAHA or in acetylated HDAC substrates (Figure 1.7). The aromatic phenyl group of TSA and SAHA are located towards the solvent exposed region. At the bottom part of the 11 Å channel is a catalytic metal ion that interacts with the hydroxamic groups of SAHA and TSA (Figure 1.7). The function of the 14 Å channel is unknown. Several biochemical and computational studies have postulated that the 14 Å channel has two main functions: serving as the exit path for the acetate by-product of the

deacetylation reaction and a shuttling channel for the catalytic water needed in the active site (Figure 1.8) [20-22].

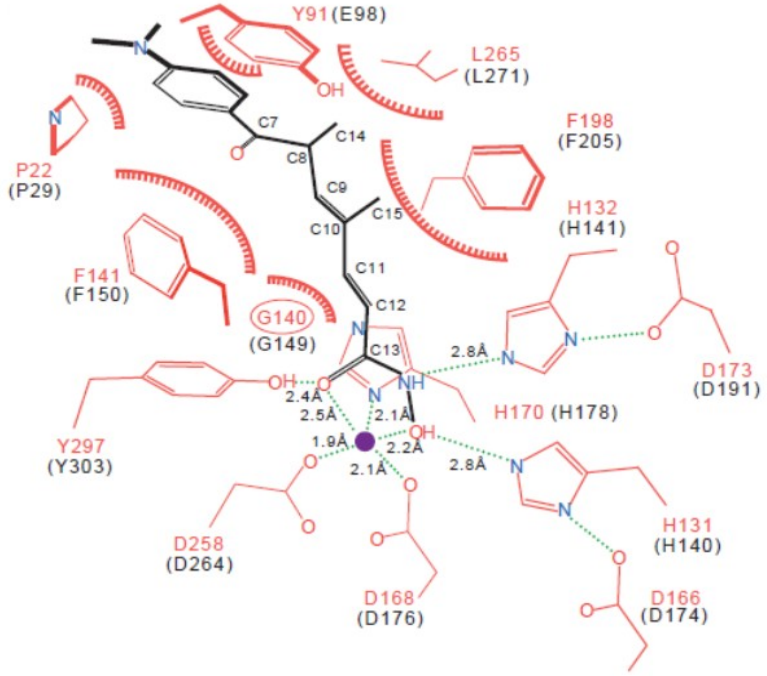

Figure 1.7: A schematic representation of Trichostatin A (TSA) in the active site of HDLP [20]. TSA is in black and the protein is in red. HDLP residues are labeled in red with their counterparts in HDAC1 indicated in black. Thatched semi-circles indicate van der Waals contacts between hydrophobic protein residues and TSA. Hydrogen bonds are shown as green dashed lines. *Reproduced with permission from Nat., 1999, 401 (6749), 188-93.*

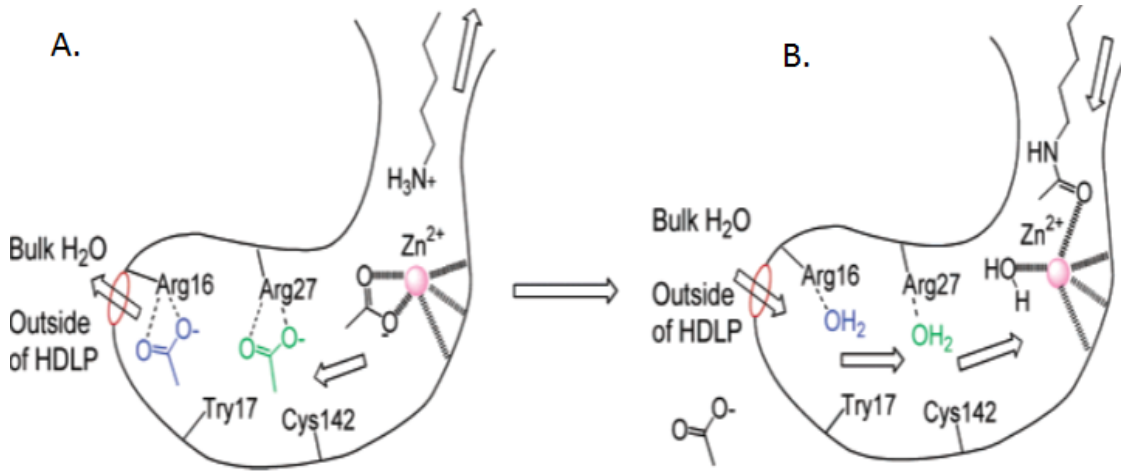

Figure 1.8: Picture of the internal cavity after deacetylation [21]. (A) After deacetylation, the lysine chain leaves the 11 Å channel while the byproduct, acetate, passes through the 14 Å channel (see arrows). (B) After escape of acetate, the catalytic center accepts water through the 14 Å channel and acetylated lysine via the 11 Å channel for the next cycle of deacetylation. *Reprinted with permission from the J. Med. Chem., 2004, 47 (13), 3409-17.*

The HDLP structure has been widely used for rational HDAC inhibitor design because the amino acids in the catalytic domains of HDLP and most metal-dependent HDACs are similar and highly conserved. From this crystallographic data, a plausible mechanism for metal-dependent HDAC proteins was deduced (section 1.4.3, Scheme 2) [20]. In addition to HDLP, the crystal structures for HDAC2, HDAC3, HDAC4, HDAC7 and HDAC8 have been solved [23-26]. The class II HDACs 4 and 7 gave insights into the active sites of class II deacetylases. HDAC4 is a tetramer unlike monomeric HDAC7, which has a structure very similar to HDLP [23, 24]. The focus of this project is the class I HDAC isoform HDAC1. The crystal structure of the class I isoform HDAC8 will be discussed further; the class I isoform HDAC2 structure is not thoroughly detailed [27].

The HDAC8 structure is quite distinct from the HDLP structure. It has a dimeric structure where the monomers are identical and each binds one Zn^{2+} and two K^+ ions [25]. Similar to the HDLP structure, the Zn^{2+} metal ion in the HDAC8 active site coordinates to the hydroxamic acid part of the inhibitors. The K^+ ions are thought to influence the deacetylation reaction of HDAC8. Specifically, one K^+ is located closer to and coordinates with the Zn^{2+} binding amino acids and is

therefore likely to influence the correct orientation and properties of bound residues involved in catalysis (Figure 1.9) [25]. Interestingly, the capping groups of the two inhibitor molecules could facilitate dimer formation by stacking interactions as well as interactions with nearby residues in HDAC8. Similar to HDLP, the 14 Å channel is hypothesized to be involved in acetate release [20, 25].

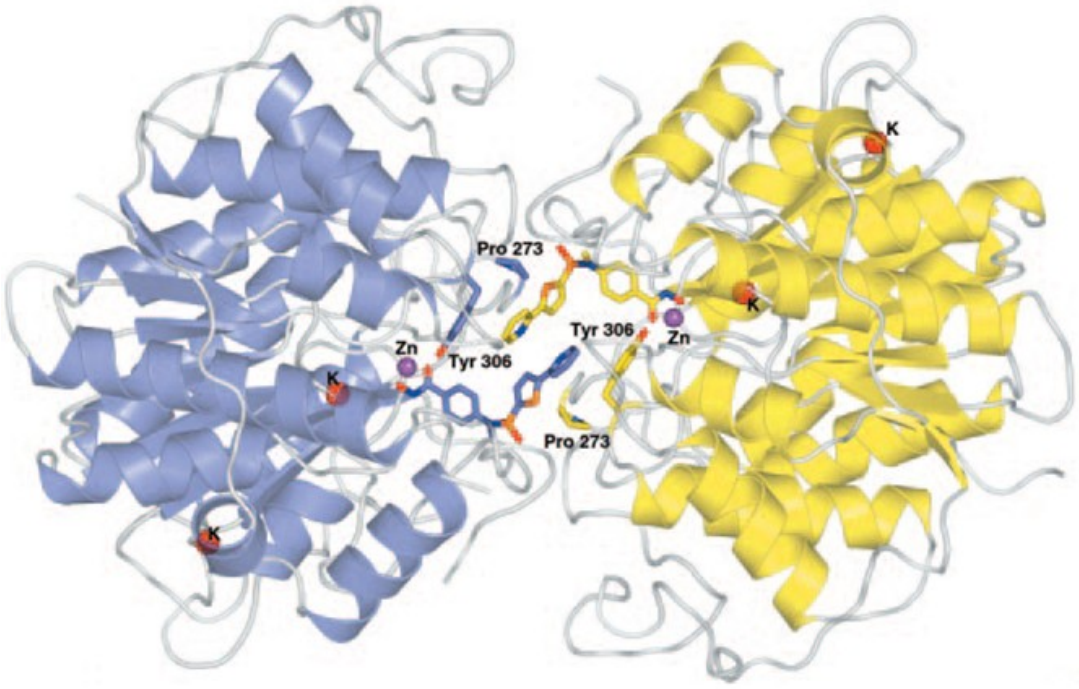

Figure 1.9: Ribbon diagram of the dimeric structure of HDAC8 shown in yellow (monomer A) and indigo (monomer B) colors [25]. The bound inhibitors in the two active sites are shown as sticks packed head to tail. Red=oxygen; blue=nitrogen; orange=sulfur. Carbon is shown in indigo (molecule A) and yellow (molecule B). Violet spheres, Zn^{2+} ions; red spheres, K^{+} ions. *Reprinted with permission from Proc. Natl. Acad. Sci. U S A., 2004, 101 (42), 15064-9.*

1.4.3: HDAC reaction mechanism

From the HDLP crystal structure, a plausible deacetylation mechanism for the metal dependent HDACs was proposed (Scheme 1.2).

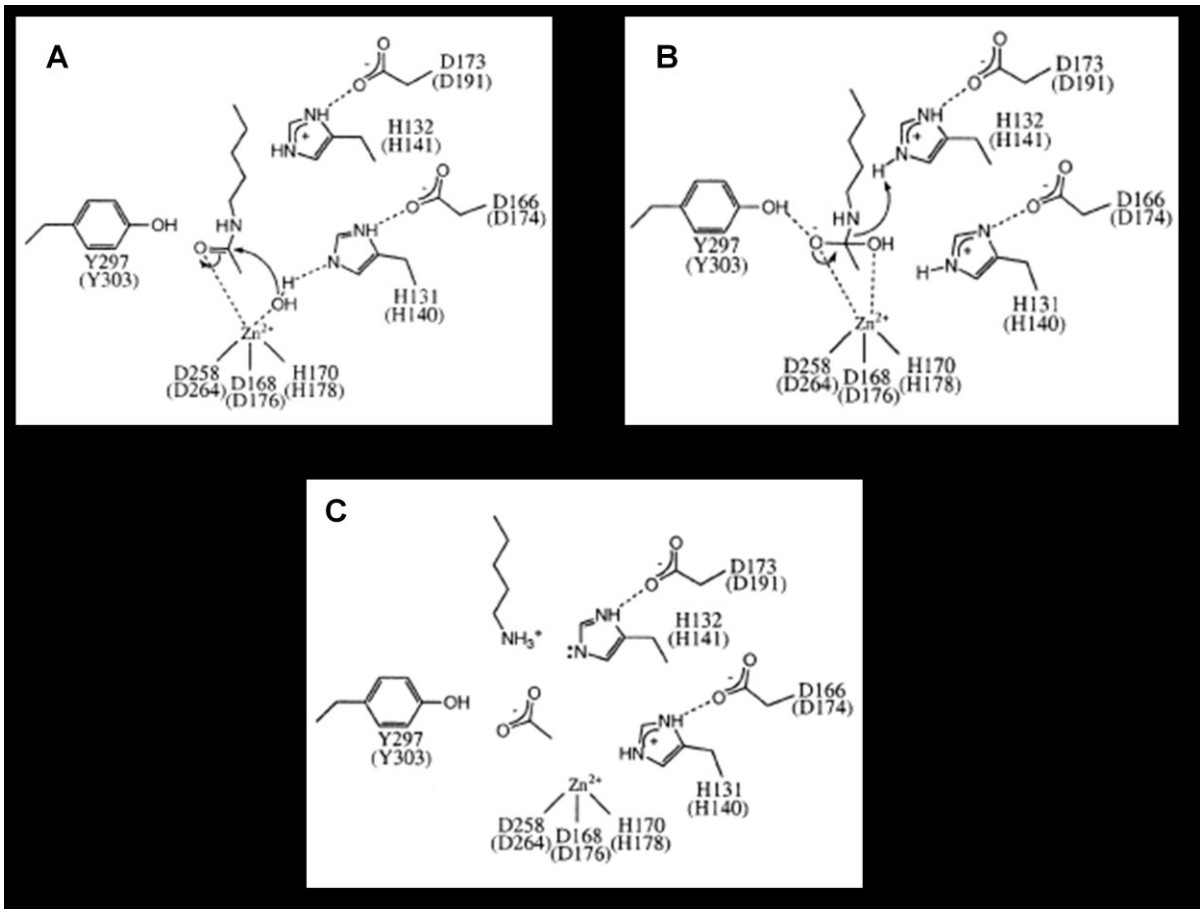

Scheme 1.2: Proposed chemical mechanism for class I, II and IV HDACs [20]. HDLP-active site residues and their proposed HDAC1 counterparts (in parenthesis) are labeled. *Reproduced with permission from Nat.,1999, 401 (6749), 188-93.*

The deacetylation reaction involves catalytic His and Asp residues acting as general acid/base pairs. A catalytic metal ion (can be Zn^{2+}, Co^{2+} or Fe^{2+}), which coordinates to the Asp, the two His residues and a nearby tyrosine residue, form hydrogen bonds to the carbonyl oxygen making the carbonyl carbon a better electrophile. Water in the active site is activated by the two histidine residues to attack the carbonyl carbon. The resulting tetrahedral intermediate is stabilized by the metal ion and the Tyr residue (Scheme 1.2B), and collapses to form the acetate leaving group and lysine (Scheme 1.2C). This process is followed by restoration of the active site. Although the active site residues are highly conserved among the metal-dependent

deacetylases, the class II HDACs, HDAC4, HDAC5 and HDAC7, have a histidine residue in place of the tyrosine residue (Y297), which explains their reduced deacetylase activities [28]. Further, the class I HDAC8 possesses a mono-valent ion containing second site (K^+), which is close to the active site and is required for HDAC8 stability and deacetylase activity [25]. Due to the amino acid differences in the active sites of class I versus class II HDACs and the presence of a second metal in the active site in HDAC8, further work is needed to decipher the similarities and differences in the catalytic mechanisms of these enzymes. It is important to note that efforts to understand the active site of the individual HDACs are frustrated by a lack of crystal structures and the fact that bacterially expressed HDAC proteins are inactive, except HDAC8 [29, 30]. Lack of deacetylase activities for recombinant HDACs might be explained by the requirement of associated proteins to promote HDAC activity or folding (Section 1.4.3).

1.4.4: HDAC associated proteins

Histone modifying enzymes are usually part of protein complexes that recognize and bind to specific histone modification(s) and are recruited at promoter regions leading to activation or silencing of target genes [31]. HATs are part of activator protein complexes. Protein complexes with intrinsic HAT activities include the GNAT super family found in yeast, humans and mouse; the MYST family in yeast, humans and drosophila; the complex p300/CBP in various multicellular organisms; the SRC-1, ACTR and TIF2 family of nuclear receptor coactivators in humans and mice; $TAF_{II}250$ in humans and mice, and the TFIIIC transcription factors in humans [32]. Transcription activators whose function is influenced by histone acetylation include; p53, c-Myp, GATA-1, EKLF, E3F, HIV Tat, dTCF and the general transcription factors TFIIE and TFIIF [32]. Notably, the activity of the tumor suppressor gene p53 in cell cycle regulation and apoptosis is highly regulated and acetylation is one key regulatory mechanism. In addition, acetylation of the basal RNA, III machinery, TFIIIC, by the p300/CBP-associated factor PCAF, is required for transcription initiation, whereby the initiation complex RNA polymerase III-TFIIIB

binds to the promoter region of DNA, further indicating that acetylation is not tied to histone proteins only [33].

Similar to HATs, HDACs are part of transcriptional co-repressor complexes *in vivo,* for instance the Mi-2-NuRD, RbAp48-mSin3A or mSin3B complexes (known as Sin3 in yeast) and NCoR (nuclear hormone co repressor)/SMRT (silencing mediator of retinoid and thyroid receptors) [34, 35]. Mechanistically, HDACs associating with co-repressor complexes at promoter regions to deacetylate nucleosomal DNA of target transcription factors, leading to gene repression. The repressor activities of HDAC proteins involve DNA-bound transcription factors. For example, Mad:Max and Ume6 DNA-binding transcription repressors interact with the mSin3A/B complex which in turn recruits the mammalian deacetylases, HDAC1 or HDAC2, leading to gene repression [36]. Transcriptional repression by HDAC1 associating with the Mad-Max heterodimer, is essential for suppression of cell transformation, which ties HDAC1 deacetylase activity to cancer formation [37].

1.5: HDAC proteins in cancer

Aberrant epigenetic coding can lead to diseased states notably cancer, neuron-diseases, inflammation, and metabolic disorders [38-40]. Granted, clinically relevant therapies targeting epigenetic marks on histone proteins and DNA are currently in use and a lot more are in clinical trials, which make the epigenome a relevant area of research [41]. HDAC proteins have been implicated in a number of diseases, most notably cancer. Cancers are one of the leading causes of death not only in the United State but also in many other countries, according to the World Health Organization. But despite the isolation and identification of the various HDAC isoforms, the individual functions of each HDAC isoform are poorly understood. However, overexpression of HDAC proteins has been observed in several cancers. The class I HDAC proteins, HDAC1, HDAC2, HDAC3 and HDAC8, are overexpressed in a number of cancers. HDAC1, HDAC2 and HDAC3 are overexpressed in colorectal cancer and higher levels of

expression correlate with reduced patient survival [42, 43]. Further, inhibiting HDAC1, 2, and 3 expression by short interfering RNAs reduces tumor growth [43]. In patients with gastric cancer, HDAC1, HDAC2 and HDAC3 proteins are up regulated and higher levels of expression were seen in patients with advanced stage cancer suggesting that overexpression advanced tumor growth and aggressiveness [44, 45]. HDAC3 is over expressed in patients with lung cancer, as shown by gene micro-array profiling studies in lung cancer patients [46].

A study involving prostate carcinomas showed that HDACs 1, 2 and 3 are up regulated and higher expression levels are associated with tumor cell proliferation and differentiation [47, 48]. HDAC1 is over expressed in pancreatic cancers and regulates the activity of the hypoxia induced transcription factor α, with higher levels of HDAC1 expression correlating to a decrease in patient survival [49]. Overexpression of HDACs 1 and 2 correlates with cervical dysplasia and invasive carcinoma [50]. Children with neuroblastoma have higher levels of HDAC8 and disease progression and death correlates with increasing HDAC8 expression levels [51]. Overexpression of the class II HDAC 4 and 6 is seen in breast cancer tumors with HDAC6 shown to be an estrogen-maintaining gene in patients with breast cancer [52]. Further, high levels of endogenous HDAC6 augment breast cancer motility and invasion [52]. HDAC6 is over expressed in oral squamous cell carcinoma [53]. HDACs 5 and HDAC 7 are up regulated in colorectal cancer [42].

Despite the observed overexpression patterns of HDAC proteins in several cancers, little is known about the mechanisms via which HDAC overexpression lead to cancer formation and maintenance. Aberrant cell growth and proliferation are hallmarks for tumor genesis and HDAC1 plays a crucial function. Specifically, HDAC1 is critical for proper cell differentiation and regulation of cell cycle check point genes [54]. Inhibition of HDAC1 and HDAC3, using small interring RNAs, led to a reduced proliferative phenotype in HeLa cells suggesting that HDAC1 and 3 regulate the proliferation of cancer cell [55]. A similar study showed that siRNA

knockdown of HDAC1 and HDAC2 in prostate cancer cells renders them anti-proliferative and the cells fail to grow *in vitro,* further proving that HDAC1 and HDAC2 participate in maintaining proliferation of cancer cells [43]. These combined studies show that overexpression of HDAC proteins in cancer cells generally renders them proliferative. This phenomenon can be attributed to transcriptional repression of tumor suppressor genes and cell cycle check point genes by HDACs [56].

Apart from regulating the proliferative state of tumors, HDAC proteins have been implicated in multi drug resistance. siRNA mediated inhibition of HDAC1 in drug resistant neuroblastoma cells rendered the cells sensitive to drug treatment *in vitro* [57]. In addition, HDAC proteins are indicators in the control of the biology of cancer cells by inhibiting apoptosis, angiogenesis of tumor cells from dormant to malignant states, cancerous cell migration and invasion, proliferation and dedifferentiation of cancerous cells. Therefore, HDAC inhibitors have been explored as potential anti-cancer drugs.

1.6: HDAC Inhibitors are cancer drugs

Because of their involvement in cancer biology, small molecules targeting HDAC proteins are attractive anti-cancer agents. HDAC inhibitors (HDACi) exert their inhibitory effects via binding to the active site pocket and the catalytic metal ion [58]. Two HDAC inhibitors, suberoylanilide hydroxamic acid (SAHA, Zolinza, Varinostat) and FK-228 (a depsipeptide) have been approved by the FDA for the treatment of cutaneous T-cell lymphoma (Figure 1.10) [59-61]. Several HDACi are also in clinical trials for cancer treatment [62]. But, because the metal-dependent HDAC proteins have conserved binding pockets and catalytic residues, most HDACi interact with most, if not all, of the HDAC family. Efforts to characterize the inhibition patterns of HDACi are complicated by the fact that most recombinant purified proteins are inactive [63]. The observed inactivity with recombinant HDACs can be explained by the fact that HDAC proteins require associated protein partners to remain active, that are lacking in recombinant proteins.

Non-selective HDAC inhibitors (pan inhibitors) are problematic due to the involvement of HDAC proteins in important cellular functions, and patients therefore typically experience a lot of side effects. On the other hand, pan-inhibitors have been very useful in characterizing HDAC proteins and elucidating their functions in cancer cells.

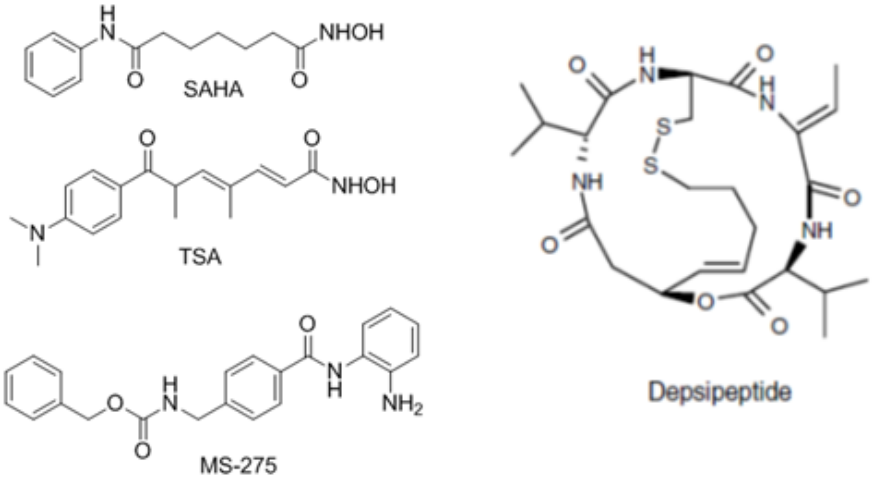

Figure 1.10: Structures of the HDAC inhibitors SAHA, TSA, MS-275 and FK-228.

HDACi are not only useful as anti-cancer agents but have been widely used as chemical tools to study HDAC proteins. The HDAC inhibitor trapoxin was used to identify and isolate the first human HDAC protein, human HDAC1, from nuclear cell extracts, paving the way for identification of the rest of the human HDAC family isoforms [7]. HDACi are indispensable tools in HDAC chemistry and the most commonly used ones are TSA and SAHA (Figure 1.10). The usage of HDACi as chemical tools has been demonstrated in many studies. For instance, treating murine erythroleukemia cells with HDAC inhibitors induced cell differentiation [64]. Malignant colorectal cancer cells displayed apoptotic effects upon treatment with the HDAC inhibitors TSA and butyrate [65]. The expression patterns of multiple genes involved in cell proliferation, cell differentiation and apoptosis were influenced by HDAC inhibitors, as shown by gene profiling studies [66, 67]. In vitro studies with HDAC 1, 2 and 3 treated with HDAC

inhibitors FK-228 and SAHA reduced ovarian cell growth and this was also observed using siRNA silencing [68].

1.7: This thesis project

To develop better anti-cancer drugs targeting HDAC proteins, more studies with HDAC proteins need to be done. Specifically, the individual roles of each HDAC isoform and their contributions to cancer are critical to aid in the design of isoform selective inhibitors. ***The long term goal of the HDAC project in the Pflum lab is to determine the individual roles of each HDAC protein and their contribution to cancer formation.*** As a first step towards achieving this goal, studies in this thesis project focus on HDAC1. HDAC1 is an attractive target for anti-cancer drugs because of its role in regulating cell proliferation and cell cycle, the main events that can lead to cancer development (see discussion in section1.6).

Due to a lack of crystallographic structural information on HDAC1, mutagenesis studies are a good alternative to give information on the involvement of amino acid residues in the active site on HDAC1 deacetylase activity. As discussed in section 1.4.2, the active site contains an 11 Å hydrophobic channel where the long hydrophobic linker region of TSA and SAHA is sandwiched. Mutagenesis studies in this channel demonstrated that most of the amino acids within are crucial for deacetylase activity (Chapter 2, section 2.2.1) [69]. A 14 Å exit channel is next to the active site and has been hypothesized to be the exit patch for the acetate byproduct of the deacetylation reaction. ***Studies outlined in the second chapter of this dissertation seek to understand the roles of the amino acids in the 14 Å channel of human HDAC1 using alanine scanning.***

The third chapter of this thesis focuses on efforts towards understanding the involvement of HDAC proteins in cancer formation using small molecule HDAC inhibitors. Previous methods used to study HDAC1 include genetic methods, such as siRNA and knockout embryonic stem cells [54, 55]. HDAC1 knockout caused lethality on embryonic day 9.5 in mice, whereas siRNA required 48 hours time during which HDAC2 compensated for HDAC1. Therefore, genetic

methods are not suitable for characterizing HDAC1 in cancer biology. Small-molecule inhibitors are excellent alternatives to genetic methods. For example, small molecules influence protein activity quickly and do not give the cell time to express proteins, particularly other HDAC isoforms that might compensate for the abolished activity. It is also possible to evaluate a dose-dependent effect for partial inhibition as opposed to total inhibition. Additionally, only the active site of the enzyme is affected, having the advantage of not affecting protein-protein associations which might be crucial to activity. With the advantages of inhibitors, the use of modified inhibitor analogues to characterize the individual functions of HDAC1 and their relevance to cancer formation is practical. ***Towards this goal, efforts to create the first HDAC1-inhibitor bump-hole pair will be detailed in the third chapter*.**

Chapter 2

2.1: Mutagenesis studies in HDAC1 14Å channel

HDAC1 is an attractive anti-cancer target (see section 1.5 chapter 1) and therefore HDAC1-selective inhibitors would be valuable tools for studying the involvement of HDAC1 in cancer formation and provide better anti-cancer drugs. The lack of structural information for HDAC1 has frustrated efforts to design selective inhibitors. Currently, HDAC inhibitor design relies on the crystal structure of a histone deacetylase like-protein (HDLP), which displays 35.2% sequence homology to HDAC1 [20]. A HDAC1 homology model based on HDLP revealed that the active site contains a hydrophobic 11 Å channel with a catalytic metal ion at the bottom of the channel [69]. HDAC inhibitors have been designed that fit in this long channel by making favorable hydrophobic interactions with amino acids lining the channel.

At the bottom of the active site and next to the catalytic metal ion is the 14 Å internal cavity whose function remains unclear [20, 21]. The 14 Å channel of Class 1 HDAC isotypes has been hypothesized to be the exit cavity for acetate following deacetylation [20, 21, 70]. The amino acids lining this cavity are very similar suggesting the role of the cavity is relevant to all class I HDACs. Computational and homology model studies identified charged amino acids that are likely to facilitate acetate escape by forming favorable ionic interactions (Figure 2.1) [71]. In one study, docking showed that both acetate and acetic acid localize next to the metal ion, R16 and R27 in HDLP (Figure 2.1) [21]. These interactions were not present in the 11 Å channel (Figure 2.2) [21]. In contrast, similar studies with N-hydroxyacetamide, which is similar to HDAC inhibitors SAHA or TSA, revealed less binding.

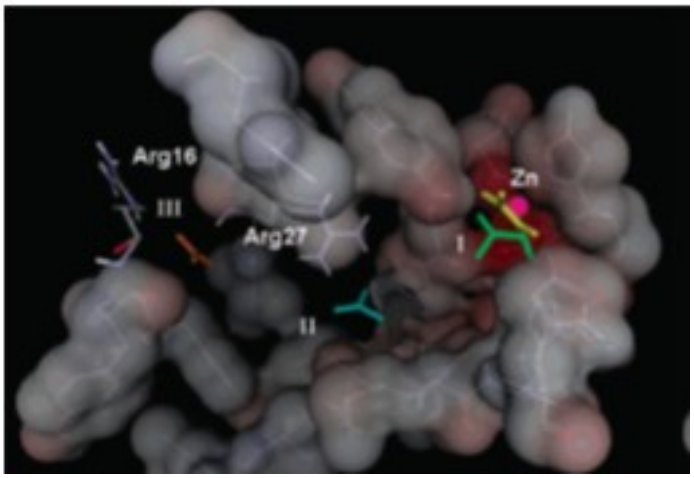

Figure 11: Docking acetate in the 14 Å channel of HDLP revealed important amino acids involved in acetate escape [21]. Acetate localized next to R16 (indicated by III) and R27 (indicated by II) in HDLP presumably by forming ionic interaction, but failed to localize next to Zn (I) or in the 11 Å channel Similar results were shown with acetic acid (data not shown). *Reprinted with permission* from *J. Med. Chem.*, *2004, 47 (13), 3409-17.*

In addition to facilitating acetate escape, the internal cavity may act as an inlet for catalytic water following deacetylation to restore the active site configuration for the next cycle of catalysis, as illustrated in Figure 2.2 [21]. Further, residues located towards the solvent exposed regions of HDAC1 demonstrate flexibility, indicating that side chain movement near the solvent exposed region of the 14 Å channel could exchange cavity contents with the bulk water for the next cycle of deacetylation [20, 21].

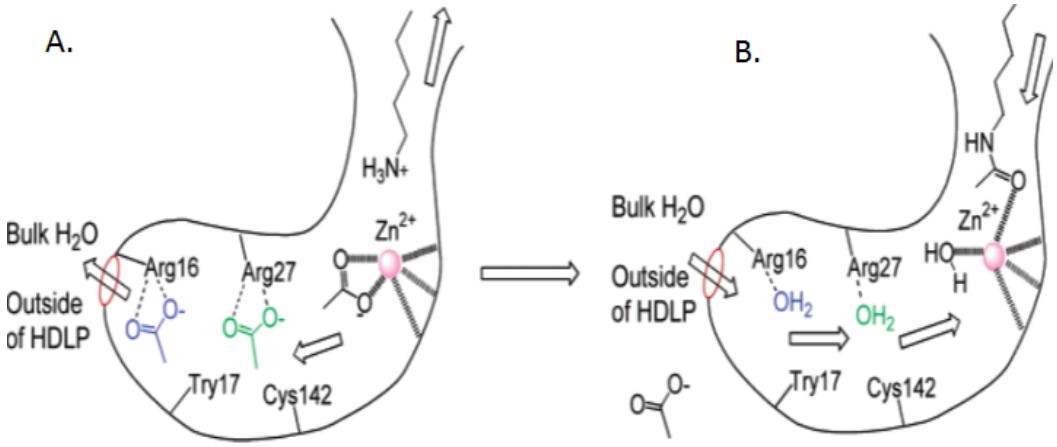

Figure 12.2: Picture of internal cavity after deacetylation [21]. (A) While the free lysine chain leaves the 11 Å channel, the byproduct, acetate, passes through the 14 Å cavity (see arrows). (B) The catalytic center therefore is ready to accept water and an acetylated lysine for the next cycle of deacetylation. *Reprinted with permission from J. Med. Chem., 2004, 47 (13), 3409-17.*

The 14 Å channel has been exploited in inhibitor design. Several isoform selective HDACi designed to fit the 14 Å channel have been created [18, 19]. In one study, docking MS-275 into a HDAC1 homology model revealed that a large aromatic substituent on the metal binding moiety could access the 14 Å channel [19]. In addition, the presence of M30 and C151 suggested that para-thienyl substituted amino benzamide MS-275 derivatives could benefit from potential sulfur interactions. This led to the synthesis of compounds **1** with an IC_{50} of 0.02 μM and 0.5 μM against recombinant HDAC1, and 2 respectively (5-fold selectivity for HDAC1 over HDAC2) but is non selective towards HDAC3 and 8. Further studies led to the synthesis of compounds **2** (IC_{50}=0.06 μM for HDAC1 and IC_{50}=0.2 μM for HDAC2) and 3 (IC_{50}=0.05 μM for HDAC1 and IC_{50}=0.2 μM for HDAC2), which represents 100-400-fold selectivity for HDAC1 and 2 over HDAC3 and 8 (both compounds **2** and **3** have IC50>20 μM for HDACs 3 and 8). The observed increases in selectivity are attributed to additional beneficial interactions between MS-275 derivatives and the enzyme resulting from potential sulfur interactions with amino acids located in the 14 Å channel.

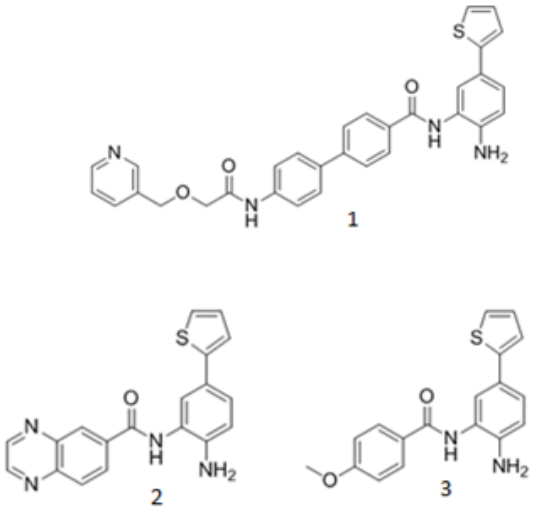

Figure 13: HDAC1 and 2 selective MS-275 derivatives designed to fit the 14Å channel [19].

In a separate study, several other HDAC inhibitors designed to fit the 14 Å channel were created (Figure 2.4) [72]. Compound **4** was 30-fold selective for HDAC1 over HDAC2 (HDAC1 IC_{50}=6 nM and HDAC2 IC_{50}=190 nM) and is only weakly bound to HDAC3 (IC_{50}=27 μM) and HDAC8 (IC_{50}=31 μM). Similarly, compound **5** was 10-fold selective for HDAC1 (IC_{50}=10 nM) over HDAC2 (IC_{50}=105 nM) with very weak HDAC3 and 8 affinity (IC_{50}>50 μM). Combined, both studies suggest that isoform selective HDAC inhibitors can be designed to bind the 14 Å channel [18].

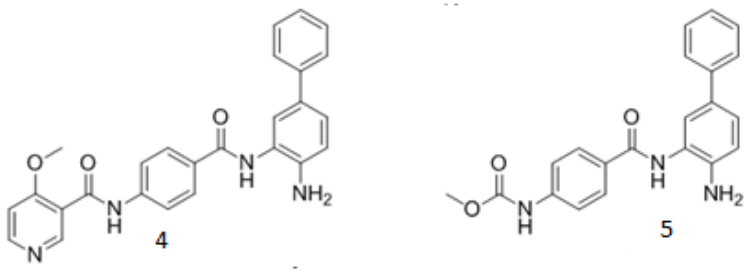

Figure 14: HDAC1 and 2 selective MS-275 derivatives designed to fit the 14 Å channel [72].

With no structural information for HDAC1, the role of the 14 Å channel in acetate binding and substrate/inhibitor binding is still unclear. Without crystallographic information, mutagenesis can offer insight into the influence of amino acid residues in the 14 Å cavity to HDAC1 activity.

2.2: Prior HDAC1 mutagenesis studies in the Pflum lab

Residues lining the 11 Å channel of HDAC1 form hydrophobic contacts with the acetylated Lys substrate in the active site (Chapter 1, figure 1.7). Amino acids lining the 11 Å channel are well conserved among the HDAC isoforms suggesting that their roles are relevant to all isoforms (Figure 2.5). Previous mutagenesis studies in the 11 Å channel of HDAC1 revealed that residues in this channel influence enzymatic activity (Figure 2.6) [69].

	H28 P29	E98 D99	G149 F150	Y204 F205	L271
HDAC1	HP	ED	GF	YF	L
HDAC2	HP	ED	GF	YF	L
HDAC3	HP	DD	GF	FF	L
HDAC4	HP	SD	GF	FF	L
HDAC5	HP	SD	GF	FF	V
HDAC6a	FP	YD	GY	FW	A
HDAC6b	HP	FD	GF	FF	V
HDAC7	HP	TD	GF	FF	V
HDAC8	LA	YD	GF	FF	M
HDAC9	HP	SD	GF	FF	V
HDAC10	EI	FD	GF	FW	A
HDAC11	HP	PN	GF	IY	I

Figure 15: A Clustal W alignment of the residues lining catalytic domains of class I, II and IV human HDAC proteins [69]. Amino acid residues located in the substrate binding region (the 11 Å channel) are shown. Highlighted in red are the residues that differ from the most conserved residue at the specified position. The numbering on top is for HDACI.

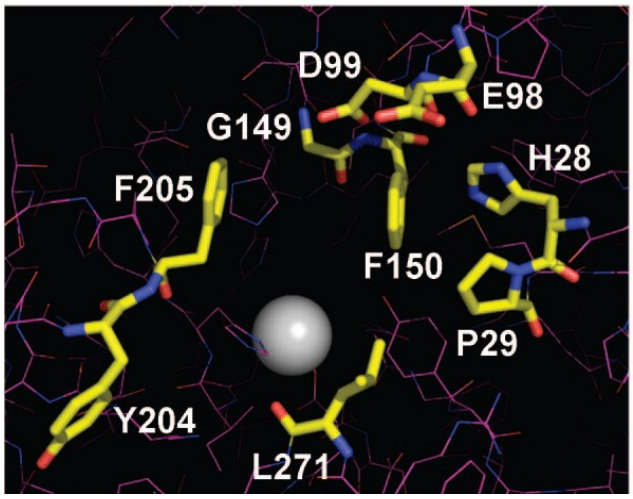

Figure 16: A human HDAC1 homology model showing residues lining the 11 Å channel of HDACI [69]. Channel residues are shown as ball and stick structures. The gray ball shows the catalytic zinc, whereas the yellow, red and blue represent carbon, oxygen, and nitrogen atoms respectively. *Reproduced with permission from J. Med. Chem., 2008, 51 (18), 5542-51.*

To study the 11 Å channel amino acids, a homology model was used to identify nine amino acids that line this channel in human HDACI. An alanine scan for these nine amino acid residues identified eight residues crucial for enzyme activity (Figure 2.7) [69]. Specifically, mutating H28, P29, D99, G149, F150, Y204, F205 and L271 to alanine led to a 62-91% reduction in HDAC1 enzymatic activity compared to wild type (Figure 2.7A) [69]. The only exception was the E98A mutant, located in the solvent exposed region of HDAC1, that

maintained deacetylase activity to levels comparable to HDAC1 (Figure 2.7A [69]. Further, mutating channel residues did not compromise HDAC1 binding to its associated proteins (Figure 2.7B). These combined data suggest that residues lining the 11 Å channel govern substrate binding and that mutations lead to a reorganization of the channel residues which compromise HDAC1 deacetylase activity.

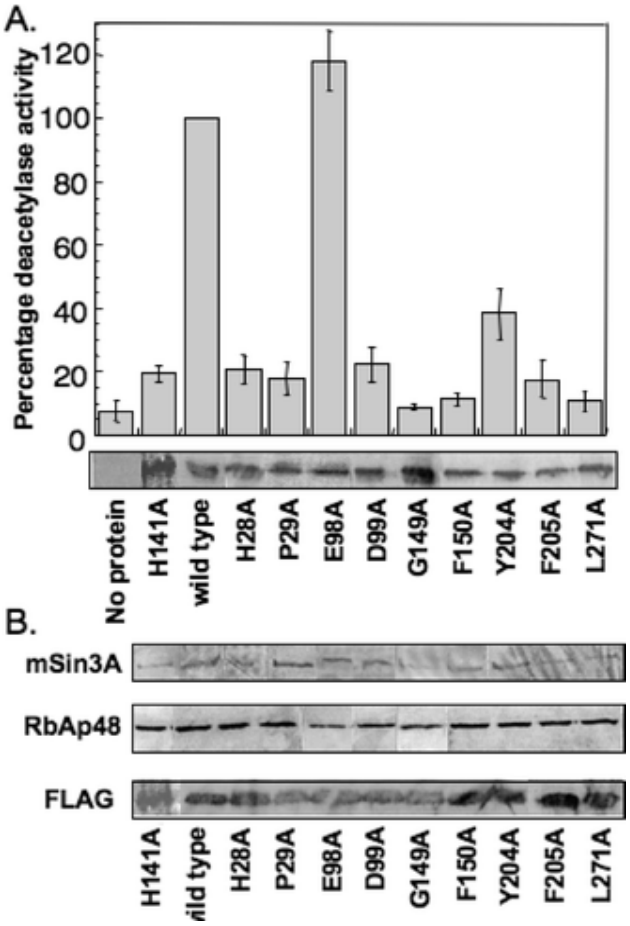

Figure 17: Residues lining the 11 Å channel of HDAC1 promote enzyme activity but not protein associations [69]. (A) HDAC1 wild-type or alanine mutants were expressed as FLAG-tagged fusion proteins and were immunoprecipitated with anti-FLAG-agarose resin. The immunoprecipitated proteins were used in fluorescence HDAC assays (histogram). The mean percent activity of five independent trials compared with that of the wild-type protein (100%) with standard error is shown. The immunoprecipitated proteins were also separated by SDS-PAGE and were probed with anti-FLAG (gel image) to ensure that equivalent protein quantities were used (Figure A.1). (B) Immunoprecipitated proteins in part A were further probed with anti-mSin3A, anti-RbAp48, and anti-FLAG to assess protein association. *Reproduced with permission from J. Med. Chem., 2008, 51 (18), 5542-51.*

Studies outlined in this chapter were geared towards understanding the importance of amino acid residues in the 14 Å internal cavity for HDAC1 activity. We used alanine scanning mutagenesis and substitution mutagenesis to determine the importance of channel residues to HDAC1 activity. Further, we performed an acetate competition assay to determine whether alanine mutants affect HDAC1 binding to acetate. Our results suggest that amino acids lining the 14 Å channel are important to maintain HDAC1 catalytic activity and that mutating them to alanine leads to a loss in activity. The acetate competition experiments reveal that several residues affect the interaction of HDAC1 with acetate. The mutagenesis studies identified amino acid residues involved in acetate or inhibitor binding and will aid in HDAC1 inhibitor design that includes the 14 Å channel.

2.3: Results

2.3.1: Residues in the 14Å channel of HDAC1 are critical for activity

Computational and homology studies have predicted that in HDAC1 Y23 (aligned with R16 in HDLP) and R34 (aligned with R27 in HDLP) form a charged pocket in the 14 Å channel and bind to and thereby stabilize the acetate by-product of the deacetylation reaction (Figure 2.1 and 2.2) [21]. The polar residues C151 and Y24 line the other side of the cavity and are likely to influence acetate binding and restoration of the active site configuration (Figure 2.2). In addition, these four amino acids might influence substrate binding and orientation of the active site due to their close proximity to the active site. Not surprisingly, C151 and R34 are strictly conserved among all class 1 isoforms, while Y23 and Y24 maintain 75% similarity (Figure 2.8B), indicating that the role of the 14 Å channel is relevant to all class 1 HDACs.

A.

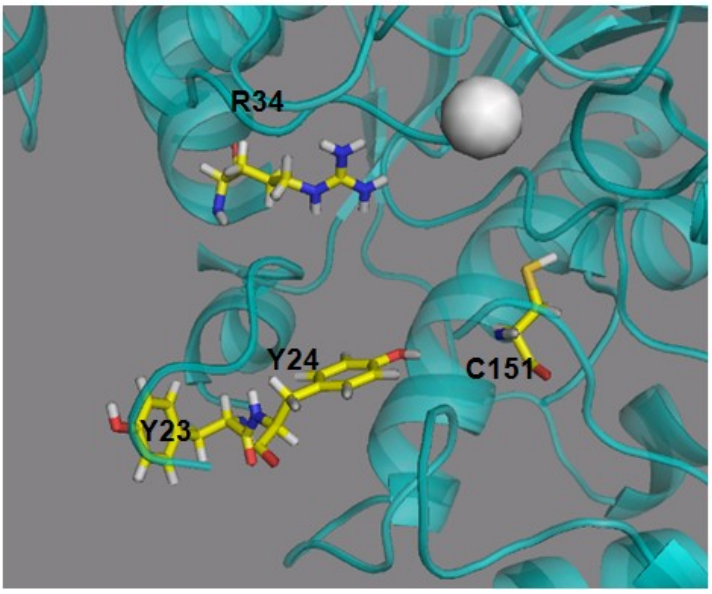

B.

	Y23	Y24	R34	C151
HDAC 1	Y	Y	R	C
HDAC 2	Y	Y	R	C
HDAC 3	F	H	R	C
HDAC 8	V	S	R	C
HDLP	R	Y	R	C

Figure 18: (A) Amino acid residues in the acetate-escape patch of HDAC1. The four amino acids (stick structures) lining the 14 Å channel of an HDAC1 homology model are shown. (B) Amino acid residues lining the 14 Å channel are shown for class I HDACs and HDLP. The catalytic domains of class 1 HDAC isoforms were aligned used Clustal W. Residues highlighted in red differ at Y23 (HDAC1) and Y24 (HDAC1).

To determine the influence of Y23, Y24, R34 and C151 in the 14 Å channel on HDAC1 enzymatic activity, each amino acid was individually mutated to alanine. Alanine mutants or the wild-type were expressed in T-Ag Jurkat cells as FLAG-tagged fusion proteins, immunoprecipitated with α-FLAG agarose beads, and tested for deacetylase activity using an in vitro fluoresence assay (Figure 2.9). The catalytically inactive mutant H141A was included for comparison purposes [20].

These alanine mutants each significantly influenced HDAC1 catalytic activity. The highly conserved R34 and C151 alanine mutants demonstrated only 31±6.5% and 21±4.5% remaining activity, compared to the wild type (100%) and which is comparable to the inactive H141A (19%±1.5). Mutating the two Tyr residues, Y23 and Y24 to alanine led to a 34± 7.0% and 25± 6.0% catalytic activity, respectively, compared to the wild type (100%). The HDAC1 homology model predicts that R34 and C151 are closer to the active site than Y23 and Y24, which are closer to the solvent exposed region of the 14 Å channel (Figure 2.8). These alanine scan

results suggest that Y23, Y24, R34 and C151 are critical to maintain the catalytic activity of HDAC1.

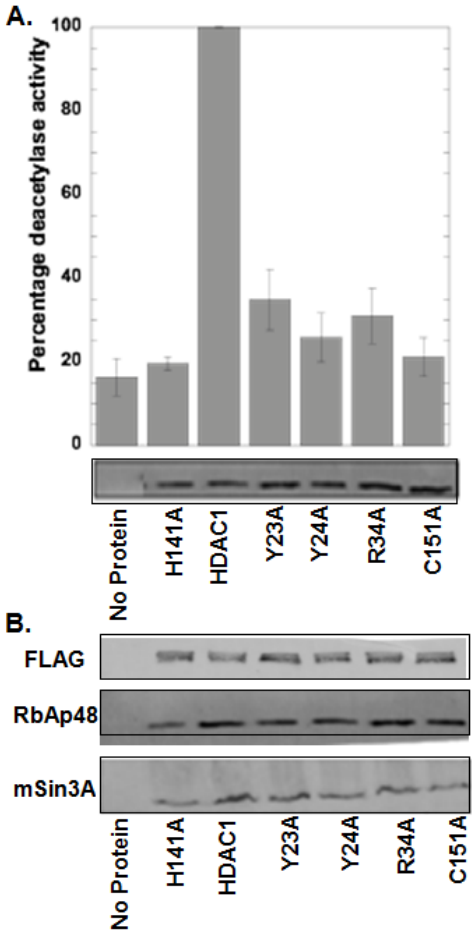

Figure 19: Y23A, Y24A, R34A and C151A mutants affect HDAC1 deacetylase activity, but not protein association. (A) Wild type or mutant proteins were expressed in T-Ag Jurkat cells as FLAG-tagged fusion proteins, immunoprecipitated with anti-FLAG-agarose beads, and tested for catalytic activity using an in vitro fluorescence assay (histogram) or separated on SDS-PAGE and probed with anti-FLAG antibody (gel image). The histogram shows the mean percent of at least four independent trials, which were normalized to wild type deacetylase activity (set to 100%). The standard error is shown as error bars (Table A.1). (B). Immunoprecipitated wild type and alanine mutants in A were further probed with anti-FLAG, anti-RbAp48 and anti-mSin3A to assess protein association.

To study the influence of other amino acids lining the 14 Å channel on catalytic activity, the HDAC1 homology model was used to identify V19, M30, I35, R36, S113, L139 and Y303 for further analysis (Figure 2.10). With the exception of R36, most of these amino acids are hydrophobic or polar, and are therefore not expected to bind to acetate. Because of their

location in the 14 Å channel and proximity to the active site, these seven amino acids may influence substrate binding or restoration of the active site configuration.

A.

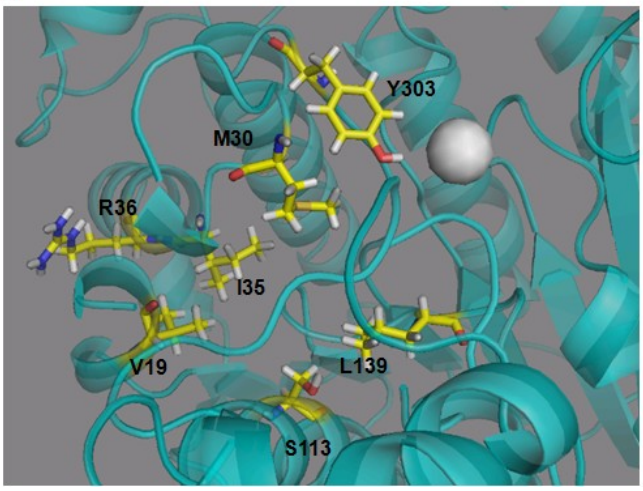

B.

	V19	M30	I35	R36	S113	L139	Y303
HDAC 1	V	M	I	R	S	L	Y
HDAC 2	I	M	I	R	S	L	Y
HDAC 3	V	M	L	A	Y	L	Y
HDAC 8	P	K	A	S	I	W	Y
HDLP	Y	L	V	S	A	M	Y

Figure 20: Residues in the 14 Å channel of HDAC1 (A).The seven additional amino acids (stick structures) lining the 14Å channel of the HDAC1 homology model are shown. (B) ClustalW alignment of the amino acids noted in A. Highlighted in red are the residues differing at each position.

To determine the influence of seven additional amino acids in the 14 Å channel on HDAC1 enzymatic activity, each amino acid was individually mutated to alanine, over expressed, immunoprecipitated, and tested for activity as discussed earlier. These alanine mutants all significantly reduced HDAC1 catalytic activity (Figure 2.11). The strictly conserved Y303 alanine mutant displayed 6.7±1.5% remaining activity relative to the wild type HDAC1 (100%). The homology model predicts that Y303 is close to the active site, near the catalytic metal ion (Figure 2.10). The dramatic loss of activity in the alanine mutation suggests that Y303 promotes HDAC1 deacetylase activity. The alanine mutations of hydrophobic residues V19, I35 and L139, which display 50% similarity among the class 1 isotypes, displayed between 5-39% deacetylase activities suggesting that all are important for HDAC1 deacetylase activity. Mutation of the amino acids M30 and S113 to alanine resulted in 19±6% and 62±4% deacetylase activities. The R36A mutant had 25±4% remaining activity, which is comparable to the inactive H141A mutant (19±1.5%). The combined mutagenesis data suggests that except for S113, the other six amino

acids in the 14Å channel are critical for maintaining HDAC1 enzymatic activity but do not appear to be involved in acetate release.

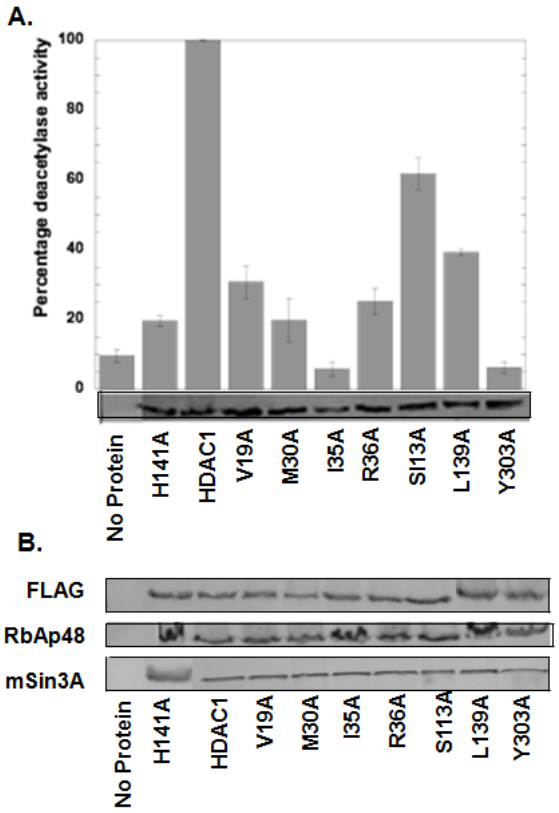

Figure 21: The 14 Å channel alanine mutants affect HDAC1 deacetylase activity, but have no effect on protein association. (A) Wild type or mutant proteins were expressed in T-Ag Jurkat cells as FLAG-tagged fusion proteins, immunoprecipitated with anti-FLAG-agarose beads, and tested for catalytic activity using an in vitro fluorescence assay (histogram) or separated on SDS-PAGE and probed with anti-FLAG antibody (gel image). The histogram shows the mean percent of at least four independent trials that were normalized to wild type deacetylase activity (set to 100%). The standard error is shown with error bars. (B) Co-immunoprecipitation of alanine mutants in A with, anti-FLAG, anti-RbAp48 and anti-mSin3A to assess protein association.

2.3.2: HDAC1 rescue mutants are inactive

According to computational and homology studies, the strictly conserved R34 is located closer to the active site, whereas the poorly conserved R36 residue is adjacent to R34 but farther from the active site in HDAC1 (Figures 2.6 and 2.8) [69]. The acetate by-product of the deacetylation reaction could form favorable ionic interactions to R34 and Y23 (similar to R16 in HDLP) located farther from the active site and close to the solvent exposed region of the 14 Å channel. These computational studies predict that acetate is exchanged with the bulk water outside the channel. Substitution of a similar charged functional group capable of forming ionic bond at R34 or R36 in HDAC1 could maintain enzymatic activity. Similarly, the C151 residue (located next to the catalytic metal ion and in the 14 Å channel) could be replaced by serine with a similar polar functional group, which could maintain interactions with acetate or the active site. Additionally, to probe the importance of the aromatic phenyl group of Y23, 24 and 303 in HDAC1, Y23F, Y24F and Y303F substitution mutants were created. In this case, if aromaticity is critical, aromatic amino acids should replace tyrosine.

To test the rescue mutations, Y23F, Y24F, R34K, R36K, C151S and Y303F single point mutants were expressed in T-Ag Jurkat cells as FLAG-tagged fusion proteins, immunoprecipitated with FLAG-agarose beads, and tested for deacetylase activity using an in vitro fluoresence assay, as described earlier. The substitution mutants were unable to restore HDAC1 catalytic activity except for the Y24F mutant (Figure 2.12). R34K, R36K and C151S HDAC1 mutants demonstrated 17±3.0%, 33±3.5% and 30±1.0% remaining activity respectively. Mutating the residues Y23, Y24 and Y303 to Phe led to 12±3.5%, 56±9.0% and 38±4.0% deacetylase activity respectively. Collectively, these mutagenesis data suggest that Y23, Y24, R34, R36, C151 and Y303 are uniquely suited to promote HDAC1 deacetylase activity, and that F partially substitutes for Y24 and Y303 in HDAC1.

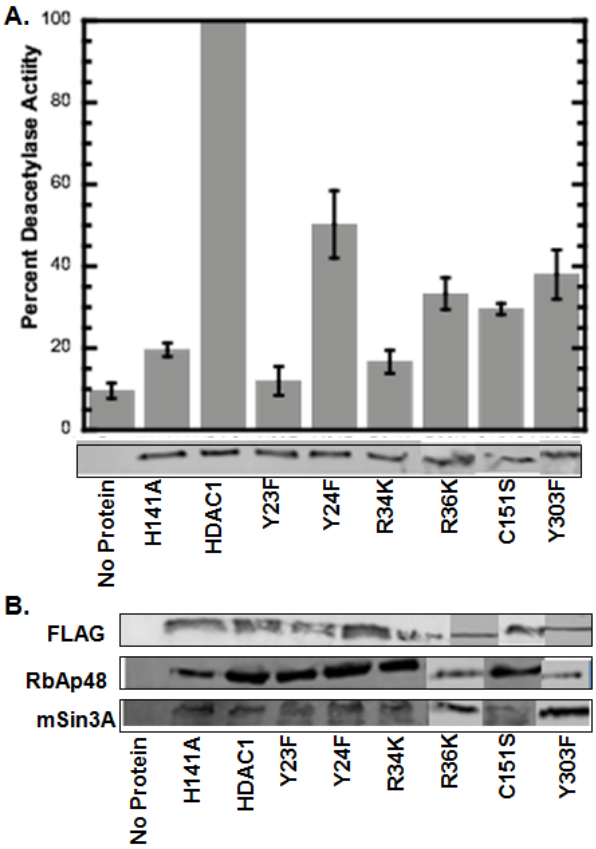

Figure 22: HDAC1 Y23F, Y24F, R34K, R36K, C151S and Y303F substitution mutants are inactive. (A) Wild type or mutant proteins were expressed in T-Ag Jurkat cells as FLAG-tagged fusion proteins, immunoprecipitated with anti-FLAG-agarose beads, and tested for catalytic activity using an in vitro fluorescence assay (histogram) or separated on SDS-PAGE and probed with anti-FLAG antibody (gel image). The histogram shows the mean percent of at least three independent trials that were normalized to wild type deacetylase activity (set to 100%). The standard error is shown as error bars (Table A.2). (B) Co-immunoprecipitation of mutants in (A) with anti- FLAG, anti- RbAp48 and anti-mSin3A to assess protein association.

2.3.3: Mutation of amino acids lining the 14 Å channel of HDAC1 does not disrupt protein association

The mammalian co-repressor complexes mSin3A and RbAp48 tie HDAC1 to promoter-bound transcription factors, leading to transcriptional gene silencing (discussed in section 1.4.3 chapter 1) [70, 73-75]. The binding of HDAC1 to co-repressors not only recruits the deacetylase to promoter regions but also leads to an increase in deacetylase activity [73]. Our results suggest that alanine and substitution mutants abolish HDAC1 activity. It is therefore possible that mutations lead to protein misfolding and/or that mutant proteins fail to bind to co-repressor

complexes. To test whether the loss in activity observed in mutant proteins was a result of failure of the mutant proteins to bind to its associating partners, biochemical purification was performed. Alanine and substitution mutants were immunoprecipitated with FLAG-agarose beads, separated on SDS-PAGE, and probed with anti-mSin3A or anti-RbAp48 antibodies. Alanine and substitution mutants displayed equal co-immunoprecipitation activities independent of deacetylase activity (Figure 2.9B, 2.11B and 2.12B). The inactive H141A recovered similar levels of mSin3A and RbAp48 comparable to the wild type as previously reported [69]. Collectively, our results suggest that the loss in activity in 14Å channel is not due to a failure of mutant proteins to bind to the co-repressor complexes.

2.3.4: R34 and R36 affect interaction of HDAC1 with acetate

To facilitate passage of acetate through the 14 Å channel, computational studies predicted that charged amino acids R34 and R36 in HDAC1 would form favorable ionic/hydrogen bond interactions with acetate [21]. Polar residues Y23, Y24, C151 could also hydrogen bond to acetate [70].Further, side chain movement of Y23 and Y24 located towards the solvent exposed region of the 14 Å channel could help exchange acetate with the bulk water solvent [21, 70]. Our mutagenesis results demonstrate that mutations of the amino acids thought to bind to acetate abolish HDAC1 enzymatic activity.

To determine the influence of mutant proteins to acetate binding in HDAC1, acetate inhibition of the activities of Y23, Y24, R34, R36, and C151 mutants were determined and compared to wild type. The F205Y mutant located in the 11 Å channel was included as a control because it should not affect acetate binding [69]. Mutant or wild type proteins were immunoprecipitated with FLAG-agarose beads and the extent of inhibition by acetate was determined at constant substrate concentration. All 14 Å tunnel mutations displayed altered acetate inhibition. The R34A and R36A mutants displayed 1.7 and 2.8 fold reduced IC_{50} values (12 mM and 15 mM, respectively) compared to the wild type (7.2 mM) and F205Y (7.5 mM)

controls (Figure 2.13). Similarly, the Y23A, Y24A and C151A mutants displayed close to 2-fold reduction in acetate binding compared to wild type (Figure 2.14). Collectively, these acetate competition data suggest that both charged and polar amino acid residues in this channel influence HDAC1 binding to acetate and confirms the involvement of these amino acids in acetate binding or release.

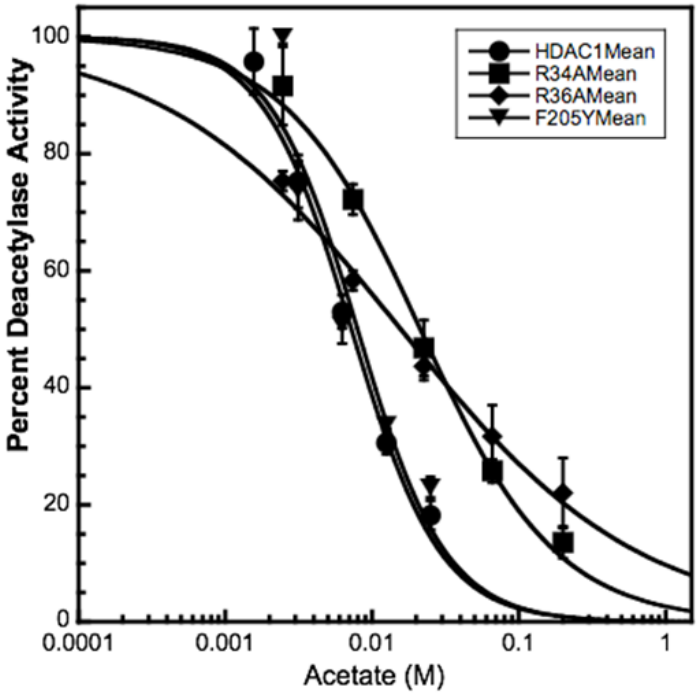

Figure 23: R34 and R36 mutations affect HDAC1 binding to acetate. Wild type or mutant proteins were expressed in T-Ag Jurkat cells as FLAG-tagged fusion proteins, immunoprecipitated with anti-FLAG-agarose bead, and tested for catalytic activity in the presence of varying concentrations of acetate (0-200 mM). The standard error for at least three trials is shown. (Table 1.1).

Table 1.1: IC_{50} values on acetate inhibition of HDAC1 and mutant proteins[a]

HDAC1	IC_{50} (mM)
Wild type	7.2 ± 0.5
Y23A	21 ± 2
Y24A	19 ± 1
R34A	12 ± 0.3
R36A	15 ± 1
C151A	13 ± 1
F205Y	7.6 ± 1.1

[a]Calculated from at least three trials; errors are the standard error of the mean.

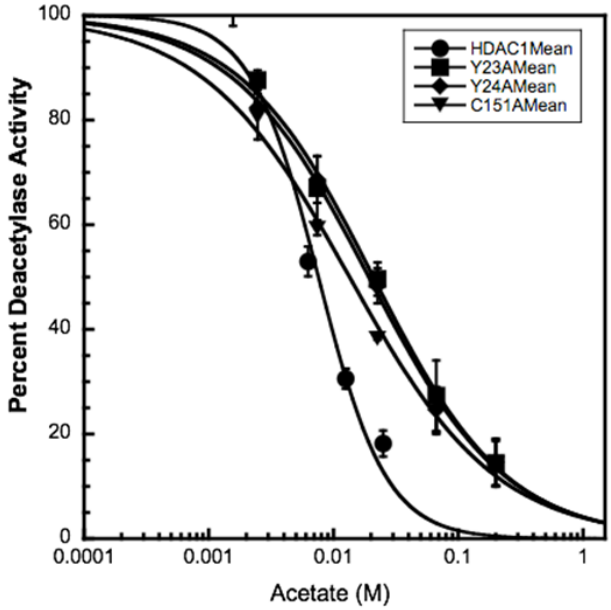

Figure 24: Y23, Y24 and C151 affect HDAC1 binding to acetate. Wild type or mutant proteins were expressed in T-Ag Jurkat cells as FLAG-tagged fusion proteins, immunoprecipitated with anti-FLAG-agarose bead, and tested for catalytic activity in the presence of varying concentrations of acetate (0-200 mM). The standard error for at least three trials is shown (Table 1.1).

2.4: Discussion

The 14 Å channel of Class 1 HDAC isotypes has long being hypothesized to be the exit cavity for acetate release by deacetylation [20, 21, 70]. The amino acids lining this cavity are very similar among the HDAC isoforms, suggesting the role of the cavity is relevant to all HDACs proteins. In one study, docking showed that both acetate and acetic acid localize next to the metal ion, and amino acids R16 and R17 in HDLP. In contrast, in similar studies, N-hydroxyacetamide, which is related in structure to HDAC inhibitors SAHA or TSA, was bound to the 11 Å channel,but less to the 14 Å channel [21]. In addition, amino acids located towards the solvent exposed regions of HDAC1 demonstrate flexibility, indicating that side chain movement of these amino acids could help exchange cavity contents with bulk water for the next cycle of deacetylation [20, 21]. To date, no experimental data confirm these speculations with HDAC1.

An alanine scan was used to determine the influence of amino acid residues lining the 14 Å channel of HDAC1 in enzymatic activity and binding to acetate [22, 69]. HDAC1 V19A, Y23A, Y24A, M30A, R34A, I35A, R36A, L139A, C151A and Y303A mutants reduced HDAC1 deacetylase activity significantly to levels ranging from 6 to 34% compared to the wild type. The S113A mutant, which is located near the solvent exposed region of the internal cavity, maintains significant deacetylase activity at 61% compared to the wild type (100%). Because polar and charged residues lining the 14 Å channel of HDAC1 are implicated in acetate binding and release, more conservative mutations were examined to see if they could restore deacetylase activity. These mutants also displayed reduced deacetylase activities suggesting functional group specificity. Y24F is the only mutant that maintained a significant deacetylase activity at 56% compared to that of the wild type. These combined mutagenesis studies suggest that the 14 Å channel is critical to maintain HDAC1 activity and influence acetate binding and release.

Mutating the 14 Å cavity residues does not globally affect HDAC1 structure as shown by the protein association studies. The loss in enzymatic activity for mutant proteins can therefore be attributed to two possibilities. One, mutating channel residues might influence substrate binding and govern the organization of the active site residues, which ultimately affect HDAC1 activity. Alternatively, mutating channel residues might influence the release of the acetate by-product. To probe this hypothesis further, we determined the influence of mutation on HDAC1 binding to acetate. Both polar and charged residues showed a two-fold reduction in the half-maximal inhibition by acetate compared to the wild type. It is likely that mutating these residues remove key contacts required for acetate binding and release. These findings are consistent with previous work on HDAC8, where acetate competition assay with recombinant HDAC8 R37A resulted into 160-fold difference in IC_{50} values (HDAC8R37A IC_{50} of 400 mM versus the HDAC8 wild type IC_{50} of 2.5 mM) [22]. The small differences observed here with HDAC1 could be a result of mammalian proteins versus bacterially-expressed proteins in the two separate studies. Combined, our results indicate that the 14 Å channel mutants do not significantly alter the active site configuration, but rather affect the substrate binding and acetate release.

HDAC1 has been linked to certain cancers, making it an attractive target for cancer therapy. Characterization of HDAC1 structure will aid in drug-design efforts and will facilitate the understanding of its involvement in cancer formation. In addition, HDAC1 selective inhibitors may be valuable cancer therapeutics. The lack of structural information on the HDAC1 active site has frustrated efforts to design HDAC1 selective inhibitors. Structural characterization of HDAC1 has been hindered by lack of active enzyme from heterologous bacteria culture [76]. As an alternative, mutagenesis offers insight into the influence of amino acid residues in the enzyme pocket to HDAC1 activity. The combined mutagenesis data confirm the importance of V19, Y23, Y24, M30, R34, I35, R36, S113, L139, C151 and Y303 in the 14 Å channel of HDAC1, as predicted earlier[21,71].

The mutagenesis studies in this work will aid in the design of HDAC1 selective inhibitors. Importantly, selective HDAC1 inhibitors designed to fit the 14Å channel have been created [19]. Subtle differences in amino acids give rise to distinct channel regions and can be exploited to design selective HDAC1 inhibitors as previously reported [19, 71]. The acetate competition results suggest that designing HDAC1 inhibitors with acetate mimics targeting interactions with Y23 can create a HDAC1 selective inhibitor. Future inhibitor design which includes the 14Å channel will benefit from these findings.

2.5: Experimental procedures

2.5.1: General biochemical equipment

Equipment available in the Pflum lab includes centrifuges (Eppendorf models 5415D and 5810R), bacterial incubator/shaker (New Brunswick Scientific C25 Incubator Shaker Classic Series), Tecan GENios Plus spectrophotomer, Biorad gel electrophoresis systems and an Eppendorf Mastercycler Gradient.

2.5.2: Single point mutagenesis

Asymmetric was used to create HDAC1 single-point mutants using the primers shown below; mutants were cloned into the pBJ5HDAC1-Flag expression plasmid using *Not1* and *EcoR1* restriction sites [70]. All mutants were confirmed by DNA sequencing. The primers used were as follows (mutation bolded):

pBJ5 *Not1* start: GCCAGAATGCGGCCGCATGGCGCAG

pBJ5 153 rev: TATCATGTCTGGATCCGG

HDAC1 V19A rev: CATCCCCGTCGTAGTAGTAACAGAC

HDAC1 V19A for: GTTACTACTACGACGGGGAT**GCT**GGAAATTACTATTATGG

HDAC1 Y24A rev: GTAATTTCCAACATCCCCG

HDAC1 Y23A for: CGGGGATGTTGGAAATTAC**GCA**TATGGACAAGGCCACCCAATG AAGCC

HDAC1Y23Ffor: CGGGGATGTTGGAAATTAC**TTC**TATGGACAAGGCCACCCAATGAAGCC

HDAC1 Y24A for: CGGGGATGTTGGAAATTACTAT**GCA**GGACAAGGCCACCCAATGAAGCC

HDAC1 Y24F for: CGGGGATGTTGGAAATTACTAT**TTC**GGACAAGGCCACCCAATGAAGCC

HDAC1 M30A rev: GGGTGGCCTTGTCCATAATAG

HDAC1M30A for: GGACAAGGCCACCCA**GCG**AAGCCTCACCGAATC

HDAC1 R34A rev: GGCTTCATTGGGTGGCCTTGTCC

HDAC1 R34A for: GGCCACCCAATGAAGCCTCAC**GCA**ATCCGCATGACTCATAATTTGCTG

HDAC1 R34K for: GGCCAC CCAATGAAGCCTCAC**AAG**ATCCGCATGACTCATAATTTGCTG

HDAC1 I35A rev: CGGTGAGGCTTCATTGGGTGG

HDAC1 I35A for: CCCAATGAAGCCTCACCGA**GCC**CGCATGACTCATAATTTGCTGC

HDAC1 R36A for: CCCAATGAAGCCTCACCGAATC**GCC**ATGACTCATAATTTGCTGC

HDAC1 R36K for: CCCAATGAAGCCTCACCGAATC**AAA**ATGACTCATAATTTGCTGC

HDAC1 S113A rev: CAACTGACAGAACTCAAACAGGCC

HDAC1 S113A for: GGCCTGTTTGAGTTCTGTCAGTTG**GCA**ACTGGTGGTTCTGTGGC

HDAC1 L139A rev: GCCCCCAGCCCAATTCACAGCG

HDAC1 L139A for: GGGCTGGGGGCGC**GCA**CCATGCAAAGAAGTCCGAGGC

HDAC1 C151A rev: GAAGCCAGATGCCTCGGACTTC

HDAC1 C151A for: GTCCGAGGCATCTGGCTT**CGC**TTACGTCAATGATATC

HDAC1 C151S for: GTCCGAGGCATCTGGCTTC**TCT**TACGTCAATGATATC

HDAC1 Y303A rev: CCACCGCCTCCCAGCATCAGC

HDAC1 Y303A for: GGGAGGCGGTGG**GCT**CACCATTCGTAACGTTGCCCGG

HDAC1 Y303F for: GGGAGGCGGTGG**TTT**CACCATTCGTAACGTTGCCCGG

2.5.3: Polymerase Chain Reaction (PCR)

Two-step (touchdown PCR program) PCR was used to generate PCR inserts with the mutagenic primers described in section 2.5.2. A typical reaction mixture contained the following reagents: water (30 µL), DMSO (5 µL), 10X Pfu buffer (5 µL of 200 mM Tris, 100 mM $(NH4)_2SO_4$, 100 mM KCl, 1% TritonX-100, 20 mM $MgSO_4$, 1 mg/mL BSA, pH 8.8), DNA plasmid template (1 µL of 0.5 µg/µL), forward primer (1 µL of 25 µM), reverse primer (1 µL of 25 µM), and dNTPs (2µL of 10 mM ; 2.5mM of each base). PCR reaction mixtures were mixed thoroughly by pipetting and then heated in a thermocycler (Eppendorf Mastercycler Gradient) for 1 minute at 95 °C and 2 µL Pfu enzyme was added. After addition of the enzyme, initial 10 cycles of the touchdown program were run as follows: 1 minute 95 °C, 1 minute annealing, 2 minutes elongation at 72°C. The initial and final annealing temperatures in the 10 cycles were 60 °C and 50 °C respectively with lowering of the temperature by 1 °C per cycle. After another 25 cycles at

the final annealing temperature of 50 °C, the PCR cycles ended with a 10 minute elongation period at 72 °C before cooling to 4 °C. DNA products were purified by gel electrophoresis as described below in section 2.5.4.

The second step PCR was similarly run to create the full length HDAC1-FLAG mutant insert for homologous recombination using 5 µL of gel purified PCR1 products to replace the DNA template and the volume of water adjusted to final 50 µL total volume. PCR2 products were similarly gel purified (section 2.5.4).

2.5.4: DNA agarose gel electrophoresis and gel purification

Gel electrophoresis was done using 1% agarose in 1X Tris-Acetate-EDTA buffer (TAE; 40 mM Tris, 20 mM acetic acid, 1mM EDTA, pH 8.8, 0.5 µg/mL ethidium bromide) for 60 minutes at 120V Separated DNA was purified using the QIAgen gel extraction kit (cat # 28704) and used for homologous recombination (section 2.5.6).

2.5.5: Restriction digest

pBJ5HDAC1[70] was digested with *EcoRI* and *NotI* restriction enzymes (both from Promega). The restriction digest reaction contained, pBH5HDAC1 (50 ng of 1 µL) buffer H (2 µL; Promega), BSA (1 µL of 0.1 mg/mL), of *Not1* and *EcoRI* (1 µL each) and water (14 µL). The reaction mixture was incubated for 2 hours at 37 °C with shaking at 250rpm. The DNA was recovered by gel electrophoresis (section 2.5.4) followed by extraction using the QIAgen gel extraction kit.

2.5.6: Homologous recombination in KC8 cells

KC8 cells (50 µL section 2.5.10) were mixed with PCR insert (5 µL; section 2.5.3), restriction-digested DNA (5 µL; section 2.5.5), KCM buffer (10 µL of 0.1M KCl, 30 mM $CaCl_2$, 50 mM $MgCl_2$) and 30 µL water. The mixture was incubated on ice for 20 minutes followed by a 60-90 second heat shock at 42 °C. The cells were then cooled on ice for 2 minutes, before 500 µL of LB medium (1% peptone, 0.5% yeast extract and 1% NaCl) was added. Cells were incubated for 90 minutes at 37 °C with shaking at 250 rpm. Cells were collected by spinning at 13200 rpm for

10 minutes and all but 100 µL of the supernatant was removed. The remaining media was used to resuspend the cell pellet followed by plating on 20 µg/mL kanamycin (to select for KC8) and 50 µg/mL ampicillin LB agar plates (to select for pBJ5HDAC1). The cells were grown overnight at 37 °C. The DNA from individual colonies was mini-prepped as described in section 2.5.8 and sequenced by the University of Michigan DNA sequencing core.

2.5.7: Bacterial plasmid transformation

Wild type pBJ5HDAC1-Flag or mutant expression plasmids were transformed into chemocompetent DH5α *E. coli* (section 2.5.9). DH5α competent cells (100 µL) were thawed on ice and 1 µL plasmid DNA was added and mixed. Next, the solution was incubated for 20 minutes on ice and heat-shock treated for 60-90 seconds at 42 °C. The cells were quickly transferred into ice for 2 minutes, after which 0.5 mL of LB media was added. The cells were grown for 1 hour at 37 °C with shaking at 250 rpm. Cells were collected by spinning at 13000 rpm for 10 minutes and all but 100 µL of the supernatant removed by aspiration. The cell pellet was resuspended into the remaining 100 µL and plated on LB agar plates containing 50 µg/mL ampicillin. Plated cells were grown overnight at 37 °C.

2.5.8: Plasmid mini and midi-preps

One colony of DH5α cells expressing wild type pBJ5HDAC1-Flag or mutant expression plasmids (section 2.5.7) or KC8 cells containing a new clone (section 2.5.6) was inoculated into 5 mL (mini-prep) or 100 mL (midi-prep) LB containing 50 µg/mL ampicillin. The culture was grown overnight at 37 °C at 250 rpm. Cells were recovered by spinning at 13200 rpm for 10 minutes at 4 °C. The supernatant was removed by aspiration and the cell pellet was resuspended into 300 µL (mini-prep) or 4 mL (midi-prep) cold P1 buffer (50 mM Tris-Cl, pH 8.0, 10 mM EDTA, 100 µg/mL RNAse A). Room temperature 300 µL (mini-prep) or 4mL (midi-prep) P2 buffer (200 mM sodium hydroxide, 1% SDS) was added and mixed by inversion prior to incubation for 5 minutes at room temperature with constant gentle mixing. Cold P3 buffer (300 µL for mini-prep or 4 mL for midi-prep of 3.0 M potassium acetate, pH 5.5) was added, mixed by

inversion, and incubated on ice for 15 minutes (inversion every 5 minutes). The cell debris was removed by spinning at 13200 rpm for 10 minutes and the supernatant was loaded on a QIAgen column (midi-prep; needed for mammalian transfection) or a pre-chilled tube containing 540 µL of isopropanol. Midi-prep DNA was prepared as per the Qiagen protocol. The mini-prep was incubated on ice for 5 minutes after which the DNA was collected by spinning at 13200 rpm for 10 minutes, the supernatant was removed by aspiration, and the DNA was redissolved in 20 µL water and stored at -20 °C.

2.5.9: Preparation of chemocompetent DH5α *Blue E. coli*

DH5α *E. coli* was made chemocompetent by calcium chloride treatment to allow for plasmid uptake or transformation for subsequent replication to produce large amounts of plasmid. A single colony of DH5α was inoculated into 25 mL LB and grown overnight at 37 °C with shaking at 250 rpm. On day 2, 4 mL of the overnight culture was diluted into 400 mL LB and similarly grown until OD_{600}=0.375. Portions of the growth culture (50 mL) were transferred into 50 mL pre-chilled centrifuge tubes and cooled on ice for 10 minutes, followed by spinning at 4000 rpm, for 10 minutes at 4 °C. The liquid supernatants were removed via aspiration and the cell pellets were washed 3 times with 10 mL cold $CaCl_2$ solution (60 mM $CaCl_2$, 10 mM PIPES, and 15% v/v glycerol). After the last wash, the cell pellets were resuspended in 2 mL of $CaCl_2$, split into 100 µL aliquots, and stored at -80 °C until use.

2.5.10: Preparation of KC8 competent cells

KC8 cells were obtained from the Finley lab (Wayne State University). An overnight culture (5 mL) grown at 37 °C with 250 rpm shaking was diluted into 500mL LB media. The cells were further grown for about 3-4 hours at the same growth conditions until OD_{600} reached about 0.5. Cells were recovered by spinning at 3500 rpm for 15 minutes at 4 °C and the LB was poured out. Cells were resuspended into 25 mL cold LBSB (LB diluted with HCl to pH 6.1, 10% (w/v) PEG 3400, 5% (v/v) DMSO, 10% glycerol, 10 mM $MgCl_2$, 10 mM $MgSO_4$) and incubated on ice for 10 minutes. The cells were split into 250 µL aliquots and stored at -80 °C until use.

2.5.11: Mammalian cell growth and storage

TA-g Jurkats cells [77] were grown in RPMI-1640 media (GIBCO) supplemented with 10% FBS (GIBCO) and 1% antibiotic-antimycotic (GIBCO). Cells were grown at 37 °C in 5% CO_2 to a maximum confluency of 1 million cells/mL. Cells were passaged each day and cell count was determined using Tryptan blue stain (GIBCO) and a hemocytometer. For storage, approximately 10 million cells were harvested by spinning at 1000 rpm at 4 °C for 5 minutes and the growth medium was removed by aspiration. The cell pellet was re-suspended in 1 mL RPMI -1640 medium containing 5% glycerol. Cells were transferred into cryovials, which were wrapped in styroform and slowly frozen, first at -20 °C overnight, and then transferred to -80°C for a day before moving them to liquid nitrogen.

2.5.12: DNA transfection

Plasmid DNA purified using the QIAgen kit (see section 2.5.8, 20 µg, pBJ5HDAC1-Flag or mutants) was separately transiently transfected into 40 X 10^6 TA-g Jurkat cells by electroporation using 4 mM electroporation cuvettes. Briefly, cells were harvested by spinning at 1000 rpm for 5 minutes at 4 °C. The supernatant was removed by aspiration and the cell pellet was resuspended in 20 mL RPMI medium without FBS and phenol red pH indicator (GIBCO) followed by spinning and medium removal. The cell pellet was resuspended in 800 µL RPMI media (no pH indicator or FBS) and transferred into eppendorf tubes. Plasmid DNA was added, mixed, set at room temperature for 10 minutes, and transferred into BTX 4 mM gap electroporation cuvettes (Fischer Biotech). Electroporation was carried out using a BTX Electro cell manipulator 630. For every 10 X 10^6 cells in 200 µL media the following settings were used: S-250 V, T-500V/capacitance and resistance, C-800 µF and R-129 Ohms. The µF output was varied depending on the quantity of cells as follows; 10 X 10^6 cells: 800 µF, 20 X 10^6 cells: 1600 µF, 30 X 10^6 cells: 2100 µF and 40 X 10^6: 2800 µF. The pulse length (1/e) was around 35 msec

for optimal electroporation and the presence of a frothy precipitate due to dead cells is normal. Electroporated cells were set at room temperature for 10 minutes, transferred to 10 mL of warm (37 °C) RPMI-1640 (with 10% FBS and 1% antibiotic) for every 10 X 10^6 cells and grown for 48 hours as described in section 2.5.11. The cells were harvested by spinning at 1000 rpm for 5 minutes at 4 °C and washed with 1 mL of PBS (137 mM NaCl, 2.7 mM KCl, 4.3 mM Na_2HPO_4, 1.4 mM KH_2PO_4 pH 7.3). PBS was removed by spinning at 1000 rpm, for 5 minutes at 4 °C and the cells were used immediately or stored at -80 ˚C until use.

2.5.13: Immunoprecipitation

TA-g Jurkat (40 X 10^6) cells expressing HDAC1-FLAG wild type or mutant proteins were lysed in cold Jurkat lysis buffer (50 mM Tris pH 8, 150 mM NaCl, 10% (v/v) glycerol, 0.5 % (v/v) Triton X-100) containing 1X protease inhibitor cocktail set V (Calbiochem). Briefly, the cells were lysed by pipetting in 0.5 mL of cold JLB buffer for every 20 X10^6 cells and incubating with rotation at 4 °C for 30 minutes. The soluble fraction was separated from cell debris by spinning at 15000 rpm for 10 minutes at 4 °C. Anti-Flag agarose beads (10 µL of bead slurry, Sigma) were used to immunoprecipitate HDAC1-Flag wild type or mutant proteins in 1 mL cold TBS buffer (50 mM Tris HCL, with 150 mM NaCl, pH 7.4). The beads were prepared by washing three times with 0.5 mL TBS followed by spinning at 1000 rpm for 5 minutes at 4 °C, with buffer removal in between washes. Immunoprecipitation was carried out at 4 °C for 2 hours with rotation by incubating 400 µL lysates with the washed beads. Immunoprecipitated proteins were harvested by spinning at 3200 rpm for 5 minutes at 4 °C. Immunoprecipitates were split in half: half was used for gel analysis (section 2.5.14) and the other half for HDAC assays (section 2.5.15). For gel analysis, FLAG-fusion proteins were eluted from the agarose bead by adding 40 µL of 0.1M glycine HCl, pH 3.5, and incubating for 5 minutes at 4 °C with gentle shaking. The supernatant containing the FLAG-fusion protein was recovered by spinning at 3200 rpm for 5 minutes at 4 °C. The supernatant was neutralized by transferred into a clean tube containing

10μL 0.5 M Tris HCl, pH 7.4, and 1.5 mM NaCl. The eluted protein was used immediately in SDS-PAGE experiments (section 2.5.14)

2.5.14: SDS-PAGE

β-mercaptoethanol (1 μL) and 5XSDS loading buffer (10 μL of 50 mM Tris-Cl pH 6.8, 100 mM dithiothreitol, 2% (w/v) SDS electrophoresis grade, 0.1% bromophenol blue, 10% (v/v) glycerol)) was added for every 40 μL immunoprecipated FLAG-fusion proteins. Each solution was incubated at room temperature for 5 minutes. The mixtures were heat at 95 °C for 1 minute and quickly cooled on ice prior to loading onto the gel. When using lysates, 10 μL lysates was added to 10 μL SDS loading buffer with 10% β-mercaptoethanol. The separating layer of the SDS-PAGE gel was prepared to contain 10% 37:1 acrylamide/ bisacrylamide (Acros) by mixing 1 mL 4X Tris/SDS buffer (0.4% SDS, 1.5 M Tris, 0.24 M HCl; pH 8.8), 1.96 mL water, 1 mL 40% 37:1 acrylamide/bisacrylamide, 40 μL ammonium persulfate and 2 μL 10% TEMED (N, N, N', N'-tetramethylthylenediamine; Acros). The mixture was mixed thoroughly and immediately poured into a BioRad mini-Protean tetra cell casting module. The surface of the gel was covered with methanol and allowed to polymerize. The stacking layer was prepared by mixing 1.24 mL water, 250 μL 40% 37:1 acrylamide/bisacrylamide, 500 μL 4X Tris/SDS buffer (0.4% SDS, 1.5 M Tris, 0.24 M HCl; pH 6.8), 10 μL of 10% ammonium persulfate and 1 μL TEMED. Methanol was removed from the polymerized separating layer and the stacking layer mixture was poured followed by the addition of a comb; the layer was allowed to polymerize. The gels were inserted into the BioRad (Protean III) gel apparatus, which was filled with SDS running buffer (0.1% SDS, 25 mM Tris, 250 mM glycine; pH 8.3). The gel wells were loaded with samples and run at 200 V for 60 minutes.

2.5.15: Western blot and co-immunoprecipitation

To probe protein bands with anti-Flag (Sigma), anti-mSin3A (Santa Cruz) or anti-RbAp48 (Sigma) antibodies, the proteins in the SDS gel were transferred onto a polyvinylidene (PVDF) membrane (Millipore Immobilon-P, 0.45 micron). The membrane was activated for protein transfer by soaking in methanol. Both the membrane and gel were assembled between filter paper and padding and transferred into the BioRad gel electrophoresis chamber containing an ice cooling tray. The chamber was filled with CAPS/methanol transfer buffer prepared by mixing 100 mL 10X CAPS (0.1 M CAPS, pH adjusted to 10.5 with 10 M NaOH) and 800 mL distilled water. The transfer was run for 1 hour at 90 Volts. The membrane was carefully removed and air dried to ensure proteins were bound. The membrane was wet in methanol and blocked overnight with 10% low fat dry milk in 10 mL of PBST (PBS with 0.1% Tween). After blocking, blocking solution was removed and the membrane was washed three times with 5 mL of PBST to remove unbound milk. The membrane was probed with primary antibody (1:10,000 dilution in 10% low fat dry milk and PBST, containing 0.002% sodium azide preservative) by rocking for 2 hours. After 2 hours, the membrane was washed 3 times with 5 mL PBST to remove unbound antibody. The membrane was coated with a fluorescently labeled secondary anti-mouse (1: 5000, Alexa Fluor 647; Life Technologies) or anti-rabbit (1:3000, Alexa Fluor 647; Life Technologies) antibody solutions in PBST containing 10% low fat dry milk for 1 hour. The antibody solution was removed and the membrane was washed three times with 5 mL PBST to remove unbound antibody. Proteins were visualized using a Typhoon 9210 variable mode imager (Amersham Biosciences) by measuring the fluorescence at 670 nM.

2.5.16: HDAC activity assay

The Fluor de Lys™ fluorescence activity assay (Biomol) was used to determine HDAC activity. Approximately 20 µg total protein was immunoprecipitated as described in section 2.5.13 and used in this assay. The bead-bound HDAC immunoprecipitates were incubated with 25 µL HDAC assay buffer (50 mM Tris/Cl, pH 8.0, 137 mM NaCl, 2.7 mM KCl, 1 mM $MgCl_2$) and 25 µL substrate (100 µM; Prod. No. BML-KI104) at 37 ˚C for 45 min with shaking (900 rpm). Then, 50 µL 20X developer (Prod. No. BML-KI105) was added and incubated for 5 min at 37 °C. The reaction mixture was transferred into a white microplate (Prod. No. BML-K571) and the fluorescence signal was measured using the GENios plus plate-reader fluorimeter (Tecan) with an excitation wavelength of 360 nm and emission of 465 nm wavelength. The fluorescence signal for each mutant was normalized to the wild type (set at 100%) and standard errors from at least four independent trials are provided in the appendix (Table A.1 and A.2).

2.5.17: Acetate competition assay

To perform the acetate competition assay, the activity of mutant proteins was determined using the Fluor de Lys™ kit with some modifications. Immunoprecipitation was done as described in section 2.5.13 and then split into 5 equal aliquots. Each aliquot was incubated with 25 µL HDAC assay buffer containing 0-200 mM sodium acetate (Table A.3-A.9) for 15 minutes at 37 ˚C with shaking. The deacetylase activity was determined as described in section 2.5.16. The percent deacetylase activity was determined by normalizing the fluorescence signal at each concentration to the no acetate control for each mutant (no acetate=100%) and standard errors from at least four independent trials are shown in the appendix (Table A.3-A.9).

Chapter 3

Introduction

3.1: Efforts towards the first HDAC1-'bump hole' inhibitor pair

(Portions of the text in this chapter were reprinted or adapted with permission from Weerasighe S.V., Wambua M., and Pflum M.K (2010) A Histone dependent screen in Yeast, *Bioorg. Med. Chem., 18, 7586-7592.*)

Overexpression of one or more histone deacetylase (HDAC) proteins is observed in many cancers (Chapert 1, section 1.5). Unfortunately, it is still unclear which HDAC isoform(s) are involved in cancer formation. Understanding the involvement of each HDAC isoform in cancer is critical to aid in the design of isoform selective inhibitors. Use of HDAC inhibitors has been shown to reduce malignancies but, unfortunately, most HDAC inhibitors interact with all or most of the eleven known human isoforms. With FDA approval of the HDAC inhibitors FK-228 and suberoylanilide hydroxamic acid (SAHA) for the treatment of cutaneous T-cell lymphomas, the discovery of more HDAC inhibitors is a promising area of cancer research. Consequently, various HDAC inhibitors are in different phases of clinical trials to treat cancer [62].

HDAC1 is an attractive target for anti-cancer drugs (see chapter 1, section 1.5). HDAC1 regulates the cell cycle, cellular proliferation and development, key events that can lead to cancer development if aberrant. HDAC1-deficient mouse embryonic stem cells deciphered the dominant role of HDAC1 in growth, development and cellular proliferation [54]. Specifically, deletion of HDAC1 resulted in embryonic lethality at E10.5 in mice, which was attributed to severe defects in proliferation and retarded growth [54]. The observed reduction in proliferation correlated with the upregulation of cyclin-dependent kinase inhibitors p21 and p27 and an overall reduction in deacetylase activity. Importantly, loss of HDAC1 led to induction of HDAC2 and 3, but both isoforms were unable to compensate for the HDAC1 deletion, suggesting that HDAC1 plays a critical role in development and cellular proliferation by regulating cell cycle check-point genes. Further, mouse fibroblast cells lacking HDAC1 are anti-proliferative and

exhibit G1-cell cycle arrest accompanied by the up-regulation of CDK inhibitors p21 and p53 [56]. In addition, B-cell development was blocked following HDAC1 deletion, which was accompanied by G1-cell cycle arrest and induction of apoptosis. Combined, these studies showed that HDAC1 regulates G1-S phase transition in the cell cycle by repressing the expression of p21 and p53. Aberrant cell cycle regulation and proliferation are hallmarks of cancer formation, and HDAC1 is thus a potential target for Dace drug design. Currently, no HDAC1 selective inhibitor is yet available.

To achieve better therapies for cancer treatment, it is important to understand the individual functions of each HDAC isoform, which will aid in design of isoform selective HDAC inhibitors. As a first step towards this goal, studies in this chapter are focused on HDAC1. Conventional genetic strategies have revealed that HDAC1 regulates cell cycle, tissue differentiation and development [54, 55]. In addition, the use of mouse knock-out models and siRNA silencing has been useful in understanding the individual functions of other HDAC proteins (see section 3.1). As an alternative to genetic methods, small molecules offer a temporal, time-dependent, and reversible control of gene silencing which is unattainable with genetic methods. *Studies outlined here examine the bump-hole approach, a combination of genetic manipulations and small molecules incubation, to understand the involvement of HDAC1 in cancer formation*. Understanding the role of HDAC1 in cancer formation will aid in developing better cancer therapies targeting HDACs.

3.1.2: The utility of a bump-hole pair:

3.1.2.1: The kinase bump-hole

The bump-hole strategy has been used successfully to design allele-specific inhibitors to probe kinase signaling (Figure 3.1) [78]. Protein kinases have highly conserved domains, making the design of selective highly specific inhibitors very difficult. Chemical biology has allowed the design of allele specific kinases to probe kinase signaling for individual kinases.

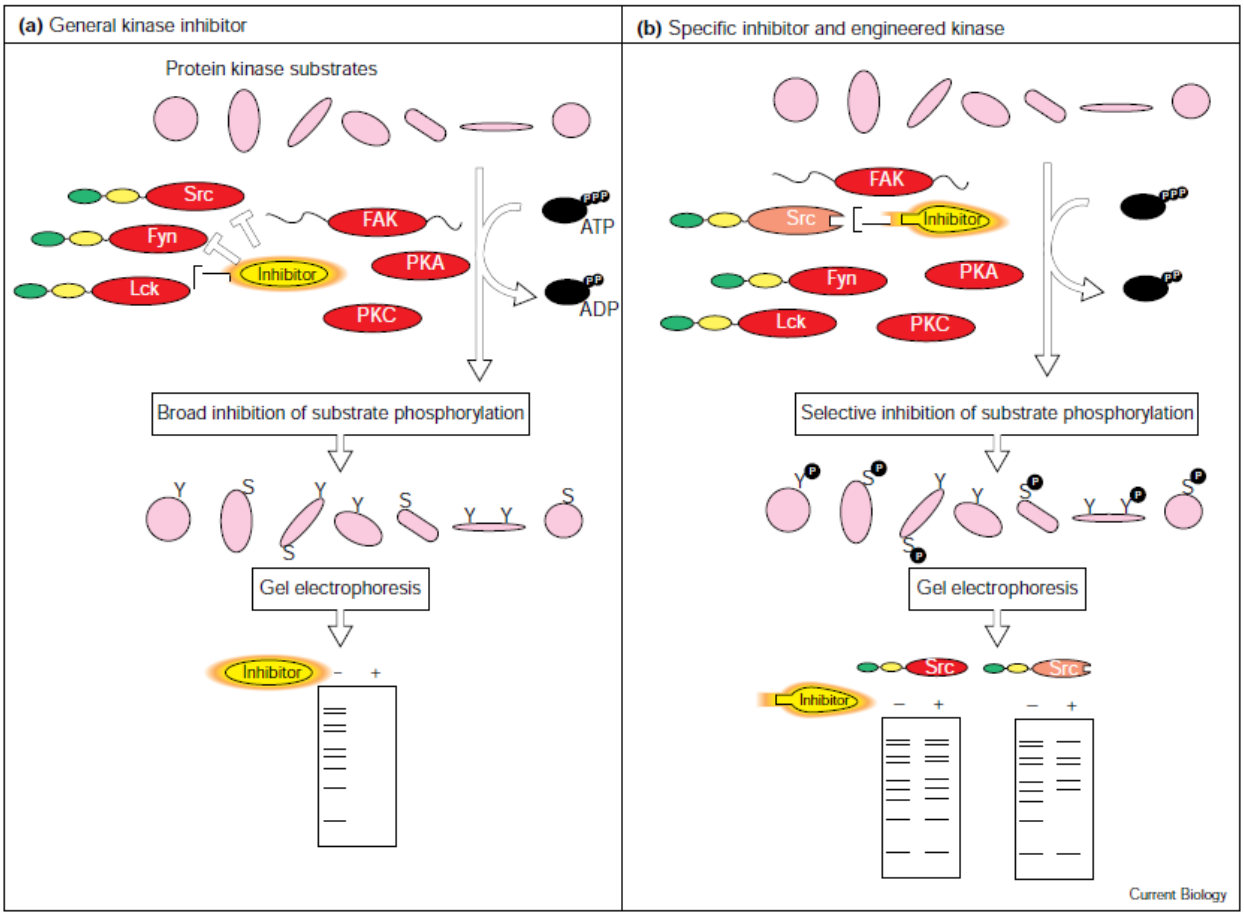

Figure 25: The kinase bump-hole to probe kinase signaling [78]. A) Kinase catalytic domains are highly conserved (red ovals) and therefore the majority of potent kinase inhibitors (red oval) would block the activity of closely related kinase and their pathways regulated by kinase activity. Gel analysis for phosphorylated proteins shows completed blockage of kinase activity by potent inhibitors shown at the bottom.B). Src kinase is engineered to contain a hole that is uniquely complementary to a small molecule inhibitor, allowing for selective inhibition of one kinase as opposed to all kinases. The panel shows gel analysis for phosphorylated proteins with selective blockage of an engineered kinase activity by the modified inhibitor (Pink ovals represent kinase substrates; Y and S represent tyrosine and serine respectively). *Reproduced with permission from Curr. Bio.,1998, 8: 257-266.*

To create a bump-hole, the kinase protein is mutated to contain a hole and a small molecule inhibitor is modified to contain a bump that is complementary to the hole. A kinase bump-hole study focused on two structurally related Src kinases, v-Src and Fyn, which display 85 % sequence homology in their catalytic domains. A functionally silent threonine to isolecucine mutation for the kinase of interest was created in the active site to give rise to a unique pocket that could accommodate a bumped adenosine mimic inhibitor [78]. Importantly,

the ATP mimic inhibited the engineered kinase more potently than the wild type or other non-Src family kinases (>100-fold selectivity). Treating NIH3T3 fibroblasts transfected with the engineered v-Src kinase with the adenosine-mimic inhibitor blocked tyrosine phosphorylation; this phenotype was not observed with the wild type kinase. To further demonstrate selective inhibition of the engineered v-Src kinase variants by a bumped ATP mimic, mammalian cellular transformation by the Rous sarcoma virus, which is dependent on v-Src activation, was determined. NIH3T3 cells expressing engineered v-Src, but not the wild type v-Src, exhibited flat cell morphology upon treatment with the adenosine mimic inhibitor; this morphology is attributed to reversal of cellular transformation. Importantly, the engineered Fyn kinase with a mutation at a similar position was selectively inhibited by the same adenosine-mimic inhibitor, demonstrating that the bump-hole strategy can be extended to other kinase families.

Other such bump-hole studies have been done in recent years. For instance, mutation of the highly conserved phenylalanine 338 to glycine in the active site of the cyclin-dependent kinase Cdc28 (CDK1) creates a unique ATP-mimic inhibitor binding pocket in [79]. The smaller glycine residue acts as a gate keeper to allow for bulkier ATP analogs to access the active site and sensitizes Cdc28 to specific inhibitors. The allele-sensitive Cdc28 was used to understand the biology of budding yeast. Specifically, inhibiting the mutant Cdc28, but not the wild type enzyme, *in vivo* caused pre-mitotic cell cycle arrest and thereby facilitated a functional characterization of this kinase [79]. A different study focused on the *Toxoplasma gondii* calcium-dependent protein kinase 1 (TgCDPK1) [80]. Unlike other protein kinases in *T. gondii*, the presence of a glycine residue at the gate-keeper position renders TgCDPK1 sensitive to pyrazolopyrimidine-derived inhibitors and mutating the glycine to a methionine residue leads to insensitivity [80]. Specific inhibition of TgCDPK1 revealed that TgCDPK1 controls calcium-dependent secretion of specialized organelles, the micronemes, which blocks parasite motility, host-cell invasion and egress [80]. These observations were recapitulated using conditional knock-out models as well as expression of a resistant mutant kinase or other *T. gondii* protein

kinases [80]. A recent development was reported in 2012 [81]. In this study, the methionine residue at the gatekeeper position of calcium-dependent protein kinase 3 (TgCDPK3) was mutated to glycine and thereby rendered sensitive to a pyrazolopyrimidine-derivative inhibitor (PPI). Inhibiting the allele-specific TgCDPK3 with PPI derivatives demonstrated that TgCDP3 is essential for parasite egress but not host invasion or motility [81]. These combined studies demonstrate the successful use of allele-specific kinases along with enlarged inhibitor compounds with increased potencies for functional characterization of closely related protein kinases in *T. gondii.*

3.1.2.2: HDAC1-inhibitor bump-hole

Allele-specific kinase inhibitor pairs have been used to understand kinase signaling and biological relevance (section 3.1.2.1). Similar to kinases, an allele specific HDAC1-inhibitor pair would be useful for understanding HDAC1 biology. Importantly, the bump-hole is a great alternative to the development of isoform selective HDAC inhibitors, in order to explore HDAC1 biology.

A functional characterization of the role of HDAC1 in cancer can be conducted using the bump-hole strategy in cell based assays (Figure 3.2). Our proposition is that HDAC inhibitors (HDACi) can be modified to contain a steric bump which is accommodated by a mutant HDAC1 with a complementary hole (Figure 3.2A). Importantly, the modified HDACi must be excluded from binding the wild type HDAC1 (Figure 3.2B). The HDAC1-inhibitor bump-hole pair can be used to study the expression profiles of cancer related genes influenced by HDAC1.

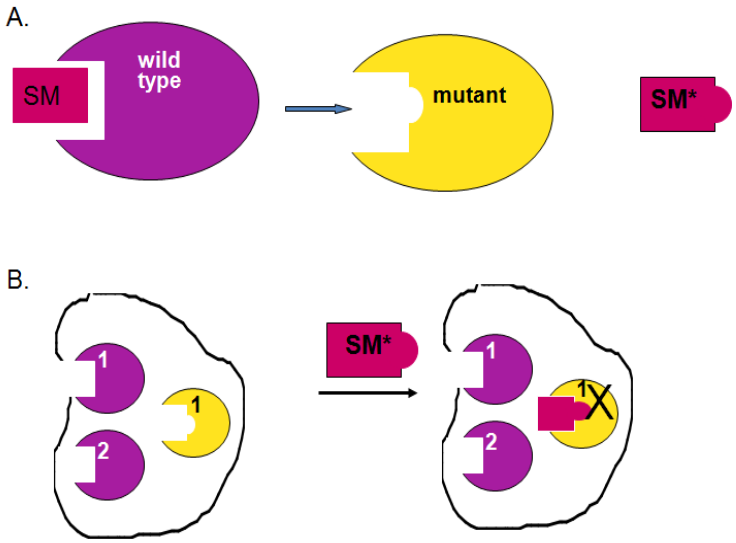

Figure 26: A cartoon showing the rationale of the bump-hole approach. (A) Wild-type HDAC1 is mutated to contain a hole. A small molecule inhibitor is modified to contain a bump. The bumped inhibitor fits into the hole of the mutant but not the wild type. B) In a cellular context, the modified inhibitor analogue inhibits the mutant HDAC1 but not the wild type or the other HDAC isoforms.

The HDAC1-inhibitor bump-hole pair is summarized in Figure 3.3. The wild type HDAC1 is knocked down using siRNA (Figure 3.3B). The active HDAC1 mutant containing a 'hole' is expressed (Figure 3.3C) at the same time that the wild type HDAC1 is knocked down by siRNA. A small molecule inhibitor analogue is used to inhibit the mutant but not the other HDAC isoforms (Figure 3.3D). The expression profile of cancer related genes influenced by HDAC1 alone but not the other HDAC isoforms is determined by comparing the results from panels C and D. Further, inhibiting all HDAC isoforms can be done using a pan-HDAC inhibitor (Figure 3.3E or F) and comparative studies for expression profiles gives the cancer related genes influenced by all the other HDAC isoforms but not HDAC1.

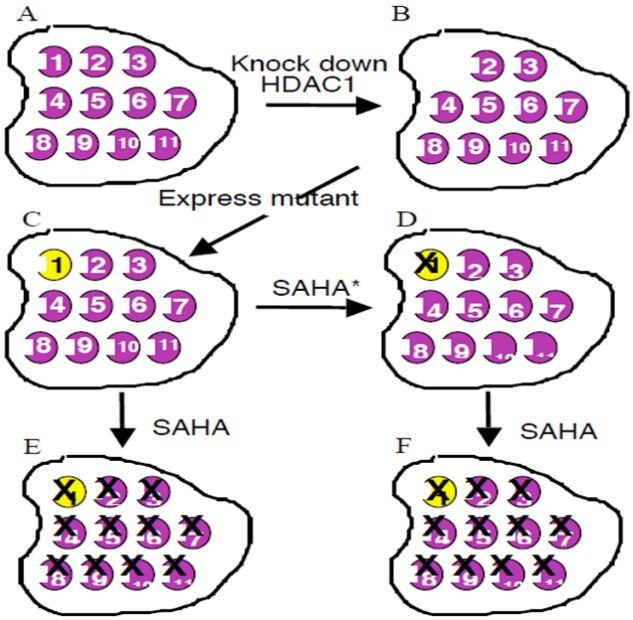

Figure 27: Dissecting the individual functions of HDAC1 using the bump-hole strategy. siRNA is used to knock-out HDAC1 (B). The engineered HDAC1 mutant is expressed (C). Cells are treated with a bumped-inhibitor analogue which selectively inhibits the mutant HDAC1 but not the other HDAC isoforms (D). Pan-HDAC inhibitor is introduced to inhibit all

3.1.2.3: Approaches to obtain an HDAC1-inhibitor bump-hole pair

Unfortunately, the creation of active HDAC1 mutants for use in the bump-hole has been challenging (Chapter 2). With over 80 HDAC1 mutants characterized so far in the Pflum lab, only the E98A mutant was catalytically active, making it challenging to proceed with the bump-hole project (Chapter 2, figure 2.7). As an alternative, we envisioned creating combinations of several point mutations, which might restore catalytic activity. This approach is only feasible in the more tractable yeast system, which is easier to manipulate. HDAC1 is homologous to the yeast Rpd3 protein and therefore active mutations in Rpd3 are often conserved in HDAC1. Our second approach for creating a bump-hole pair was to screen the active HDAC1E98A protein against libraries of SAHA analog compounds produced in the Pflum lab. Both of these strategies are discussed in this chapter.

3.2: Results

3.2.1: Development of an HDAC dependent yeast gene reporter screen

Rpd3, the yeast histone deacetylase shares 60% sequence identity with its human HDAC1 homologs and is a component of the Sin3 corepressor complex [82]. However, unlike HDAC1, which regulates growth, development, cell cycle and proliferation, the Rpd3-Sin3 repressor complex negatively regulates genes involved in potassium transport, meiosis, phospholipid metabolism, phosphate metabolism and cell-type specificity [82]. The high sequence similarity between Rpd3 and class I HDACs makes Rpd3 an ideal model to study class 1 proteins in the more tractable yeast system. Therefore, it is probable that active mutants obtained in Rpd3 will be transferable to human HDAC1. A major challenge, however, is to have a functional screen for selecting active mutants from a large mutant library. This issue necessitated the development of a yeast reporter screen dependent on Rpd3 activity.

A high throughput screen capable of testing a library of Rpd3 mutants for activity is ideal. The current fluorimetric assay used in chapter 2 is sensitive and is the most widely used in the field. The assay is dependent on fluorophore-labeled peptide substrate and has been widely used for mutant and inhibitor studies. In addition, several other assays developed in the past have relied on radio-labeled acetylated histones or peptide substrates [7]. Unfortunately, the HDAC is usually sourced from HeLa nuclear extracts and is therefore disadvantageous in inhibitor screens because the inhibition profile is a reflection of the overall HDAC activity and cannot be attributed to a specific HDAC isoform. Efforts to purify individual isoforms for selectivity studies are hindered by the fact that bacterially expressed HDACs are inactive, presumably due to the lack of associated proteins, which are needed for catalytic activity. As an alternative, baculovirus-expressed HDAC sources, which have shown 70% reduction in enzymatic activities, have also has been explored but this loss in deacetylase activity limits their use. In addition, these assays are cost prohibitive and would therefore not be ideal for a high

throughput, library screening. The development of a high throughput cost effective screening assay will be ideal for identification of active mutants and inhibitor screen. Further, the histone deacetylase screen developed in Rpd3 is dependent on native substrates unlike the commercial kits.

3.2.1.1: Design of a yeast gene reporter screen

The Rpd3 dependent yeast gene reporter screen utilizes the *LACZ* gene product β-galactosidase, which cleaves 5-Bromo-4-chloro-3-indolyl-β-D-galactopyranoside (X-Gal), giving a blue color, or 2-Nitrophenyl β-D-galactopyranoside (ONPG), giving a yellow color (Figure 3.4A). These color changes can be monitored to assess HDAC activity. Rpd3 is expressed as a LexA fusion protein; LexA recruits Rpd3 to the LexA DNA binding promoter region upstream of the *LACZ* gene. The yeast FT5ΔRpd3 strain, with a deletion of the endogenous Rpd3, is transformed with reporter plasmid and the Rpd3 expression construct. Transformation of the *LACZ* reporter alone gives basal *LACZ* expression under a constitutively active promoter and results into a colored cell (Figure 3.4A). Expression of Rpd3-LexA together with the reporter results in recruitment of Rpd3 to the LexA DNA binding region in the promoter region. Rpd3 will deacetylate nucleosomal DNA turning off *LACZ* gene transcription. Lack of β-galactosidase activity then yields a white cell (Figure 3.4.B). A catalytically inactive mutation in Rpd3 or inhibition of the wild type Rpd3 leaves DNA acetylated, *LACZ* gene transcription is turned on and the cells are colored (Figure 3.4C). The *LACZ* gene reporter can screen Rpd3 mutants for activity or inhibitor selectivity.

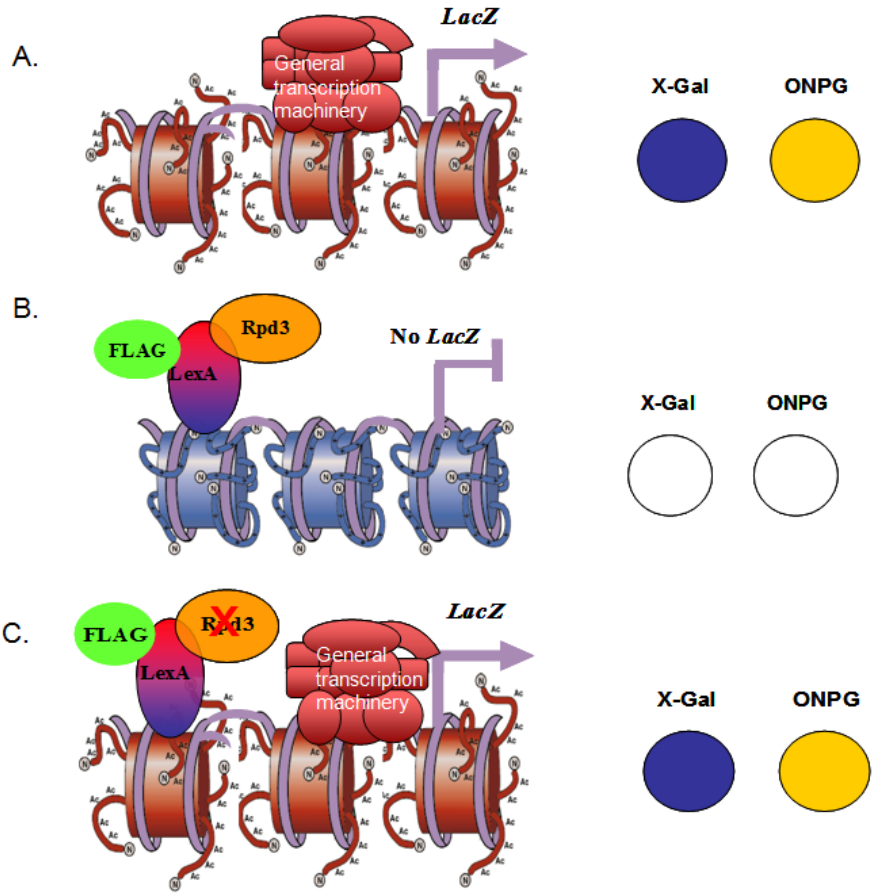

Figure 28: Schematic diagram of yeast based *LACZ* gene reporter screen. (A) When the *LACZ* reporter is transformed alone, the *LACZ* gene under the control of a constitutively active promoter, expresses β-galactosidase (β-gal) which hydrolyzes the 5-Bromo-4-chloro-3-indolyl-β-D-galactopyranoside substrate (X-Gal), resulting a blue color, or the 2-Nitrophenyl β-D-galactopyranoside substrate (ONPG), resulting in a yellow color. The color changes can be monitored to assess the HDAC activity. (B) When the catalytically active Rpd3 LexA fusion is expressed and recruited to the reporter, the nucleosomal DNA will be deacetylated and inaccessible to the transcription machinery, causing *LACZ* gene transcription to be turned off and the cells to be white. (C) A catalytically inactive Rpd3 mutant fails to inhibit *LACZ* expression and results in blue and yellow cells. Inhibiting active Rpd3 mutants or wild type with a small molecule will give similar results.

3.2.1.2: Validation of the Rpd3-dependent screen using a qualitative X-Gal agar format

To determine if the yeast screen is suitable for mutant and inhibitor screening, the assay was developed and optimized. The *LACZ* reporter plasmid, pJK1621 (obtained from Prof. Struhl), was transformed into the *FT5 Δrpd3::HIS3* yeast strain (wherein the endogenous *rpd3* is deleted) with or without the Rpd3-LexA fusion plasmid (cloned in our lab, see section 3.5.2) [69]. The *β*-galactosidase activity was monitored using X-Gal. The X-Gal assay is a qualitative agar layout that allows for an initial validation of the screen. The *LACZ* reporter alone strain showed basal *β*-galactosidase activity and a resultant blue colored yeast cell (Figure 3.5A). Transforming the *LACZ* reporter together with Rpd3 resulted in low *β*-galactosidase and a white colored cell (Figure 3.5C), suggesting that Rpd3 represses *LACZ* gene expression. As expected, the catalytically inactive Rpd3H150A151A mutant showed low *β*-galactosidase levels that were comparable to the reporter alone and gave a blue colored cell (Figure 3.5 D). Inhibiting Rpd3 with trichostatin A (TSA) resulted in high levels of *β*-galactosidase and a blue color as expected (Figure 3.5F). Endogenous HDAC activity with the *LACZ* reporter alone is negligible as TSA treatment gave similar *β*-galactosidase activities (Figure 3.5B). The solid X-Gal screen is therefore ideal for mutant and inhibitor screens.

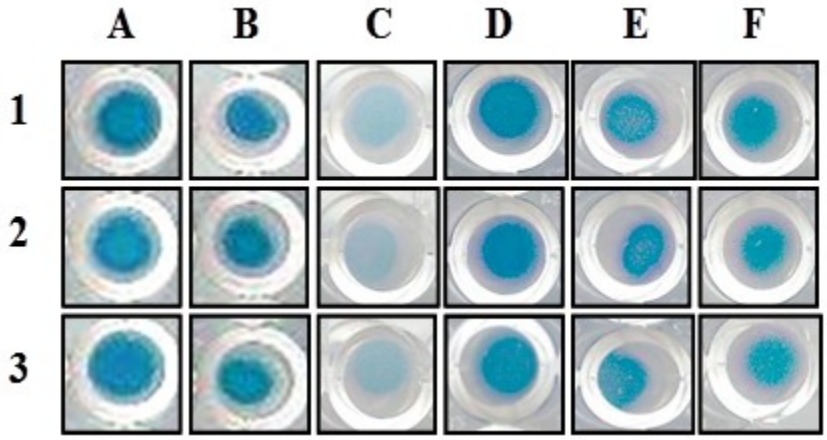

Figure 29: The Rpd3-dependent gene reporter screen (data obtained by Sujith Weerasighe) [83]. *LACZ* reporter plasmid, pJK1621, was transformed with or without wild type Rpd3 or catalytically inactive Rpd3 mutant as LexA-FLAG fusions, into *FT5 Δrpd3::HIS* yeast strain. Transformed cells were grown with or without TSA for 48 h in 96 well format and were overlaid with X-Gal substrate. The *β*-galactosidase activity was observed qualitatively by blue color formation after 3h of X-Gal incubation. Columns represent (A) *LacZ* reporter alone, (B) *LacZ* reporter + TSA 100 μM, (C) *LacZ* reporter + Wild type *Rpd3*-LexA, (D) *LacZ* reporter + *Rpd3*-LexA mutant, (E) *LacZ* reporter + wt *Rpd3*-LexA +100 μM TSA and (F) *LacZ* reporter + *Rpd3*-LexA mutant + 100 μM TSA. The experiments were carried out in triplicate (rows 1, 2 and 3). *Reproduced with permission from Bioorg. & Med. Chem., **2010**, 18, 7586-7592.*

3.2.1.3: The *LACZ* gene reporter assay can be quantified

A quantification of Rpd3 dependent repression of *β*-galactosidase activity was further determined using ONPG as a substrate. The liquid format makes it possible to quantify the amount of Rpd3 deacetylase activity by measuring the absorbance of ONPG hydrolysis product at 420 nm. The *LACZ* reporter plasmid alone gave high levels (2.4-fold compared to wild type which was normalized to 1) of β-galactosidase and is consisted with X-Gal results (Figure 3.6, column 1 reflecting basal *LACZ* expression levels from a constitutive promoter. Rpd3-LexA, together with the *LACZ* reporter resulted in loss in *β*-galactosidase activity, suggesting that Rpd3 repressed *LACZ* expression (Figure 3.6, column 3). However, this suppression was reversed by TSA treatment and resulted in 2.5-fold increase in *β*-galactosidase activity. The inactive Rpd3 H150AH151A mutant was unable to suppress *LACZ* expression and resulted in a 2.4-fold increase in *β*-galactosidase activity (Figure 3.6, column 5). Importantly, the *LACZ* reporter alone gave similar β-galactosidase activity with and without TSA, suggesting that endogenous HDAC activity is negligible, as previously observed with the X-GAL assay (Figure

3.6 lane B). The combined results indicate that both the qualitative X-Gal and quantitative ONPG assays are dependent on the activity of Rpd3-LexA, making the yeast screen ideal for identifying active mutants as well as inhibitor screen.

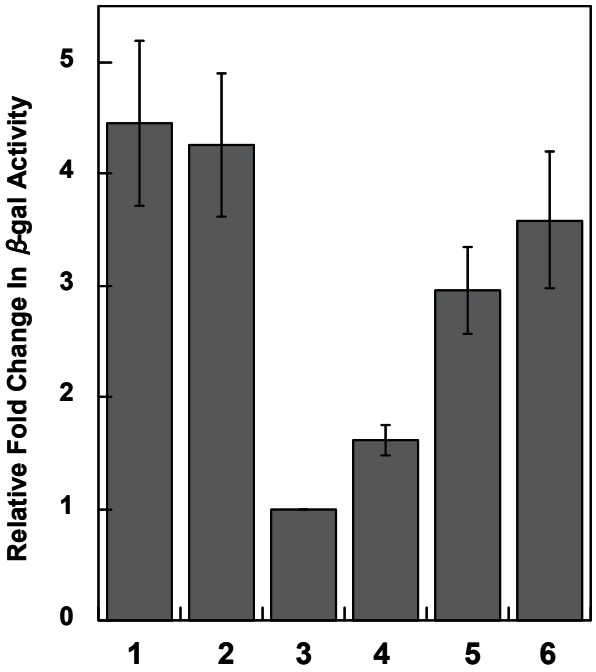

Lac Z Reporter	+	+	+	+	+	+
TSA 100 µM		+		+		+
Wt Rpd3			+	+		
Rpd3 mutant					+	+

Figure 30: Quantitative inhibition of *Rpd3* activity; data obtained by Sujith Weerasighe [83]. *LacZ* reporter plasmid, pJK1621, was transformed with or without wild type Rpd3 or catalytically inactive Rpd3 mutant as LexA-FLAG fusions into *FT5 Δrpd3::HIS* yeast strain. Transformed cells were grown with or without TSA for 6h at 30 °C and β-galactosidase activity was measured quantitatively using ONPG and absorbance at OD_{420}. Relative fold change in *β-galactosidase* activity was calculated with respect to wild type Rpd3 and mean of three trials is shown with standard error (as error bars). Relative fold changes observed in each trial are summarized in Appendix B (Table B.1). *Reproduced with permission from Biorg. & Med. Chem., **2010**, 18, 7586-7592.*

3.2.1.4: Screening yeast libraries for active mutants

The *LACZ* gene reporter assay was used to screen a 15,000 member library (see experimental section 3.5.1 and 3.5.2) previously generated by Sujith Weerasighe (unpublished work). The amino acids F214, F215, and L281 positions were mutated to create this Rpd3 library. These amino acids are located near the solvent exposed region of the enzyme's active site and their contributions to the catalytic activity of Rpd3 has never been reported (F214, F215 and L281, are similar to F204, F505 and F271 in HDAC1 respectively and are located further from the active site (Chapter 2, figure 2.6). We envisioned that random mutagenesis would create a combination of mutants that could be active; loss of activity as a result of a mutation of one amino acid could be compensated for by another amino acid in the same mutant, therefore increasing the chances of creating an active mutant for the bump-hole approach. In order to screen the 15,000 mutants for activity using the yeast gene reporter assay as described in section 3.2.1.1, mutants were transformed into the *FT5ΔRpd3::HIS* strain cell line together with the *LACZ* gene reporter plasmid, pJK1621. Transformed yeast cells were subjected to blue-white screening as discussed in section 3.5.6. A representative result of the X-Gal blue-white screen is shown in Fig. 3.7 (white colonies are shown by arrows). The expectation was that cells containing an active Rpd3 mutant would repress β-gal expression and color change. It was necessary to do an initial selection screen to identify possible hits for further evaluation using the quantitative ONPG assay and fluorescence assay. One hundred white colonies were picked to move forward to further screening.

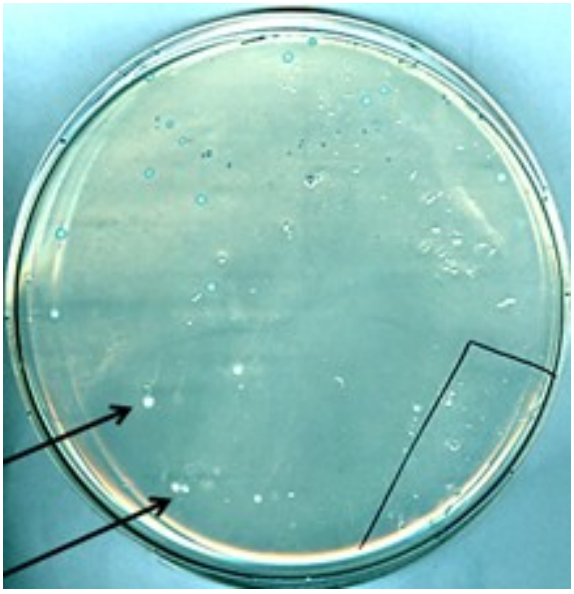

Figure 31: *LacZ* gene reporter screen for active mutants (X-gal overlay assay; Blue-white screen). Rpd3 mutant expression plasmids were transformed into the *FT5ΔRpd3::HIS* strain cell line. Yeast cells were grown for 3 days and overlaid with X-Gal solution and then incubated for 2 hours. Development of blue color was monitored visually. The arrows show white mutants that are thought to be 'active mutants' from this screen.

3.2.1.5: Quantification of β-galactosidase activity for white mutants identified in X-Gal screen

The ONPG screen allows for quantification of deacetylase activity for white colonies and is also a secondary confirmatory assay of the quantitative X-Gal plate assay. To confirm the deacetylase activities of colonies from the blue-white screen using X-Gal (Section 3.2.1.4), colonies were retrieved from the agar, re-grown for 2 days in liquid medium and the ONPG assay was applied as described in experimental section 3.5.7. A representative screen for ten white colonies (out of the hundred selected) is shown in figure 3.8. The wild type Rpd3 repressed β-galactosidase expression and showed low levels of activity as expected (Figure 3.8, column 1, positive control). The inactive Rpd3H150AH151A double mutant was unable to repress *LACZ* expression and resulted into a 4.5-fold increase in β-galactosisade activity (column 2, negative control). Out of the ten mutants screened in this representative assay, mutants 3 and 7 showed low β-galactosidase activities (Figure 3.8, columns 3 and 10). The rest of the mutants showed high β-galactosidase activities (Figures 3.8, columns 1, 2 and 4-9)

suggesting that these mutants do not repress *LACZ* expression. In total, the ONPG assay validated 60 colonies which were screened for activity using a fluorimetric assay (Section 3.2.1.6).

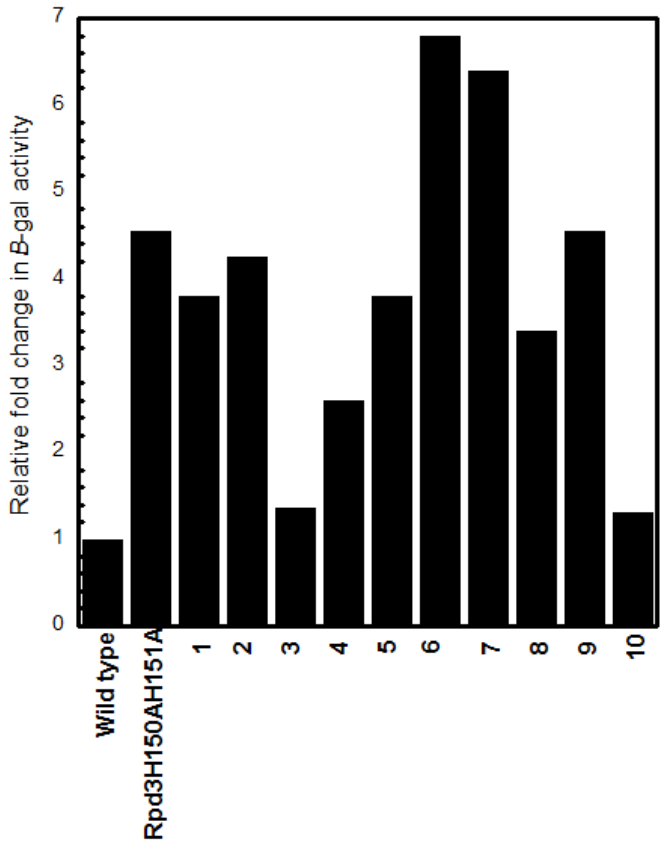

Figure 32: *LacZ* gene reporter assay screen for active mutants (ONPG assay). *LacZ* reporter plasmid, pJK1621, was transformed with wild type Rpd3 or a catalytically inactive Rpd3 mutant or the Rpd3 library plasmid DNA as LexA-FLAG fusions into the *FT5 Δrpd3::HIS* yeast strain. Transformed cell were grown overnight at 30 °C. β-galactosidase activity was measured quantitatively. Relative fold change in β-galactosidase activity was calculated with respect to wild type Rpd3 and the mean of two trials is shown (no error bars). Mutants 3 and 10 are thought to be active mutants. While data from a single trial is shown here, the relative fold change observed in two independent trials is summarized in Appendix B (Table B.2).

3.2.1.6: HDAC assay for identified mutants

In order to validate the activity of the 60 mutants form the ONPG screen, the commercially available kit, Fluor-de-Lys (Biomol), was used to confirm HDAC activity (Appendix B.3). A representative set of results is shown in Figure 3.9. The wild type Rpd3 has high deacetylase activities (set to 100%) whereas the mutant Rpd3H150AH151A mutant has low deacetylase

levels (20%) compared to wild type (Figure 3.9). Of the five mutants tested, mutants 3 and 6 maintained high deacetylase activities at 93% and 85% respectively (Figure 3.9, columns 3 and 6). The three other mutants had low deacetylase levels (10-30%) comparable to the Rpd3H150AH151A control (Figure 3.9, columns 4, 5 and 7). Using the HDAC assay, 19 of the 60 mutants were confirmed as active mutants; these were sequenced to determine the presence and identification of any mutations.

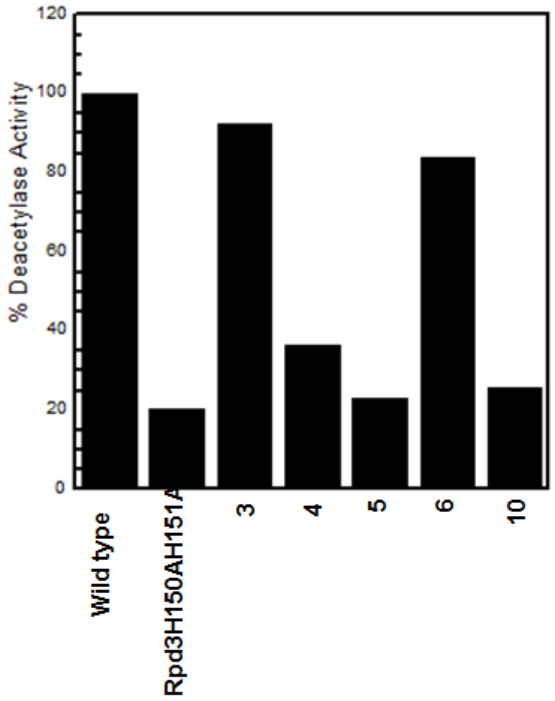

Figure 33: Representative results from an HDAC assay of active mutants identified using the *LacZ* gene reporter screen. Rpd3 wild-type, Rpd3 H150A151A mutants or the validated mutant(s) were expressed as FLAG-tagged fusion proteins and were immunoprecipitated with anti-FLAG-agarose resin. The immunoprecipitated protein were used in fluorescence HDAC assays .The percent activity is compared with that of the wild-type protein (100%). The deacetylase activities for each trial are summarized in Appendix B (Table B.3).

The sequence data for all the isolated plasmids showed wild type sequence (Figure 3.10). The data from this project reinforces the fact that it is very difficult to create active Rpd3 mutants and is consistent with our observations with human HDAC1 (Chapter 3). As an alternative to identifying a HDAC1-inhibitor bump hole pair, our attention turned to screening the only active mutant for HDAC1, E98A against SAHA analogs available in the Pflum lab.

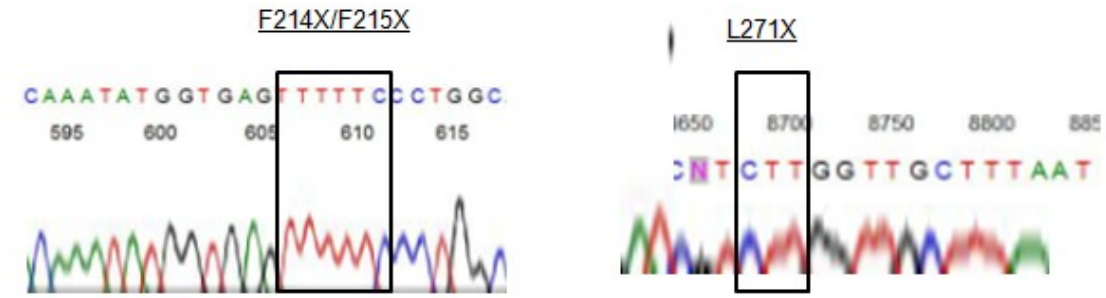

Figure 34: A representative chromatogram of an active mutant. The chromatogram shows the sequence data obtained for one mutant confirmed from the HDAC flourimetric assay. The other 19 mutants also had the wild type sequence. The three amino acid residues are boxed off and shown on top of each chromatogram.

3.3: Development of a high throughput ELISA assay to screen small molecules for bump-hole experiments

To screen a library of small molecules for selectivity against the active HDAC1E98A protein, it was necessary to develop an assay that is high throughput and inexpensive. ELISAs are luminescence-based assays that utilize luciferin, which is converted to oxyluciferin (Figure 3.11). Briefly, secondary antibody coated plates (G Bioscience) were incubated with a monoclonal anti-FLAG antibody. Next, lysates from HDAC1-FLAG or the mutant fusion protein were added and bound to the FLAG epitope. The deacetylase activities of the bound wild type or mutant protein were monitored by release of luciferin, which was converted to oxyluciferin by luciferase in the presence of Mg^{2+} and ATP. The amount of luminescence is directly proportional to deacetylase activity. Active mutant(s) exhibit high luminescence activity, comparable to wild type. A small molecule inhibitor of HDAC1 activity should abolish luminescence. Using this assay, we set out to screen E98A against all SAHA analogs produced in our lab.

Figure 35: Plate based ELISA assay to determine the deacetylase activity of wild type or active HDAC1 mutant(s). Secondary antibody coated plates (G bioscience) were incubated with α-flag antibodies and lysates from HDAC1-FLAG or mutant protein(s). The deacetylase activity of the HDAC1 or the mutant bound to the plate cleaves the acetyl group from the luciferin peptide substrate. The developer contains trypsin, which cleaves the peptide bond between luciferin and the lysine of the deacetylated product. Luciferin is converted to oxyluciferin (star with GLOW) by luciferase in the presence of Mg^{2+} and ATP. Upon deacetylation, luciferin was released and is converted to oxyluciferin. The amount of luminescence is directly proportional to the deacetylase activity of each tested protein.

3.3.1: ELISA assay is ideal for screening HDAC inhibitors

To assess whether the plate-based ELISA assay was suitable for screening HDAC inhibitors against E98A for a bump-hole design, the HDAC inhibitor trichostatin A (TSA) was tested and the amount of deacetylase activity was measured. In addition; the deacetylase activities of the catalytically active E98A mutant in the presence and absence of TSA were also determined. Importantly, the deacetylase activity of the negative control (no protein) was comparable to the assays with HDAC1 and TSA. Wild type HDAC1 and the active E98A mutant showed high deacetylase activities at 100 and 115%, respectively (Figure 3.12, columns 3 and 4). Importantly, inhibiting HDAC1 or E98A with TSA reduced deacetylase activities to 25% and 28% respectively (Figure 3.12, columns 5 and 6). The no protein control and H141A had low deacetylase activities even without TSA (Figure 3.12, columns 1 and 2). These combined

results show that the ELISA assay is suitable for screening small molecules against HDAC1 and the E98A mutant for selectivity in order to create a bump-hole pair.

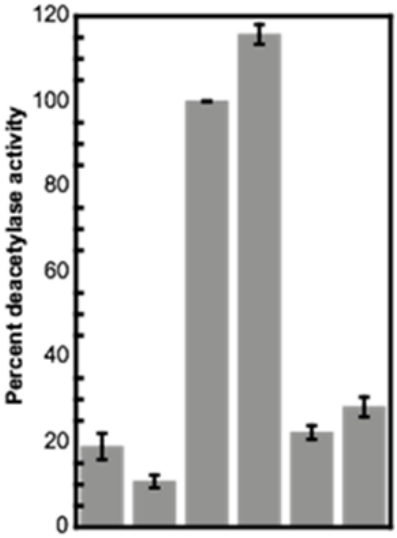

No Protein	+	-	-	-	-	-
Wild Type(HDAC1)	-	-	+	-	+	-
H141A	-	+	-	-	-	-
E98A	-	-	-	+	-	+
TSA 100nM	-	-	-	-	+	+

Figure 36: Deacetylase activities of wild type or mutant proteins were inhibited by TSA. HDAC1 wild-type or mutants were expressed as FLAG-tagged fusion proteins and were captured on α-FLAG bound to secondary antibody coated plates. The deacetylase activity of immunoprecipitated protein was determined using the luminescence assay. The percent activity is compared with that of the wild-type protein (100%) with standard errors shown. The deacetylase activities for each trial are summarized in Appendix B (Table B.4).

3.3.2: Screening SAHA- analogues to create the first HDAC1-inhibitor bump-hole pair

C-2, C-3, C-6, and N-SAHA analogues have half-maximal inhibition activities in the micromolar range against HeLa nuclear extracts. The ideal bump-hole inhibitor would have poor activity against wild type proteins [84-86]. These SAHA analogues contain steric bumps and therefore have the potential to inhibit mutant but not wild type HDACs. Each SAHA analog was screened against HDAC1E98A using the ELISA assay.

3.3.2.1 Screening C-2 SAHA analogs

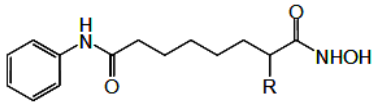

C-2-SAHA analogs

C-2-SAHA analogues, previously synthesized in the Pflum lab have IC_{50} values of 75-450 μM against HeLa lysates (Table 3.1) [84]. Attaching a bulky substituent at the C-2 position leads to a dramatic decrease in potency compared to the parent SAHA inhibitor (500-5000 fold decrease), making this class of bumped SAHA analogues potential candidates.

Table 3.1: HDAC inhibition by SAHA C-2 analogs

Compound	R	IC_{50} (μM)[a]
SAHA		0.090(0.004)
C2-a	methyl	134(6)
C2-b	ethyl	447(15)
C2-c	propyl	151(3)
C2-d	butyl	74(3)
C2-e	pentyl	45(6)
C2-f	hexyl	59(3)
C2-g	allyl	142(8)
C2-h	propargyl	87(3)
C2-i	benzyl	226(12)

[a]Values are the means of three experiments with standard error given in parentheses [84]. Structures of SAHA analogs are summarized in Appendix C, Table C.1.

The ELISA assay was used to test the C-2 SAHA analogs mutant for selectivity towards the active HDAC1E98A. We hypothesized that the glutamic acid at position 98 in HDAC1 acts as gate keeper and a mutation to alanine would allow for bulkier substituents to access the active site, as had been observed with kinases [79-81]. Because all C-2 SAHA analogs display half-maximal inhibitions in the micromolar range (Table 3.1), all analogues were included in an initial single screen to identify compounds for further evaluation.

As shown in Table 3.1, most C-2-SAHA analogs inhibited the wild type and the active HDAC1E98A mutant to the same extent, with the exception of the C-2-pentyl and C-2-hexyl

SAHA analogs. Interestingly, the C-2-hexyl and pentyl SAHA analogs, with the longest substituents, were more potent against the E98A mutant (39% and 55% remaining activity, respectively) compared to HDAC1 (95% and 98% activity, respectively). These data suggest that the E98A mutant could be allowing the bulkier pentyl and hexyl substituents to enter the active site and possibly gain access to the 14 Å channel. The observed selectivity of C-2-hexyl and C-2-pentyl SAHA for E98A encouraged us to determine the IC_{50} values for the two SAHA analogs

Table 2.2: Percent deacetylase activities for wild type or HDAC1E98A treated with C-2-SAHA analogs at indicated concentrations

	C-2-allyl (20μM)	C-2-benzyl (60μM)	C-2-ethyl (450μM)	C-2-hexyl (30μM)	C-2-methyl (40μM)	C-2-n-propyl (150μM)	C-2-propargyl (25μM)	C-2-pentyl (15μM)
HDAC1 (% Activity)[a]	23	33	30	95	44	30	16	98
E98A (% Activity)[a]	25	39	60	39	47	49	2	55

.[a]Values were determined from a single screen.

An ideal HDAC1 bump-hole pair, with the active E98A mutant and a SAHA analog, should demonstrate at least one hundred-fold lower IC_{50} compared to wild type [78]. To determine whether C-2-pentyl or C-2-hexyl SAHA showed this level of selectivity towards the E98A mutant over wild type, the half-maximal inhibition of analog was determined using the ELISA assay as described (Figure 3.11). C-2-hexyl-SAHA had an IC_{50} value of 34.5 μM and 171 μM against the E98A and HDAC1, respectively (Figure 3.13). The half-maximal inhibition of the C-2-pentyl-SAHA against HDAC1 and E98A was 18.9 μM and 100 μM, respectively (Figure 3.14). These observed 5-fold changes in IC_{50} values are not significant enough for a bump-hole pair.

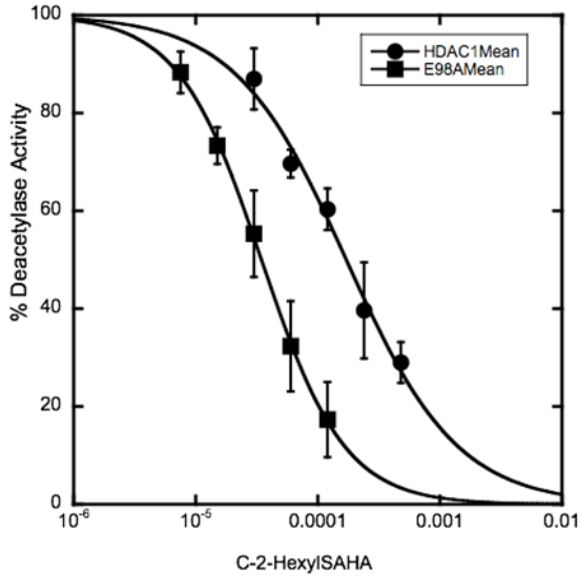

Figure 37: Deacetylase inhibitory activities of C-2-hexyl-SAHA. HDAC inhibitory activities of the C-2hexyl-SAHA measured against HDAC1 (circles) or E98A (open squares). Mean percentage deacetylase activities of three independent trials with standard errors are shown (as error bars). Deacetylase activities of individual trials are summarized in Tables B.4 and B.6 in appendix B.

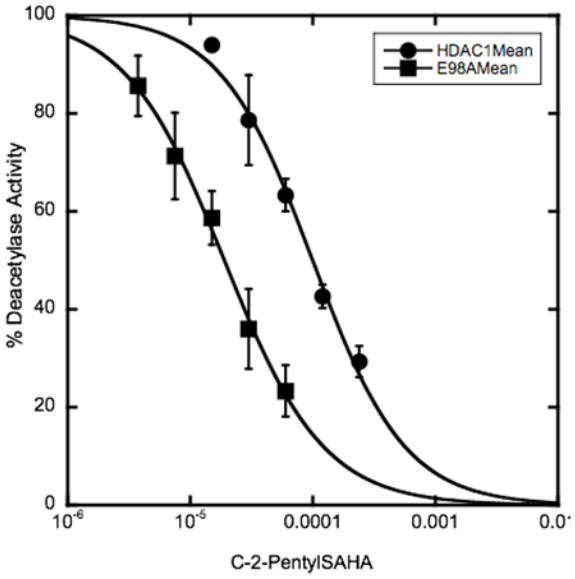

Figure 38: Deacetylase inhibitory activities of C-2-pentyl-SAHA. HDAC inhibitory activities of the C-2-pentyl-SAHA measured against HDAC1 (circles) or E98A (open squares). Mean percentage deacetylase activities of three independent trials with standard errors are shown (as error bars). Deacetylase activities of individual trials are summarized in Tables B.7 and B.8 in appendix B.

3.3.2.2: Screening SAHA analogues functionalized at C-3 position

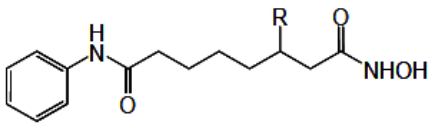

C-3-SAHA analogs

The observation that some C-2 SAHA analogs show selectivity for the active E98A mutant encouraged us to screen a C-3 library of analogs previously synthesized by Sun Ea Choi (see Appendix C, Table 3.2 for structures) [86]. Unlike the C-2 library, C-3 SAHA analogs display half-maximal inhibition in the lower micromolar range (Table 3.3). The decreased (4-2000 fold-decrease) in potency for this class of compounds compared to the C-2 analogs suggests that the C-3 position is less constrained and can be explored for designing isoform selective inhibitors. Similar to C-2 analogs, we hypothesized that bulkier substituents at C-3 would gain access to the active site in the E98A mutant compared to the wild type. An initial screen was done using the ELISA assay to identify hits for further studies (Table 3.2).

Table 3.3: HDAC inhibition by SAHA C-3 analogs

Compound	R	IC_{50} (μM)[a]
SAHA		0.090(0.004)
C3-a	methyl	0.36 (0.05)
C3-b	Vinyl	15(1)
C3-c	Ethyl	32(4)
C3-d	Phenyl	73(8)
C3-e	Butyl	185(14)

[a]Values are the means of three experiments with standard error given in parentheses.

C3-SAHA analogs inhibited both the wild type and the active E98A mutant to the same extent (Table 3.4). Specifically, the bulkier substituent C-3-butyl and C-3-phenyl-SAHA analogs abolished deacetylase activites for both the wild type and E98A enzymes to similar levels (50% versus ~60% respectively). Interestingly, both the C-3-vinyl and C-3-ethyl-SAHA analogs demonstrated a two-fold selectivity for E98A over in HDAC1. Collectively, our results indicate that the C-3 library is equally as potent for the E98A mutant and the wild type. We speculate

that, unlike the C-2-library which showed more preference for the mutant E98A, the C-3-SAHA analogs are unable to access the 14 Å channel as might be the case with the C-2-library. With these results, the analogs were not studied for IC_{50}.

Table 3.4: Percent deacetylase activities for wild type or HDAC1E98A treated with C-3-SAHA analogs at indicated concentrations.

	DMSO (1%)	C-3 butyl (400μM)	C-3 Phenyl (100μM)	C-3 Ethyl (40μM)	C-3 Vinyl (20μM)
HDAC1 (% Activity)[a]	100	49	58	15	17
E98A (% Activity)[a]	100	50	77	32	40

[a]Values were determined from a single screen.

3.3.2.3: Screening SAHA analogues functionalized at the hydroxamic acid nitrogen.

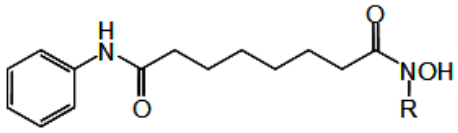

N-SAHA analogs

Our results from the C-2 library screen encouraged us to screen SAHA analogs functionalized at the metal binding moiety. Our hypothesis was that since a long carbon chain in the C-2 library shows preference for the mutants, possibly by accessing the 14 Å channel, the N-library could also access this channel easily since the metal binding moiety is next to the channel. Our previous results from mutagenesis studies indicated that residues in the 14 Å channel are critical for maintaining HDAC1 activity (Chapter 2). Further, selective HDAC1 inhibitors targeting this channel have been created. We thus wondered if E98A would bind N-SAHA analogs (see Appendix C, Table 3.2 for a summary of N-SAHA analogs) with the ability to access the 14 Å channel to allow us to selectively inhibit the mutant over the wild type to generate a bump-hole pair.

Table 3.5: HDAC inhibition by N-SAHA analogs

Compound	R	IC_{50} (μM)[a]
SAHA		0.090(0.004)
N-a	methyl	794 (46)
N-b	Pentyl	153(14)
N-c	Benzyl	293(32)
N-d	Homobenzyl	>250*
N-e	Biphenyl	>250*

[a]Values are the means of three experiments with standard error given in parentheses.* indicates IC_{50} value could not be determined due to solubility problems.

Using the ELISA assay, we screened N-SAHA analogs (all synthesized by Dr. Anton) for ideal candidates for the bump-hole. The HDAC inhibitory activities of the SAHA analogs were measured using the ELISA chemiluminescence activity assay against the HDAC1 and thHDAC1E98A mutant. A single screen was used to determine the potency of the small molecules (Table 3.6).

Table 3.6: Percent deacetylase activities for wild type or HDAC1E98A treated with N-SAHA analogs at indicated concentrations.

	N-methyl (1.6μM)	N-pentyl (1μM)	N-benzyl (80μM)	N-homobenzyl (150μM)	N-biphenyl (50μM)
HDAC1 (% Activity)[a]	117	49	66	57	29
E98A (% Activity)[a]	39	52	50	50	57

[a]Values were determined from a single screen.

With the exception of N-methyl-SAHA, all N-SAHA analogs equally inhibited the mutant E98A and the wild type in the micromolar range (Table 3.6). The half-maximal inhibition for N-benzyl and N-homobenzyl substituents against the mutant and the wild type were 80 μM and 150 μM, respectively. N-biphenyl-SAHA was two-fold more selective for the mutant (29% remaining activity) compared to the wild type (57% remaining activity). N-pentyl-SAHA, whose IC_{50} against HeLa lysates showed more potency against the wild type and the mutant to the same extent. Interestingly, the smallest N-SAHA analog, N-methyl-SAHA, was more selective

for the mutant over the wild type (39% versus 117% remaining activity). The methyl group could form favorable interactions with amino acids in the 14 Å cavity. With these promising results, we further characterized the N-methyl-SAHA analog by determining the IC_{50} value. N-methyl-SAHA had an IC_{50} value of 2.5 μM and 11.5 μM against E98A and HDAC1 respectively (Figure 3.15). This represents a 5-fold selectivity for the mutant over the wild type, which is insufficient bump-hole.

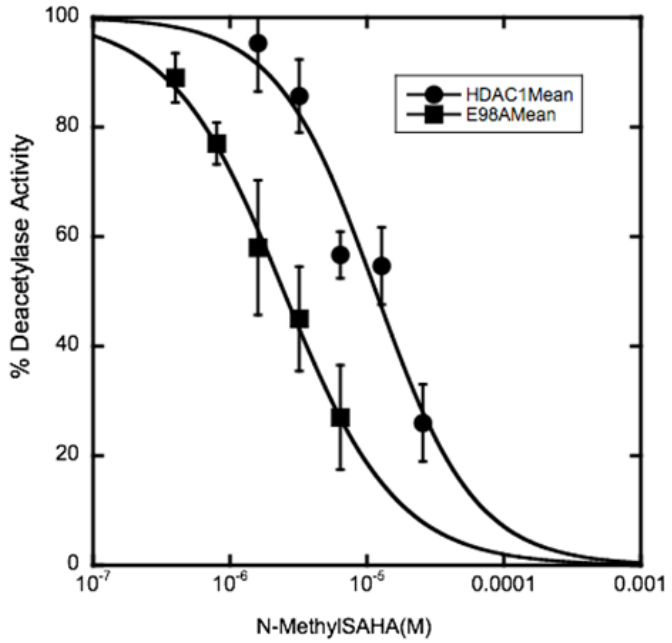

Figure 39: Deacetylase inhibitory activities of N-methyl-SAHA. HDAC inhibitory activities of N-methylSAHA measured against HDAC1 (circles) or E98A (open squares). Mean percentage deacetylase activities of three independent trials with standard error are shown (as error bars). Deacetylase activities of individual trials are summarized in Tables B.9 and B.10 in appendix B.

3.4: Discussion

Identification of isoform selective HDAC inhibitors is necessary to provide better cancer therapies. Understanding the individual functions of each HDAC isoform in cancer formation will facilitate targeted drug design. The crucial function of HDAC1 in growth, development, proliferation, cell cycle progression and cancer formation makes it an ideal target for inhibitor design. To understand the involvement of HDAC1 in cancer formation, the bump-hole approach proposed in this thesis offers great promise if actualized. Unlike, genetic methods, use of small molecules to inhibit the active site of HDAC1 would allow for temporal, dose-dependent and reversible control of cancer-related genes influenced by HDAC1. In addition, inhibiting the active site should not interfere with HDAC1 binding to associated proteins, otherwise needed for activity, with genetic methods, involving HDAC1 deletions do not offer this advantage.

Towards this goal, we used two different approaches to create the first HDAC1 inhibitor bump-hole pair that would have allowed the characterization of roles the involvement of HDAC1 in cancer formation. The bump-hole relies on successful creation of a t mutation in the HDAC1 active site, which has been unattainable for the last 10 years in the Pflum lab (Chapter 2). With only one active mutant in hand (HDAC1E98A), we first explored the creation of active mutants using the yeast Rpd3 deacetelyase, as an HDAC1 model. The second part of our effort to create an HDAC1 inhibitor bump-hole pair focused on screening this one active mutant for selectivity towards a library of small molecule SAHA analogs synthesized in the Pflum lab.

To identify active mutants from a library of Rpd3 mutants, a functional gene reporter screen dependent on Rpd3 deacetylase activity was developed and optimized. The assay can be performed both qualitatively and quantitatively. The qualitative X-Gal screen allows for identification of possible active mutants by observing blue colored colonies. The inactive Rpd3 would be unable to repress β-gal expression to give a blue color compared to the wild type, which would yield white colonies (Figure 3.4) demonstrating that active mutants can be

distinguished from inactive mutants by observing color formation. Quantification of the deacetylase activity for inactive Rpd3 mutants gave a 2.4-fold increase in β-galactosidase activity (Figure 3.6). These results indicated that the gene reporter assay is suitable for screening Rpd3 library for active mutants.

We screened a library of 15,000 Rpd3 mutants for activity using the *LACZ* gene reporter assay and validated the activity of selected plasmids using the commercially available fluorescence assay. We envisioned that cells containing active Rpd3 would be transferable to HDAC1, for use as a bump-hole. Active Rpd3 mutants showed a white color comparable to wild type (Figure 3.7). The quantified Rpd3 activities for these positive hits with the OPNG assay gave 2-23–fold increases in β-galactosidase activity (Figure 3.8). Further, these deacetylase activities were confirmed using the commercially available fluorescence assay (Figure 3.9). Upon sequencing however, we did not identify any possible mutants (Figure 3.10); only wild type Rpd3 was observed.

With these results, we turned to the active HDAC1E98A mutant and screened functionalized SAHA analogs for selectivity to create a HDAC1 inhibitor bump-hole pair. This approach necessitated the development of a high throughput ELISA assay (Figure 3.11). Consistent with previous results (Chapter 2), the E98A mutant and wild type displayed high deacetylase levels, which were abolished by the HDAC inhibitor trichostatin A (Figure 3.12). These results demonstrate that the ELISA assay is suitable for screening SAHA analogs for selectivity toward HDAC1 or the E98Amutant.

Sixteen SAHA analogs functionalized at the hyroxamic group, C-2, C-3, and C-6 with IC50 values in the micromolar range were ideal candidates for this screen. An initial screen showed that most of the SAHA analogs demonstrated equal potencies against both HDAC1 and the E98A mutant (Figure 3.13). From the initial screen, C-2-hexyl, C-2-pentyl and N-methyl-SAHA

had 5-fold increases in activity for E98A, respectively, compared to the wild type at single concentrations (Tables 3.2 and 3.6). We therefore determined the IC_{50} values for these three SAHA analogs. C-2 hexyl and pentyl SAHA had IC_{50} values of 34.5 μM and 19 μM with E98A respectively, compared to IC_{50}s of 170 μM, with the wild type. These results translate to a 5-fold increase in selectivity. Similarly, N-methyl SAHA was 5-fold selective for E98A (IC_{50}=2.5 μM) over wild type (IC_{50}= 11.5 μM). These observed 5-fold increases in selectivity are not ideal for a bump-hole (The fold-change observed with kinase bump-hole is 100-fold).

An alternative to the bump-hole technique is the isolation of HDAC1 selective isoforms. In the last year, there has been a tremendous effort in the Pflum lab to develop high throughput assays, which would allow for identification of isoform selective inhibitors for all the HDAC isoform (unpublished work). Plans are underway to screen small molecules analogs from the University of Michigan center. If HDAC1 selective inhibitors are identified, then the selective inhibitor will replace the bump-hole strategy and achieve the same goal. This approach can also be extended to other inhibitor selective HDAC isoforms resulting from the same screen.

3.5: Experimental details

3.5.1: General equipment

Standard biochemical equipment available in the Pflum lab includes centrifuges (Eppendorf models 5415D and 5810R), a yeast incubator/shaker (Barnstead labline Max^{Q}Mini 4000), a Tecan GENios Plus spectrophotometer and a VWR rocking platform.

3.5.2: Materials

Yeast Nitrogen Base without amino acids, Bacto^{TM} Agar, CSM His-Ura and CSM His-Ura-Trp were purchase from Difco. The rest of lab supplies were generally bought from Sigma Aldrich or Fisher Scientific.

3.5.3: Yeast strains and plasmids

The pJK1621 reporter plasmid and the FT5 Δrpd3::HIS3 yeast strain were obtained from Dr. Kevin Struhl.[82] The insert from the YEplac112-Rpd3-LexA-FLAG and YEplac112-Rpd3H150AH151A-LexA-FLAG fusion plasmids were generated from the YEplac112-Rpd3-Lex and YEplac112-Rpd3H150AH151A-LexA [82] plasmids via PCR using the following primers: Forward primer: CGGGGTACCATGGTATATGAAGCAACACCTTTTGATCCG; reverse primer CTGGTTAATTATAAATTAGCCATGGCCTTTATCATCATCATCTTTATAATCCAG CCAGTCGCCGTTGCG. The PCR fragments were cloned into *Nco1* digested YEp112 Rpd3-Lex –FLAG plasmid using homologous recombination (Chapter 2, section 2.5.6). Plasmids were confirmed by DNA sequencing.

3.5.4: Primer details

The three-step asymmetric 60 °C-50 °C touchdown PCR method (Chapter 2, section 2.5.3) was used to create the insert for a yeast library in the YEplac112-Rpd3LexAFLAG plasmid using the following primers:

KpnRpd3 for: CGGGGTACCATGGTATATGAAGCAACACCTTTTGATCCG

FLAG+100 rev: CCTAATTCACGTTACCCACC

F214X/F215X for: CTTTCCACAAATATGGTGAG**NNXNNX**CCTGGCACAGGTGAACTG

F214X/215X rev: CTCACCATATTTGTGGAAAGAAC

Rpd3L281 (*NcoI*) for:

CTCCTTGTCCGGCGATCGT**NNX**GGTTGCTTTAATCTTTCTATGGAAGGCC

Where X=G or T

3.5.5: Mini-prep of DNA from yeast cells

Approximately 100 mm^3 cell were obtained from a yeast plate using a sterile Pasteur pipette. The cells were dissolved in 1 mL ddH_2O and spun at 4200 rpm for 5 minutes. The supernatant was removed by aspiration and the cell pellet was resupended in 0.2 mL of Triton/SDS solution (10 mM Tris-Cl, pH 8.0, 2% (v/v) Triton X-100, 1% (w/v) SDS, 100 mM and 1 mM EDTA); the solution was filtered with 0.2 µM filters to sterilize. To the cell mixture, 1:1 equilibrated phenol: chloroform (0.2 mL) and glass beads (0.3 g) were added. The mixture was vortexed for 2 minutes at room temperature and TE buffer (0.2 mL; 10 mM Tris, pH 8.0, 1 mM EDTA) was added, followed by spinning at 5 minutes at 13200 rpm. The top aqueous layer was transferred to a clean epitube containing 1 mL ethanol, mixed by inversion, and spun for another 5 minutes at 13200 rpm. The supernatant was removed and the remaining DNA pellet was dissolved into 400 µL TE buffer containing 20 µg/mL RNase A. The mixture was incubated for 5 minutes at room temperature and centrifuged at 13200 rpm for 5 minutes. The aqueous layer was transferred into an epitube containing 1 mL ethanol and 80 µL 10 M ammonium acetate. This solution was spun at 13200 rpm for 5 minutes and the ethanol was discarded. The DNA pellet was dissolved in 20 µL ddH_2O for storage at -20 °C.

3.5.6: Yeast transformation of plasmid DNA

Approximately 10 yeast colonies from a fresh growth plate were transferred into a solution containing 333 µL 60% PEG 3350, 50 µL 1 M DTT (dithiothreitol), 50 µL of 2 N lithium acetate, and 67 µL water (this mixture is sufficient for 5 transformations). Cells were mixed thoroughly by vortexing to disperse the PEG. To this mixture, 10 µL 10 mg/mL salmon sperm DNA and 1 µL

0.5 µg/mL plasmid DNA was added. The mixture was incubated on ice for 30 minutes, then at 45 °C for 45 minutes, and finally transferred to ice for a further 5 minutes. Aliquots (100 µL) were plated on yeast plates with appropriate selection medium (CSM-His-Ura in the case of the pJK1521 plasmid; or CSM-His-Trp-Ura, in the case of pJK1561 plus Rpd3 expression plasmids) (Difco). Cells were grown at 30 °C for 3-7 days until colonies were observed. A note about making of these yeast plates: Yeast plates were prepared by mixing Yeast Nitrogen Base (6.7%), CSM-His-Ura-Trp or CSM-His-Ura (0.77%), dextrose (5%) and 2% BactoAgar in distilled water. The mixture was autoclaved and poured into petri dishes and allowed to solidify. Plates were used immediately or stored at 4 °C until use. Yeast growth media was prepared in a similar manner but without the BactoAgar.

3.5.7: X-Gal agarose overlay assay

For X-Gal assay optimization (Section 3.2.1.2 and figure 3.5), a single colony from a yeast transformation (section 3.5.8) was re-dissolved in 20 µL distilled water and spotted on wells. To make the wells, yeast nitrogen base (6.7%), CSM-His-Ura-Trp or CSM-His-Ura (0.77%), dextrose (5%) and 2% BactoAgar were mixed in distilled water, autoclaved, poured into 96-well white plates (100 µL per well) using a pipette, and allowed to solidify. After spotting the wells, cells were allowed to grow for 2-3 days at 30 °C. To perform the X-Gal overlay assay, low-melting agarose (5 mg/mL, Life technologies # No. 15517-022) was added to a 10 mL stock solution consisting of 0.5 M potassium phosphate buffer, pH 7.0, 6% DMF and 1% SDS. The 0.5M potassium phosphate buffer pH 7.0 was prepared by mixing 61 mL 1M K_2HPO_4 , 39 mL 1 M KH_2PO_4 and 100mL distilled water, followed by filtering to sterilize. DMF and SDS help to permeabilize the cell. The agarose mixture was boiled by microwaving for approximately 1 minute. To the warm mixture, X-Gal (0.1-0.5 mg/mL), 50 µL β-mercaptoethanol, and 100 µM trichostatin A (or 2% DMSO control) were added. Using a Pasteur pipette, the mixture was transferred to the surface of the well (200 µL was enough to cover the surface). The agar was allowed to cool and solidify and then incubated at 30 °C until blue color was observed (usually

4-6 hours). The colonies were retrieved by scraping off the top X-gal agar, and used for the ONPG assay (section 3.5.8)

3.5.8: Liquid β-galactosidase ONPG assay

For ONPG assay optimization (Section 3.2.1.3 and figure 3.6), colonies were retrieved from beneath the agar surface of wells (section 3.5.7) using a Pasteur pipette. Colonies were separately grown overnight at 30 °C with shaking at 200 rpm in 0.5-1.5 mL yeast media (section 3.5.6) containing the appropriate amino acid complementation; CSM-His-Ura (for *FT5 Δrpd3::HIS3* expressing pJK1621) or CSM-His-Trp-Ura (for *FT5 Δrpd3::HIS3* expressing pJK1621 and YEplac112-Rpd3LexAFLAG). The overnight culture was diluted to A_{600}=0.1, 100 μM trichostatin A added (or 2% DMSO for control), and it was grown to A_{600}=0.4-1.0. Cells were collected by spinning at 13200 rpm for 10 minutes at room temperature. The medium was removed by aspiration and the cell pellet was resuspended into 0.5 mL of buffer Z, (0.1 M $Na_2HPO_4.7H_2O$, pH 7.0, 0.04 M NaH_2PO_4, 0.1 M KCl, 2 M $MgSO_4$ and 2.7 μL/mL β-mercaptoethanol). SDS (25 μL 0.1%), chloroform (20 μL) and 100 μL of 4 mg/mL 2-Nitrophenyl β-D-galactopyranoside (ONPG, from SIGMA) was added to the mixture, followed by vortexing for 30 seconds. The mixture was incubated for 1 hour or until yellow color appeared. Na_2CO_3 (100 μL 1 M) was added to quench the reaction. Cell debris was removed by spinning at 6000 rpm for 1 minute and the OD_{420} measured from a 300 μL sample of the supernatant. Normalized units of β-galactosidase activity were calculated using the following equation: Units = (OD_{420} x 1000) / (OD_{600} x T x V), where T= ONPG incubation time in minutes, V= volume used to measure absorbance, OD_{420} in μL and OD_{600} is the absorbance of diluted overnight culture after growth for several hours. The fold change in β-gal activity for each mutant was normalized to that of the wild type Rpd3 (Normalized units were set to one).

3.5.9: Procedure for screening Rpd3 library

3.5.9.1 Rpd3 library transformation

Plasmid DNA containing Rpd3 mutants was transformed as described in section 3.5.6. Briefly, Approximately 10 yeast colonies of *FT5 Δrpd3::HIS3* from a fresh growth plate were transferred into a solution containing 333 µL 60% PEG 3350, 50 µL of 1 M DTT (dithiothreitol), 50 µL of 2 N lithium acetate, and 67 µL water (this mixture is sufficient for 5 transformations). Cells were mixed thoroughly by vortexing to disperse PEG. To the mixture, 10 µL 10 mg/mL salmon sperm DNA and 1 µL 0.5 µg/mL plasmid DNA were added. The mixture was incubated on ice for 30 minutes, and then at 45 °C for 45 minutes, and finally transferred to ice for a further 5 minutes. Aliquots (100 µL) were plated on yeast plates with amino acid complementation CSM-His-Trp-Ura. Cells were grown at 30 °C for 3-7 days until colonies were observed. Yeast plates were stored at -4 °C until use.

3.5.9.2 X-Gal overlay assay for Rpd3 library

X-Gal overlay solution was prepared and overlaid on yeast plates from section 3.5.9.1 as described in section 3.5.7. Plates were overlaid with X-Gal solution using a Pasteur pipette (10 mL was enough to cover the surface of the plate). The agar was allowed to cool and solidify and then incubated at 30 °C until blue color was observed (usually 4-6 hours). White colonies were retrieved from agar by scrapping off the top agarose solid and separately inoculated in 2 mL yeast growth medium with amino acid complementation CSM-His-Trp-Ura.

3.5.9.3: Liquid β-galactosidase ONPG assay for Rpd3 library

White colonies identified from section 3.5.9.2 were separately grown in 2 mL yeast growth medium with amino acid complementation CSM-His-Trp-Ura overnight at 30 °C with shaking at 200 rpm. ONPG assay was conducted as described in section 3.5.8.

3.5.10: Yeast lysis protocol

Yeast cells were grown at 30 ºC overnight in 5 mL CSM-His-Ura (for FT5 Δrpd3::HIS3 expressing pJK1621) or CSM-His-Trp-Ura (for FT5 Δrpd3::HIS3 expressing pJK1621 and

YEplac112-Rpd3LexAFLAG) with shaking. Cells were collected by spinning at 6000 rpm for 5 minutes. The cell pellet was resuspended in 1 mL yeast lysis buffer F (20 mM HEPES, pH 7.9, 150 mM NaCl, 10% glycerol) and 3 g glass beads were added. Protease inhibitor cocktail set V (1X, Calbiochem) was added and cells were lysed by a successive 6-8 rounds of vortexing at maximum settings for 30 seconds, followed by cooling on ice for 45 seconds. After the last vortex cycle, cells were incubated on ice for 2 min to allow glass beads to settle. The cell extract was transferred to a clean epitube and cell lysates (supernatant) were recovered by spinning at 6000 rpm for 5 minutes, followed by immediate use or storage at -80 °C until use.

3.5.11: Histone deacetylase assay and immunoprecipitation

Lysates prepared from the FT5 Δrpd3::HIS3 yeast strain expressing FLAG tagged Rpd3-LexA fusions were prepared as described in section 3.5.10. Expressed wild-type and mutant FLAG-tagged Rpd3 proteins were immunoprecipitated from the lysates (200 µg of extract for each immunoprecipitation) by incubating with 15 µL of an anti-FLAG agarose bead slurry (Sigma) in buffer F (1 mL 20 mM HEPES, pH 7.6, 1 mM EDTA, 150 mM NaCl, 20% glycerol) for 2 hours at 4 °C with inversion. After 2 hours, beads were recovered by spinning at 4000 rpm for 5 minutes at 4 °C. The supernatant was removed and beads washed three times in 1 mL buffer F by a successive spinning and supernatant removal process. The beads were split into half: one half was used for the HDAC assay, the other half was used for gel analysis (Section 3.5.11). The deacetylase activity of immunoprecipitated proteins was measured using the Fluor de Lys fluorescence activity assay kit (Biomol) as described in chapter 2 (section 2.5.16).

3.5.12: SDS-PAGE and Western

SDS-PAGE was run in s 10% gel as described in chapter 2 (section 2.5.14). The gel was transferred to PVDF membranes as described in chapter 2 (section 2.5.15), probed with anti-LexA antibodies (Promega) and visualized as described in chapter 2 (section 2.5.16).

3.5.13: Plate based ELISA assay

Anti-mouse secondary antibody coated plates (G Biosciences) were washed three times with 1X TBST wash buffer (0.2 M Tris base, 1.37 M NaCl, 0.2 M KCl and 0.0005% Tween). The anti-FLAG antibody (Sigma) was dissolved in 1XTBST containing 3% BSA to a final concentration of 10 µg/mL and 100 µL was added to the plate and was incubated at room temperature for 1 hour with rocking (Rocking platform VWR) or overnight at 4 °C. The antibody solution was removed by inverting the plate and the plate was washed ten times wish 1XTBST wash buffer using a squirt bottle. Lysates of FLAG-fusion wild type or mutant proteins were prepared as described in chapter 2, (section 2.5.13) and were diluted in 1XTBST containing 10% non-fat dry milk (3 % BSA can also be used) to a final concentration of 10 µg/mL. An aliquot (100 µL) was added to the plate and incubated for 1 hour with rocking at 4 °C. The lysates were removed by inversion and washed ten times in 1XTBST using a squirt bottle. Glo™ substrate (25µL; Promega) was added and incubated for 25 minutes without shaking at room temperature, after which the luminescence was determined using the Genios plate reader (Tecan). The luminescence signal for each mutant was normalized to the wild type (set at 100%) and standard error from at least four independent trials are shown in the appendix B.4.

3.5.14: Screening SAHA analogs using 96-well plate ELISA assay

The screen was done as described in section 3.5.10 with some modifications. After removal of the lysates and washing, the small molecule was dissolved in DMSO (see appendix B Tables, B.5-B.10 and Tables 3.2, 3.4 and 3.6 for concentrations) and incubated for 15 minutes. The DMSO concentration was kept at a constant 2% for all reactions. Then, 25 µL of the Glo™ substrate (Promega) was added and left for 25 minutes without shaking, after which the luminescence was determined using the Genios plate reader. Several controls were included; a DMSO control (2%) for both the wild type and mutant protein and a no protein control with 2% DMSO for background luminescence. The normalized deacetylase activity was determined by subtracting the amount of luminescence from the no protein control with 2% DMSO. The

percent activity at each small molecule concentration was calculated by determining the percent luminescence activity in the presence of inhibitor versus absence of inhibitor.

APPENDIX A.

Table A.3: Percent deacetylase activities for HDAC1 alanine mutants.

Protein	Trial1	Trial 2	Trial 3	Trial 4	Trial 5	Trial 6	Mean	S.E
No protein	6	25	22	13	ND	ND	16	4.0
Wild-Type	100	100	100	100	100	ND	100	0.0
H141A	18	20	25	15	20	ND	19	1.5
V19A	44	31	25	37	17	ND	31	4.5
Y23A	30	69	31	25	36	18	35	7.0
Y24A	23	49	20	35	20	8	26	6.0
M30A	20	5	36	18	ND	ND	20	6.0
R34A	42	41	13	17	42	ND	31	6.5
I35A	5	4	3	14	3	ND	5.8	2.0
R36A	38	26	16	26	20	ND	25	4.0
S113A	71	70	51	66	51	ND	62	4.0
L139A	40	39	37	41	ND	ND	39	1.0
C151A	11	21	39	11	30	15	21	4.5
Y303A	10	6	7	9	2	ND	6.7	1.5

HDAC1 wild-type or alanine mutants were expressed as FLAG-tagged fusion proteins and were immunoprecipitated with anti-FLAG-agarose bead resin. The immunoprecipitated proteins were tested for deacetylase activity using an in vitro fluorescence assay, as described in section 2.5.16. The mean percent activity for each independent trial compared to that of the wild-type protein (100%) with standard error (S.E) is shown. ND = Not determined (Data shown in Figures 2.9 and 2.11 in text).

Table 4: Percent deacetylase activities for HDAC1 rescue mutants

Protein	Trila1	Trial 2	Trial 3	Trial 4	Trial 5	Trial 6	Mean	S.E
No protein	18	11	2.7	3.0	1.9	ND	7.4	3.1
Wild-Type	100	100	100	100	100	ND	100	0.0
Y23F	5	7	13	25	10	ND	12	3.5
Y24F	57	31	81	44	69	ND	56	9.0
R34K	17	16	14	18	7	28	17	3.0
R36K	29	41	30	ND	ND	ND	33	3.5
C151S	33	25	29	30	31	ND	30	1.0
Y303F	50	33	37	31	ND	ND	38	4.0

HDAC1 wild-type or alanine mutants were expressed as FLAG-tagged fusion proteins and were immunoprecipitated with anti-FLAG-agarose bead resin. The immunoprecipitated proteins were tested for deacetylase activity by an in vitro fluorescence assay, as described in section 2.5.16. The mean percent activity for each independent trial compared with that of the wild-type protein (100%) with standard error (S.E) is shown. ND = Not determined (Data shown in figure 2.12 in text).

.

Table 5: Percentage remaining HDAC activity after incubation of acetate with HDAC1

Concentration (M)	Trial 1	Trial 2	Trial 3	Trial 4	Trial 5	Mean	S.E
2.5×10^{-2}	10	22	15	23	21	18	2.4
1.25×10^{-2}	36	31	31	24	31	31	2
6.25×10^{-3}	55	55	44	61	50	53	2.8
3.125×10^{-3}	63	83	81	74	ND	75	4.5
1.56×10^{-3}	80	107	98	98	ND	96	5.6

Deacetylase activity of wild type was determined at each sodium acetate concentration using an in vitro fluorescence assay as described in section 2.5.16. The percentage deacetylase activity of each independent trial, mean percentage deacetylase activity, and standard error (S.E) at each acetate concentration are shown. ND = Not determined.

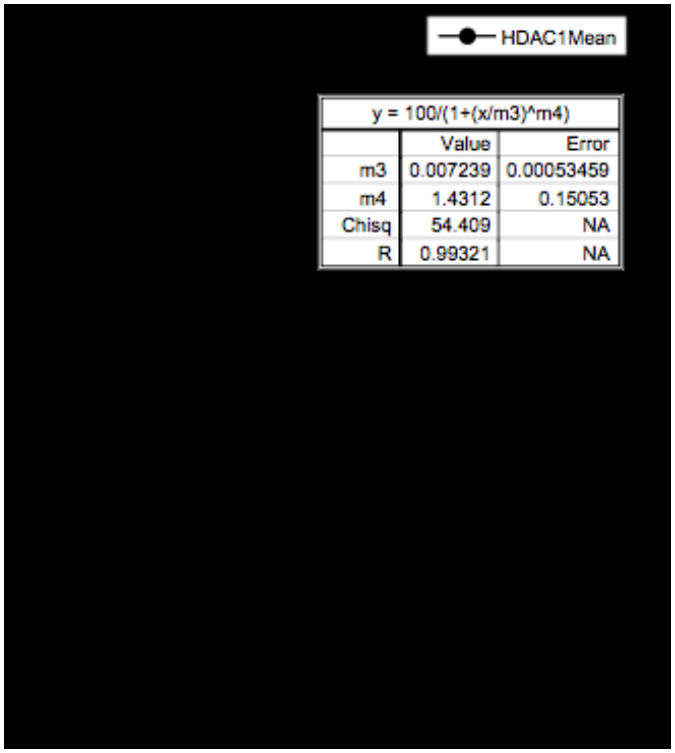

Figure 40: IC50 Curve of Acetate with wild type HDAC1. A plot showing the percentage deacetylase activity of wild type HDAC1 versus acetate concentration. Data was fit to a sigmoidal curve using Kaleidograph 4.0 (Synergy Software) to determine the IC_{50}. The inset is the results of the data analysis and the calculated IC_{50} (m3 in molar) is given with error. Graph included in Figure 2.13, Figure 2.14, and Table 1.1.

Table 6: Percentage remaining HDAC activity after incubation of acetate with HDAC1R34A

Concentration (M)	Trial 1	Trial 2	Trial 3	Trail 4	Trial 5	Mean	S.E
2.0×10^{-1}	7.8	12	20	20	8	14	3
6.6×10^{-2}	33	26	25	24	21	26	4.5
2.25×10^{-2}	50	40	64	42	38	47	8.7
7.4×10^{-3}	73	72	70	65	81	73	12
2.46×10^{-3}	96	82	82	82	116	92	16

Deacetylase activity of HDAC1R34A mutant was determined at each sodium acetate concentration using an in vitro fluorescence assay, as described in section 2.5.16.The percentage deacetylase activity of each independent trial, mean percentage deacetylase activity and standard error (S.E) at each acetate concentration are shown.

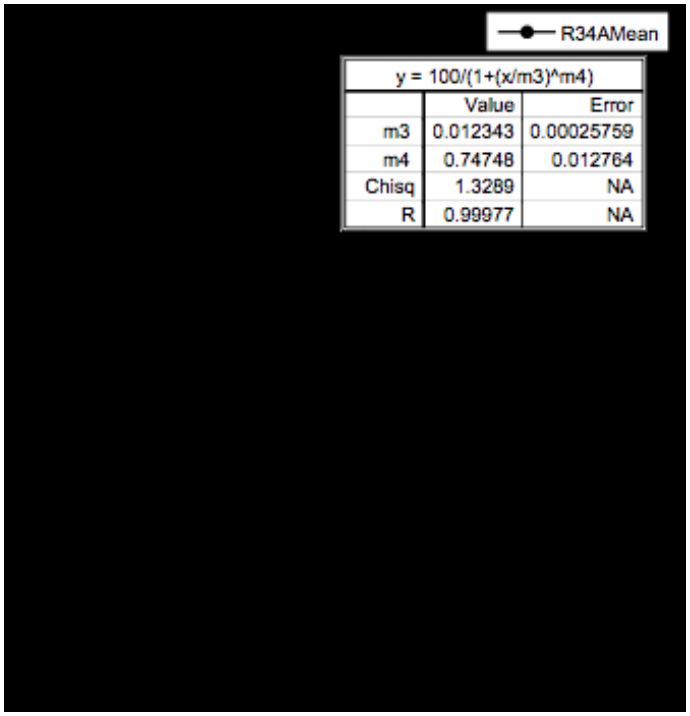

Figure 41: IC_{50} Curve of Acetate with HDAC1R34A. A plot showing the percentage deacetylase activity of HDAC1R34A versus acetate concentration. Data was fit to a sigmoidal curve using Kaleidograph 4.0 (Synergy Software) to determine the IC_{50}. The inset is the results of the data analysis and the calculated IC_{50} (m3 in molar) is given with error. Graph included in Figure 2.13 and Table 1.1.

Table 7: Percentage remaining HDAC activity after incubation of acetate with HDAC1Y23A.

Concentration (M)	Trial 1	Trial 2	Trial 3	Trial 4	Mean	S.E
2.0×10^{-1}	7.5	23	20	13	16	3
6.6×10^{-2}	17	40	25	25	27	4.5
2.25×10^{-2}	44	50	64	55	53	8.7
7.4×10^{-3}	75	55	70	71	68	12
2.46×10^{-3}	84	89	82	90	86	16

Deacetylase activity of HDAC1Y23A mutant was determined at each sodium acetate concentration using an in vitro fluorescence assay, as described in section 2.5.16. The percentage deacetylase activity of each independent trial, mean percentage deacetylase activity and standard error (S.E) at each acetate concentration are shown.

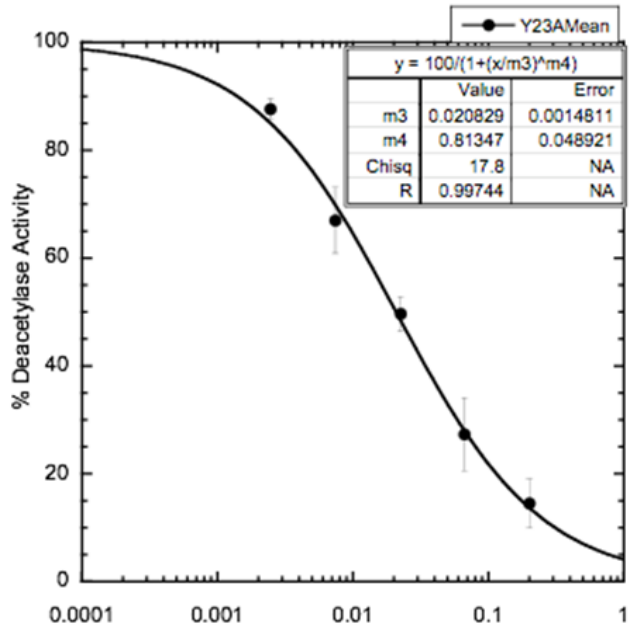

Figure 42: IC_{50} Curve of Acetate with HDAC1Y24A: A plot showing the percentage deacetylase activity of HDAC1R34A versus acetate concentration. Data was fit to a sigmoidal curve using Kaleidograph 4.0 (Synergy Software) to determine the IC_{50}. The inset is the results of the data analysis and the calculated IC_{50} (m3 in molar) is given with error. Graph included in Figure 2.14 and Table 1.1.

Table 8: Percentage remaining HDAC activity after incubation of acetate with HDAC1Y24A.

Concentration (M)	Trial 1	Trial 2	Trial 3	Mean	S.E
2.0×10^{-1}	13	23	8	15	4.4
6.6×10^{-2}	25	32	17	24	4.3
2.25×10^{-2}	55	46	44	48	3.3
7.4×10^{-3}	71	60	75	69	4.4
2.46×10^{-3}	80	83	84	82	1.2

Deacetylase activity of HDAC1Y24A mutant was determined at each sodium acetate concentration using an in vitro fluorescence assay, as described in section 2.5.16. The percentage deacetylase activity of each independent trial, mean percentage deacetylase activity and standard error (S.E) at each acetate concentration are shown.

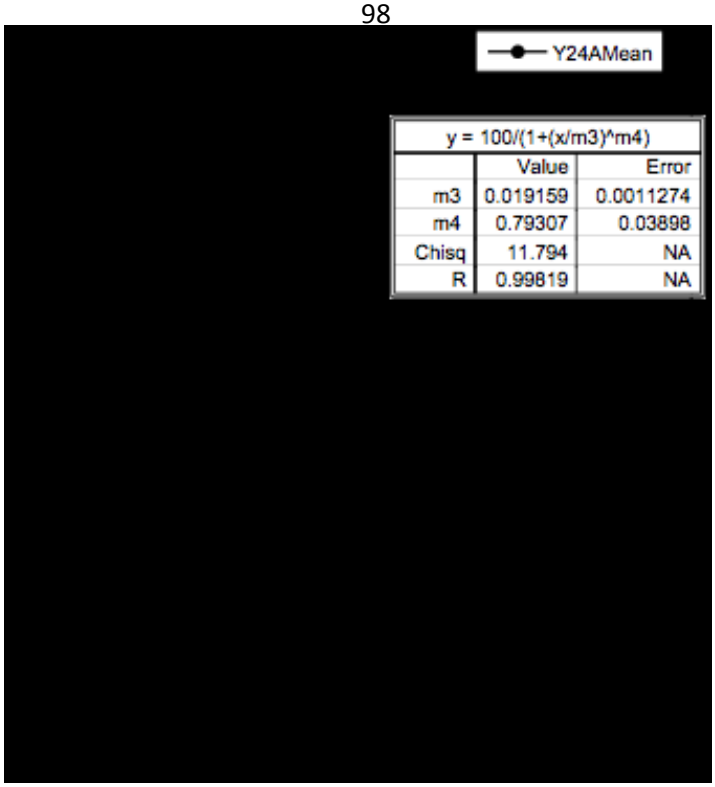

Figure 43: IC_{50} Curve of Acetate with HDAC1Y24A. A plot showing the percentage deacetylase activity of HDAC1Y24A versus acetate concentration. Data was fit to a sigmoidal curve using Kaleidograph 4.0 (Synergy Software) to determine the IC_{50}. The inset is the results of the data analysis and the calculated IC_{50} (m3 in molar) is given with error. Graph included in Figure 2.14 and Table 1.1.

Table A.9: Percentage remaining HDAC activity after incubation of acetate with HDAC1R36A.

Concentration (M)	Trial 1	Trial 2	Trial 3	Mean	S.E
2.0×10^{-1}	16	24	16	19	2.6
6.6×10^{-2}	37	21	37	32	5.3
2.25×10^{-2}	46	39	46	44	2.3
7.4×10^{-3}	60	55	60	58	1.6
2.46×10^{-3}	77	72	77	75	1.6

Deacetylase activity of HDAC1R36A mutant was determined at each sodium acetate concentration using an in vitro fluorescence assay, as described in section 2.5.16. The percentage deacetylase activity of each independent trial, mean percentage deacetylase activity and standard error (S.E) at each acetate concentration are shown.

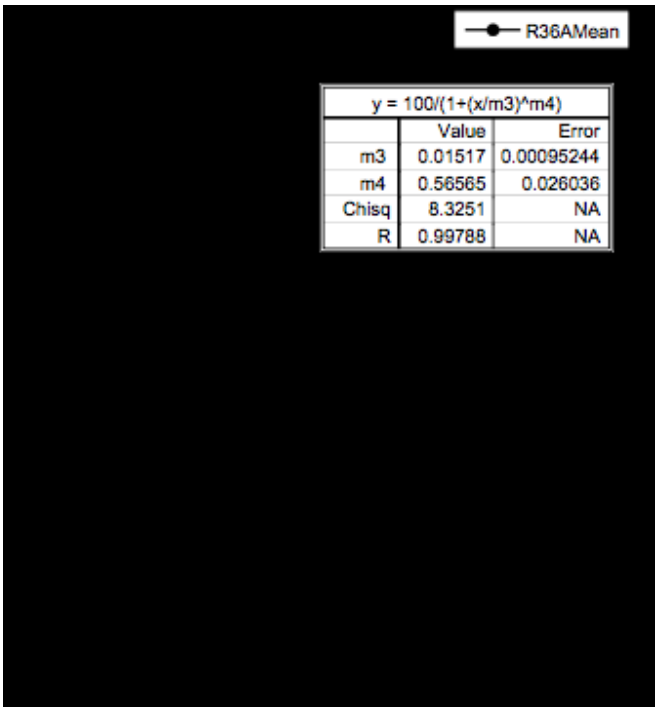

Figure 44: IC_{50} Curve of Acetate with HDAC1R36A. A plot showing the percentage deacetylase activity of HDAC1R36A versus acetate concentration. Data was fit to a sigmoidal curve using Kaleidograph 4.0 (Synergy Software) to determine the IC_{50}. The inset is the results of the data analysis and the calculated IC_{50} (m3 in molar) is given with error. Graph included in Figure 2.13 and Table 1.1.

Table A.10: Percentage remaining HDAC activity after incubation of acetate with HDAC1C151A.

Concentration (M)	Trial 1	Trial 2	Trial 3	Mean	S.E
2.0×10^{-1}	10	23	10	14	4.3
6.6×10^{-2}	20	33	20	24	4.3
2.25×10^{-2}	38	39	38	38	0.3
7.4×10^{-3}	58	62	58	59	1.3
2.46×10^{-3}	72	86	84	81	4.3

Deacetylase activity of HDAC1C151A mutant was determined at each sodium acetate concentration using an in vitro fluorescence assay, as described in section 2.5.16. The percentage deacetylase activity of each independent trial, mean percentage deacetylase activity and standard error (S.E) at each acetate concentration are shown.

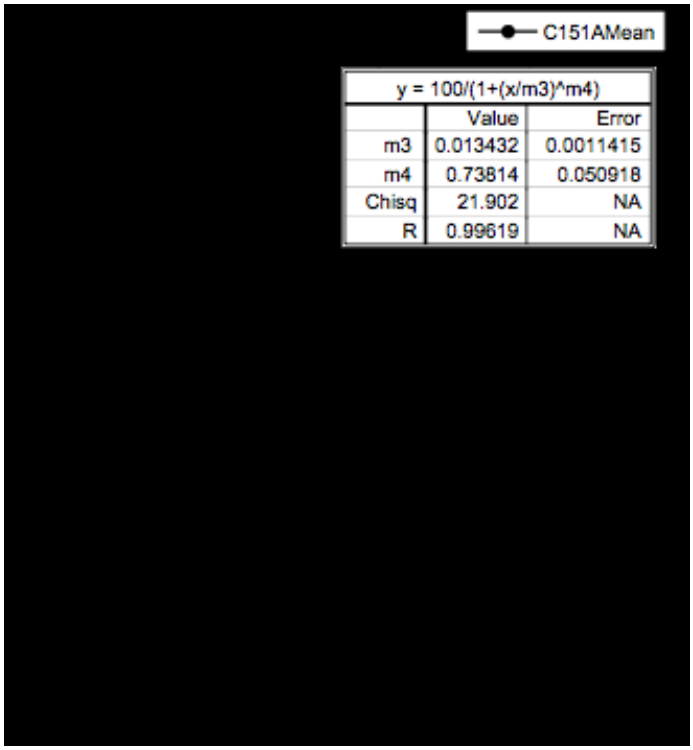

Figure 45: IC_{50} Curve of Acetate with HDAC1C151A. A plot showing the percentage deacetylase activity of HDAC1C151A versus acetate concentration. Data was fit to a sigmoidal curve using Kaleidograph 4.0 (Synergy Software) to determine the IC_{50}. The inset is the results of the data analysis and the calculated IC_{50} (m3 in molar) is given with error. Graph included in Figure 2.14 and Table 1.1.

Table A.11: Percentage remaining HDAC activity after incubation of acetate with HDAC1F205Y.

Concentration (M)	Trial 1	Trial 2	Trial 3	Trail 4	Mean	S.E
2.5×10^{-2}	19	26	21	26	23	1.7
1.25×10^{-2}	35	33	33	ND	34	0.6
6.25×10^{-3}	50	47	47	60	51	3.1
3.125×10^{-3}	65	88	88	73	79	5.0
1.56×10^{-3}	102	99	99	97	99	1.2

Deacetylase activity of HDAC1F205Y mutant was determined at each sodium acetate concentration using an in vitro fluorescence assay as described in section 2.5.16. The percentage deacetylase activity of each independent trial, mean percentage deacetylase activity and standard error (S.E) at each acetate concentration are shown. ND = Not determined.

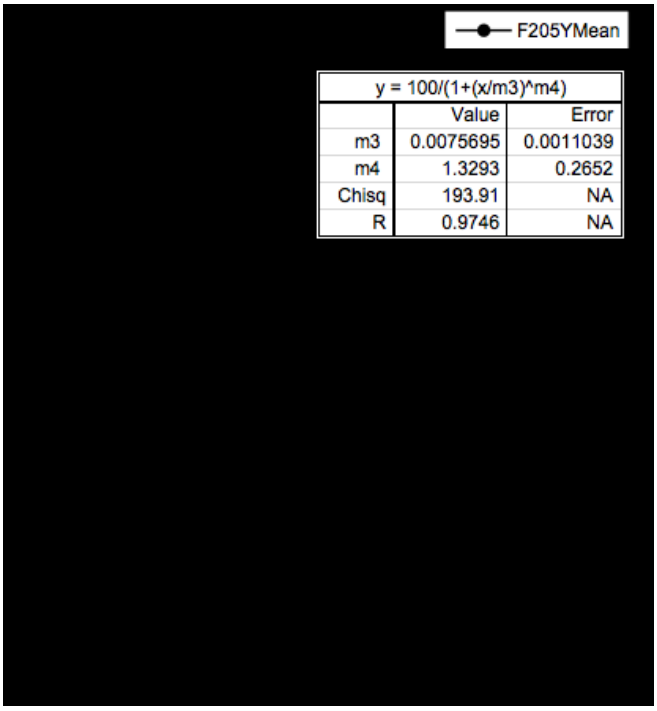

Figure 46: IC_{50} Curve of Acetate with HDAC1F205Y. A plot showing the percentage deacetylase activity of HDAC1F205Y versus acetate concentration. Data was fit to a sigmoidal curve using Kaleidograph 4.0 (Synergy Software) to determine the IC_{50}. The inset is the results of the data analysis and the calculated IC_{50} (m3 in molar) is given with error. Graph included in Figure 2.13 and Table 1.1.

APPENDIX B.

Table B.12: Quantitative inhibition of Rpd3 activity (data obtained by Sujith Weerasighe)

Sample	Trial 1	Trial 2	Trial 3	Trial 4	Trial 5	Mean	S.E
LACZ reporter	3.49	2.92	3.40	6.49	5.95	4.45	0.73
LACZ reporter + TSA 100μM	2.87	2.78	4.59	4.81	6.21	4.25	0.65
Wt Rpd3	1.00	1.00	1.00	1.00	1.00	1.00	-
Wt Rpd3 + TSA 100μM	1.42	1.47	2.16	1.58	1.44	1.61	0.12
Rpd3 mutant	2.32	2.02	2.90	3.30	4.25	2.96	0.39
Rpd3 mutant + TSA 100μM	2.21	2.50	3.20	4.81	5.2	3.58	0.61

LACZ reporter plasmid, pJK1621, was transformed with or without wild type Rpd3 or catalytically inactive Rpd3 mutant as LexA-FLAG fusions into *FT5 Δrpd3::HIS* yeast strain. Transformed cell were grown with or without TSA for 6h at 30°C and β-galactosidase activity was measured quantitatively using ONPG as the substrate. Relative fold changes in β-galactosidase activity was calculated with respect to wild type Rpd3 as described and mean fold change observed with three independent trial is shown with standard error (S.E). ND= Not determined. Data shown in figure 3.6 in the text.

Table 13: A representative quantitative ONPG inhibition of Rpd3 mutant(s) activity.

	WildType	Rpd3H150A H151A	1	2	3	4	5	6	7	8	9	10
Trial 1	1.0	4.4	4.1	4.0	1.2	2.7	3.7	7.1	6.3	3.3	4.4	1.4
Trial 2	1.0	4.7	3.5	4.5	1.5	2.5	3.9	6.5	6.5	3.5	4.7	1.2

LACZ reporter plasmid, PJK1621, was transformed with or without wild type Rpd3 (or catalytically inactive Rpd3) or plasmid DNA from Rpd3 library mutant as LexA-FLAG fusions into *FT5 Δrpd3::HIS* yeast strain. Transformed cells were grown for 6h at 30°C and β-galactosidase activity was measured quantitatively using ONPG as the substrate. Relative fold changes in β-galactosidase activity was calculated with respect to wild type Rpd3 as described and data from 2 trials is shown. Data shown in Figure 3.8 of the text.

Table 14: Deacetylase activity of immunoprecipitated wild type or Rpd3 mutants

	Wild type	RpdH150A H151A	3	4	5	6	10
Trial 1	100	16	86	33	26	79	21
Trial 2	100	25	99	40	20	80	30

Lysates were prepared from FT5 Δrpd3::HIS3 yeast strain expressing FLAG tagged Rpd3-LexA fusion proteins and immunoprecipitated as described in section 3.8. The deacetylase activity of immunoprecipitated proteins was measured using Fluor de Lys fluorescence activity assay kit. Percentage deacetylase activity for two trials is shown. Data shown in Figure 3.9 of the text.

Table 15: Validation of plate based ELISA assay

Protein	Trial 1	Trial 2	Trial 3	Trial 4	Mean	S.E
No protein	24	10	21	21	19	3.0
H141A	10	15	10	8	10	1.4
HDAC1	100	100	100	100	100	-
E98A	110	119	120	114	115	2.3
HDAC1 + TSA	25	20	25	19	22	1.6
E98A + TSA	25	30	24	34	28	2.3

Deacetylase activity was determined using ELISA assay as described (Chapter 3, section 3.5.14). Percentage deacetylase activity of each independent trial, mean percentage deacetylase activity and standard error (S.E) are shown. Data shown in Figure 3.12 of the text.

Table 16: Percentage remaining HDAC activity after incubation of SAHA C-2-hexyl with HDAC1

Concentration (M)	Trial 1	Trial 2	Trial 3	Mean	S.E
4.8×10^{-2}	35	21	31	30	4.1
2.4×10^{-2}	57	39	23	40	9.8
1.2×10^{-2}	63	52	66	60	4.2
6.0×10^{3}	72	64	73	70	2.8
3.0×10^{-3}	75	90	96	87	6.2

Deacetylase activity was determined at each SAHA C-2-hexyl concentration using ELISA assay as described (Chapter 3, section 3.5.14). Percentage deacetylase activity of each independent trial, mean percentage deacetylase activity and standard error (S.E) at each concentration are shown. Data shown in Figure 3.13 of the text.

Table 17: Percentage remaining HDAC activity after incubation of SAHA C-2-hexyl with HDAC1E98A

Concentration (M)	Trial 1	Trial 2	Trial 3	Mean	S.E
1.2×10^{-2}	32	14	6	17	7.6
6.0×10^{-3}	43	40	14	32	9.2
3.0×10^{-3}	73	47	46	55	8.8
1.5×10^{-3}	73	67	60	67	3.7
7.5×10^{-4}	91	80	94	88	4.2

Deacetylase activity was determined at each SAHA C-2-hexyl concentration using ELISA assay as described (Chapter 3, section 3.5.14). Percentage deacetylase activity of each independent trial, mean percentage deacetylase activity and standard error (S.E) at each concentration are shown. Data shown in Figure 3.13 of the text.

Table 18: Percentage remaining HDAC activity after incubation of SAHA C-2-pentyl with HDAC1

Concentration (M)	Trial 1	Trial 2	Trial 3	Mean	S.E
2.4×10^{-2}	24	29	35	30	3.1
1.2×10^{-2}	38	44	46	43	2.4
6.0×10^{-3}	65	68	57	63	3.2
3.0×10^{-3}	97	71	68	78	9.2
1.5×10^{-3}	94	94	94	94	-

Deacetylase activity was determined at each SAHA C-2-pentyl concentration using ELISA assay as described (Chapter 3, section 3.5.14). Percentage deacetylase activity of each independent trial, mean percentage deacetylase activity and standard error (S.E) at each concentration are shown. Data shown in Figure 3.14 of the text.

Table 19: Percentage remaining HDAC activity after incubation of SAHA C-2-pentyl with HDAC1E98A

Concentration (M)	Trial 1	Trial 2	Trial 3	Mean	S.E
6.0×10^{-3}	15	33	22	23	5.2
3.0×10^{-3}	23	51	34	36	8.1
1.5×10^{-3}	66	62	48	58	5.4
7.5×10^{-4}	77	83	54	71	8.8
3.75×10^{-4}	88	95	74	85	6.1

Deacetylase was determined at each SAHA C-2-pentyl concentration using ELISA assay as described (Chapter 3, section 3.5.14). Percentage deacetylase activity of each independent trial, mean percentage deacetylase activity and standard error (S.E) at each concentration are shown. Data shown in Figure 3.14 of the text.

Table 20: Percentage remaining HDAC activity after incubation of N-methyl SAHA with HDAC1

Concentration (M)	Trial 1	Trial 2	Trial 3	Mean	S.E
2.56×10^{-3}	18	40	20	26	7.0
1.28×10^{-3}	52	44	68	54	7.0
6.4×10^{-4}	65	51	54	56	4.2
3.2×10^{-4}	79	79	99	85	6.6
1.6×10^{-4}	113	87	86	95	8.8

Deacetylase activity was determined at each N-methyl SAHA concentration using ELISA assay as described (Chapter 3, section 3.5.14). Percentage deacetylase activity of each independent trial, mean percentage deacetylase activity and standard error (S.E) at each concentration are shown. Data shown in Figure 3.15 of the text.

Table 21: Percentage remaining HDAC activity after incubation of N-methyl SAHA with HDAC1E98A

Concentration (M)	Trial 1	Trial 2	Trial 3	Mean	S.E
6.4×10^{-4}	38	35	8	27	9.5
3.2×10^{-4}	62	44	29	57	9.5
1.6×10^{-4}	81	54	39	58	12
8.0×10^{-5}	83	70	78	77	3.7
4.0×10^{-5}	98	85	84	90	4.5

Deacetylase was determined at each N-methyl SAHA concentration using ELISA assay as described in Chapter 3, section 3.5.14. Percentage deacetylase activity of each independent trial, mean percentage deacetylase activity and standard error (S.E) at each concentration are shown. Data shown in Figure 3.15 in text.

APPENDIX C.

Figure 47: Structures of SAHA C2 analogs

C2-a

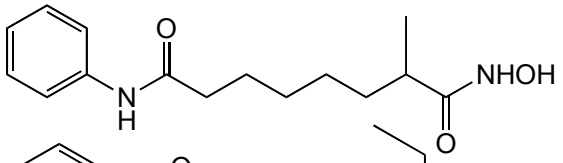

SAHA C-2-Methyl

C2-b

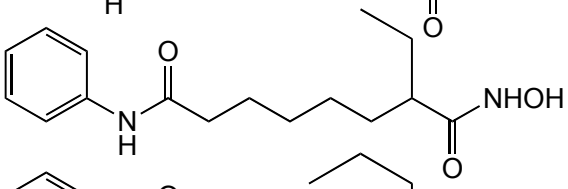

SAHA C-2-Ethyl

C2-c

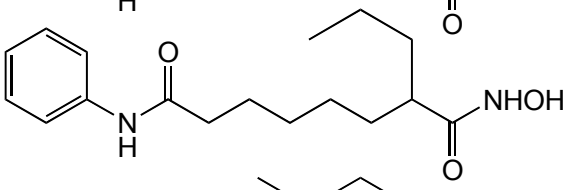

SAHA C-2-Propyl

C2-d

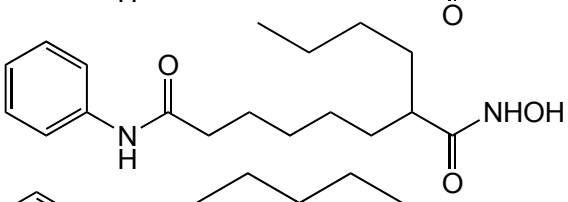

SAHA C-2-Butyl

C2-e

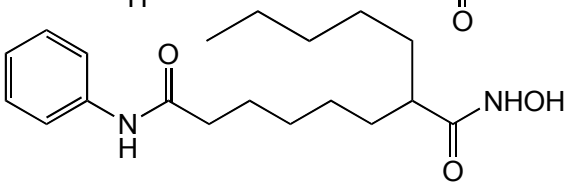

SAHA C-2-Pentyl

C2-f

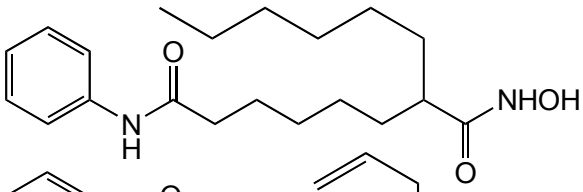

SAHA C-2-Hexyl

C2-g

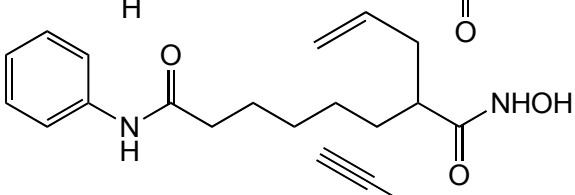

SAHA C-2-Allyl

C2-h

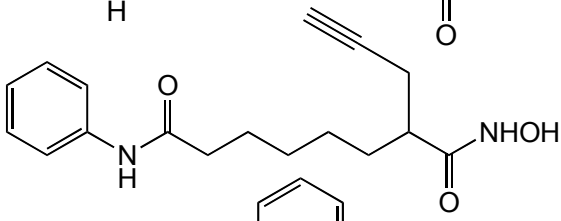

SAHA C-2-Propargyl

C2-i

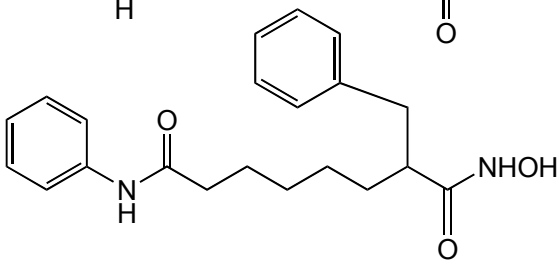

SAHA C-2-Benzyl

Figure 48: Structures of SAHA C3 analogs

C3-a

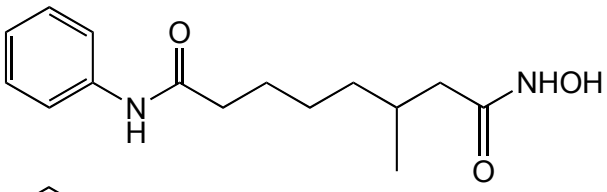

SAHA C-3-Methyl

C3-b

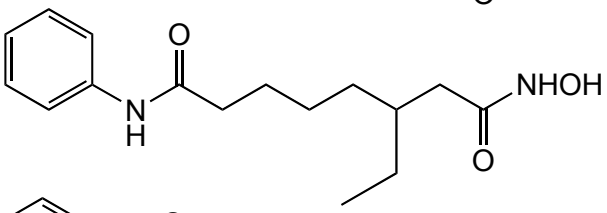

SAHA C-3-Ethyl

C3-c

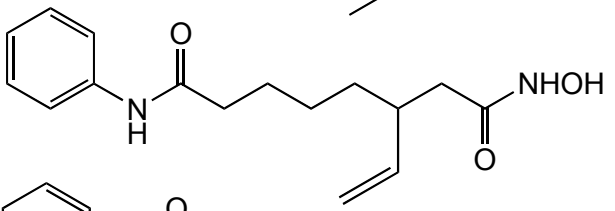

SAHA C-3-Vinyl

C3-d

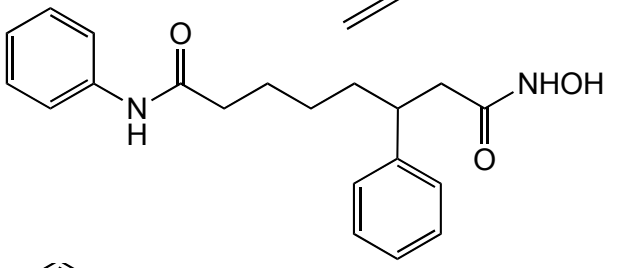

SAHA C-3-Phenyl

C3-e

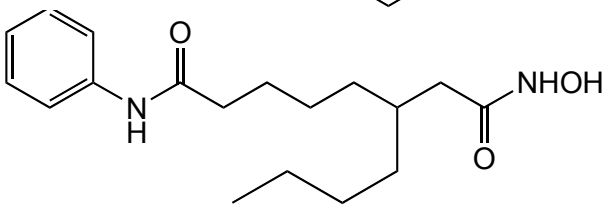

SAHA C-3-Butyl

Figure 49: Structures of N-SAHA analogs

N-a

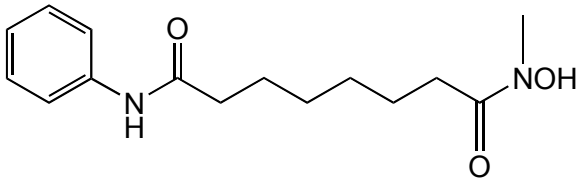

SAHA N-Methyl

N-b

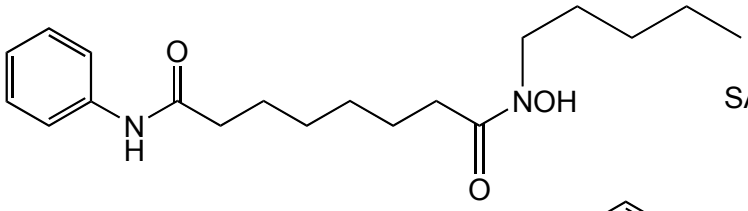

SAHA N-Pentyl

N-c

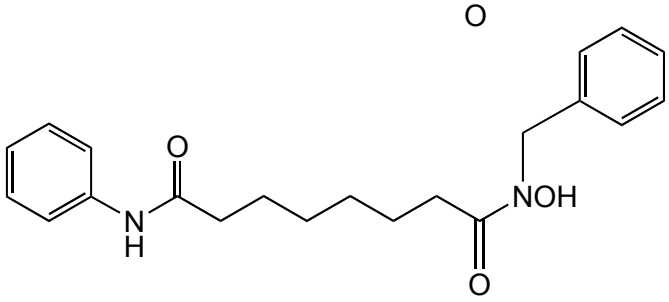

SAHA N-Benzyl

N-d

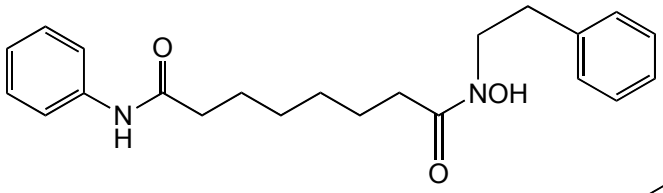

SAHA N-homoenzyl

N-e

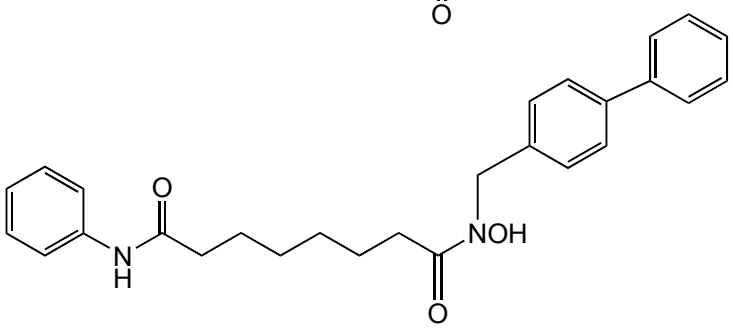

SAHA N-biphenyl

REFERENCES

1. Luger K, Mader AW, Richmond RK, Sargent DF, Richmond TJ: **Crystal structure of the nucleosome core particle at 2.8 A resolution**. *Nature* 1997, **389**(6648):251-260.
2. Turner BM: **Cellular memory and the histone code**. *Cell* 2002, **111**(3):285-291.
3. Peterson CL, Laniel MA: **Histones and histone modifications**. *Curr Biol* 2004, **14**(14):R546-551.
4. Nan X, Ng HH, Johnson CA, Laherty CD, Turner BM, Eisenman RN, Bird A: **Transcriptional repression by the methyl-CpG-binding protein MeCP2 involves a histone deacetylase complex**. *Nature* 1998, **393**(6683):386-389.
5. Costa FF: **Non-coding RNAs, epigenetics and complexity**. *Gene* 2008, **410**(1):9-17.
6. Glatt S, Alfieri C, Muller CW: **Recognizing and remodeling the nucleosome**. *Curr Opin Struct Biol* 2011, **21**(3):335-341.
7. Taunton J, Hassig CA, Schreiber SL: **A mammalian histone deacetylase related to the yeast transcriptional regulator Rpd3p**. *Science* 1996, **272**(5260):408-411.
8. Hu E, Chen Z, Fredrickson T, Zhu Y, Kirkpatrick R, Zhang GF, Johanson K, Sung CM, Liu R, Winkler J: **Cloning and characterization of a novel human class I histone deacetylase that functions as a transcription repressor**. *J Biol Chem* 2000, **275**(20):15254-15264.
9. Van den Wyngaert I, de Vries W, Kremer A, Neefs J, Verhasselt P, Luyten WH, Kass SU: **Cloning and characterization of human histone deacetylase 8**. *FEBS Lett* 2000, **478**(1-2):77-83.
10. Yang WM, Yao YL, Sun JM, Davie JR, Seto E: **Isolation and characterization of cDNAs corresponding to an additional member of the human histone deacetylase gene family**. *J Biol Chem* 1997, **272**(44):28001-28007.
11. Bernstein BE, Tong JK, Schreiber SL: **Genomewide studies of histone deacetylase function in yeast**. *Proceedings of the National Academy of Sciences of the United States of America* 2000, **97**(25):13708-13713.

12. Grozinger CM, Hassig CA, Schreiber SL: **Three proteins define a class of human histone deacetylases related to yeast Hda1p**. *Proceedings of the National Academy of Sciences of the United States of America* 1999, **96**(9):4868-4873.

13. Kao HY, Downes M, Ordentlich P, Evans RM: **Isolation of a novel histone deacetylase reveals that class I and class II deacetylases promote SMRT-mediated repression**. *Genes & development* 2000, **14**(1):55-66.

14. Zhou X, Marks PA, Rifkind RA, Richon VM: **Cloning and characterization of a histone deacetylase, HDAC9**. *Proceedings of the National Academy of Sciences of the United States of America* 2001, **98**(19):10572-10577.

15. Kao HY, Lee CH, Komarov A, Han CC, Evans RM: **Isolation and characterization of mammalian HDAC10, a novel histone deacetylase**. *J Biol Chem* 2002, **277**(1):187-193.

16. de Ruijter AJ, van Gennip AH, Caron HN, Kemp S, van Kuilenburg AB: **Histone deacetylases (HDACs): characterization of the classical HDAC family**. *Biochem J* 2003, **370**(Pt 3):737-749.

17. Gao L, Cueto MA, Asselbergs F, Atadja P: **Cloning and functional characterization of HDAC11, a novel member of the human histone deacetylase family**. *J Biol Chem* 2002, **277**(28):25748-25755.

18. Methot JL, Chakravarty PK, Chenard M, Close J, Cruz JC, Dahlberg WK, Fleming J, Hamblett CL, Hamill JE, Harrington P *et al*: **Exploration of the internal cavity of histone deacetylase (HDAC) with selective HDAC1/HDAC2 inhibitors (SHI-1:2)**. *Bioorganic & medicinal chemistry letters* 2008, **18**(3):973-978.

19. Moradei OM, Mallais TC, Frechette S, Paquin I, Tessier PE, Leit SM, Fournel M, Bonfils C, Trachy-Bourget MC, Liu J *et al*: **Novel aminophenyl benzamide-type histone deacetylase inhibitors with enhanced potency and selectivity**. *Journal of medicinal chemistry* 2007, **50**(23):5543-5546.

20. Finnin MS, Donigian JR, Cohen A, Richon VM, Rifkind RA, Marks PA, Breslow R, Pavletich NP: **Structures of a histone deacetylase homologue bound to the TSA and SAHA inhibitors**. *Nature* 1999, **401**(6749):188-193.

21. Wang DF, Wiest O, Helquist P, Lan-Hargest HY, Wiech NL: **On the function of the 14 A long internal cavity of histone deacetylase-like protein: implications for the design of histone deacetylase inhibitors**. *Journal of medicinal chemistry* 2004, **47**(13):3409-3417.

22. Haider S, Joseph CG, Neidle S, Fierke CA, Fuchter MJ: **On the function of the internal cavity of histone deacetylase protein 8: R37 is a crucial residue for catalysis**. *Bioorg Med Chem Lett* 2011, **21**(7):2129-2132.

23. Guo L, Han A, Bates DL, Cao J, Chen L: **Crystal structure of a conserved N-terminal domain of histone deacetylase 4 reveals functional insights into glutamine-rich domains**. *Proceedings of the National Academy of Sciences of the United States of America* 2007, **104**(11):4297-4302.

24. Schuetz A, Min J, Allali-Hassani A, Schapira M, Shuen M, Loppnau P, Mazitschek R, Kwiatkowski NP, Lewis TA, Maglathin RL *et al*: **Human HDAC7 harbors a class IIa histone deacetylase-specific zinc binding motif and cryptic deacetylase activity**. *J Biol Chem* 2008, **283**(17):11355-11363.

25. Vannini A, Volpari C, Filocamo G, Casavola EC, Brunetti M, Renzoni D, Chakravarty P, Paolini C, De Francesco R, Gallinari P *et al*: **Crystal structure of a eukaryotic zinc-dependent histone deacetylase, human HDAC8, complexed with a hydroxamic acid inhibitor**. *Proceedings of the National Academy of Sciences of the United States of America* 2004, **101**(42):15064-15069.

26. Watson PJ, Fairall L, Santos GM, Schwabe JW: **Structure of HDAC3 bound to co-repressor and inositol tetraphosphate**. *Nature* 2012, **481**(7381):335-340.

27. Bressi JC, Jennings AJ, Skene R, Wu Y, Melkus R, De Jong R, O'Connell S, Grimshaw CE, Navre M, Gangloff AR: **Exploration of the HDAC2 foot pocket: Synthesis and SAR of substituted N-(2-aminophenyl)benzamides**. *Bioorganic & medicinal chemistry letters* 2010, **20**(10):3142-3145.

28. Fischle W, Dequiedt F, Hendzel MJ, Guenther MG, Lazar MA, Voelter W, Verdin E: **Enzymatic activity associated with class II HDACs is dependent on a multiprotein complex containing HDAC3 and SMRT/N-CoR**. *Mol Cell* 2002, **9**(1):45-57.

29. Lee H, Rezai-Zadeh N, Seto E: **Negative regulation of histone deacetylase 8 activity by cyclic AMP-dependent protein kinase A**. *Mol Cell Biol* 2004, **24**(2):765-773.

30. Sengupta N, Seto E: **Regulation of histone deacetylase activities**. *J Cell Biochem* 2004, **93**(1):57-67.

31. Cress WD, Seto E: **Histone deacetylases, transcriptional control, and cancer**. *J Cell Physiol* 2000, **184**(1):1-16.

32. Sterner DE, Berger SL: **Acetylation of histones and transcription-related factors**. *Microbiol Mol Biol Rev* 2000, **64**(2):435-459.

33. Krumm A, Madisen L, Yang XJ, Goodman R, Nakatani Y, Groudine M: **Long-distance transcriptional enhancement by the histone acetyltransferase PCAF**. *Proceedings of the National Academy of Sciences of the United States of America* 1998, **95**(23):13501-13506.

34. Zhang Y, Reinberg D: **Transcription regulation by histone methylation: interplay between different covalent modifications of the core histone tails**. *Genes & development* 2001, **15**(18):2343-2360.

35. Ng HH, Bird A: **Histone deacetylases: silencers for hire**. *Trends Biochem Sci* 2000, **25**(3):121-126.

36. Pazin MJ, Kadonaga JT: **What's up and down with histone deacetylation and transcription?** *Cell* 1997, **89**(3):325-328.

37. Roussel MF, Ashmun RA, Sherr CJ, Eisenman RN, Ayer DE: **Inhibition of cell proliferation by the Mad1 transcriptional repressor**. *Mol Cell Biol* 1996, **16**(6):2796-2801.

38. Jones PA, Baylin SB: **The epigenomics of cancer**. *Cell* 2007, **128**(4):683-692.

39. Janssen C, Schmalbach S, Boeselt S, Sarlette A, Dengler R, Petri S: **Differential histone deacetylase mRNA expression patterns in amyotrophic lateral sclerosis**. *J Neuropathol Exp Neurol* 2010, **69**(6):573-581.

40. Hu N, Qiu X, Luo Y, Yuan J, Li Y, Lei W, Zhang G, Zhou Y, Su Y, Lu Q: **Abnormal histone modification patterns in lupus CD4+ T cells**. *J Rheumatol* 2008, **35**(5):804-810.

41. Das PM, Singal R: **DNA methylation and cancer**. *J Clin Oncol* 2004, **22**(22):4632-4642.

42. Ozdag H, Teschendorff AE, Ahmed AA, Hyland SJ, Blenkiron C, Bobrow L, Veerakumarasivam A, Burtt G, Subkhankulova T, Arends MJ *et al*: **Differential expression of selected histone modifier genes in human solid cancers**. *BMC Genomics* 2006, **7**:90.

43. Weichert W, Roske A, Niesporek S, Noske A, Buckendahl AC, Dietel M, Gekeler V, Boehm M, Beckers T, Denkert C: **Class I histone deacetylase expression has independent prognostic impact in human colorectal cancer: specific role of class I histone deacetylases in vitro and in vivo**. *Clin Cancer Res* 2008, **14**(6):1669-1677.

44. Weichert W, Roske A, Gekeler V, Beckers T, Ebert MP, Pross M, Dietel M, Denkert C, Rocken C: **Association of patterns of class I histone deacetylase expression with patient prognosis in gastric cancer: a retrospective analysis**. *Lancet Oncol* 2008, **9**(2):139-148.

45. Song J, Noh JH, Lee JH, Eun JW, Ahn YM, Kim SY, Lee SH, Park WS, Yoo NJ, Lee JY *et al*: **Increased expression of histone deacetylase 2 is found in human gastric cancer**. *APMIS* 2005, **113**(4):264-268.

46. Bartling B, Hofmann HS, Boettger T, Hansen G, Burdach S, Silber RE, Simm A: **Comparative application of antibody and gene array for expression profiling in human squamous cell lung carcinoma**. *Lung Cancer* 2005, **49**(2):145-154.

47. Weichert W, Roske A, Gekeler V, Beckers T, Stephan C, Jung K, Fritzsche FR, Niesporek S, Denkert C, Dietel M *et al*: **Histone deacetylases 1, 2 and 3 are highly expressed in prostate**

cancer and HDAC2 expression is associated with shorter PSA relapse time after radical prostatectomy. *Br J Cancer* 2008, **98**(3):604-610.

48. Halkidou K, Gaughan L, Cook S, Leung HY, Neal DE, Robson CN: **Upregulation and nuclear recruitment of HDAC1 in hormone refractory prostate cancer**. *Prostate* 2004, **59**(2):177-189.

49. Miyake K, Yoshizumi T, Imura S, Sugimoto K, Batmunkh E, Kanemura H, Morine Y, Shimada M: **Expression of hypoxia-inducible factor-1alpha, histone deacetylase 1, and metastasis-associated protein 1 in pancreatic carcinoma: correlation with poor prognosis with possible regulation**. *Pancreas* 2008, **36**(3):e1-9.

50. Huang BH, Laban M, Leung CH, Lee L, Lee CK, Salto-Tellez M, Raju GC, Hooi SC: **Inhibition of histone deacetylase 2 increases apoptosis and p21Cip1/WAF1 expression, independent of histone deacetylase 1**. *Cell Death Differ* 2005, **12**(4):395-404.

51. Oehme I, Deubzer HE, Wegener D, Pickert D, Linke JP, Hero B, Kopp-Schneider A, Westermann F, Ulrich SM, von Deimling A *et al*: **Histone deacetylase 8 in neuroblastoma tumorigenesis**. *Clin Cancer Res* 2009, **15**(1):91-99.

52. Saji S, Kawakami M, Hayashi S, Yoshida N, Hirose M, Horiguchi S, Itoh A, Funata N, Schreiber SL, Yoshida M *et al*: **Significance of HDAC6 regulation via estrogen signaling for cell motility and prognosis in estrogen receptor-positive breast cancer**. *Oncogene* 2005, **24**(28):4531-4539.

53. Sakuma T, Uzawa K, Onda T, Shiiba M, Yokoe H, Shibahara T, Tanzawa H: **Aberrant expression of histone deacetylase 6 in oral squamous cell carcinoma**. *Int J Oncol* 2006, **29**(1):117-124.

54. Lagger G, O'Carroll D, Rembold M, Khier H, Tischler J, Weitzer G, Schuettengruber B, Hauser C, Brunmeir R, Jenuwein T *et al*: **Essential function of histone deacetylase 1 in proliferation control and CDK inhibitor repression**. *The EMBO journal* 2002, **21**(11):2672-2681.

55. Glaser KB, Li J, Staver MJ, Wei RQ, Albert DH, Davidsen SK: **Role of class I and class II histone deacetylases in carcinoma cells using siRNA**. *Biochem Biophys Res Commun* 2003, **310**(2):529-536.

56. Yamaguchi T, Cubizolles F, Zhang Y, Reichert N, Kohler H, Seiser C, Matthias P: **Histone deacetylases 1 and 2 act in concert to promote the G1-to-S progression**. *Genes & development* 2010, **24**(5):455-469.

57. Keshelava N, Davicioni E, Wan Z, Ji L, Sposto R, Triche TJ, Reynolds CP: **Histone deacetylase 1 gene expression and sensitization of multidrug-resistant neuroblastoma cell lines to cytotoxic agents by depsipeptide**. *J Natl Cancer Inst* 2007, **99**(14):1107-1119.

58. Xu WS, Parmigiani RB, Marks PA: **Histone deacetylase inhibitors: molecular mechanisms of action**. *Oncogene* 2007, **26**(37):5541-5552.

59. Dokmanovic M, Clarke C, Marks PA: **Histone deacetylase inhibitors: overview and perspectives**. *Mol Cancer Res* 2007, **5**(10):981-989.

60. Mann BS, Johnson JR, Cohen MH, Justice R, Pazdur R: **FDA approval summary: vorinostat for treatment of advanced primary cutaneous T-cell lymphoma**. *Oncologist* 2007, **12**(10):1247-1252.

61. Prince HM, Dickinson M: **Romidepsin for Cutaneous T-cell Lymphoma**. *Clin Cancer Res* 2012.

62. Tan J, Cang S, Ma Y, Petrillo RL, Liu D: **Novel histone deacetylase inhibitors in clinical trials as anti-cancer agents**. *Journal of hematology & oncology* 2010, **3**:5.

63. Bolden JE, Peart MJ, Johnstone RW: **Anticancer activities of histone deacetylase inhibitors**. *Nat Rev Drug Discov* 2006, **5**(9):769-784.

64. Richon VM, Emiliani S, Verdin E, Webb Y, Breslow R, Rifkind RA, Marks PA: **A class of hybrid polar inducers of transformed cell differentiation inhibits histone deacetylases**. *Proceedings of the National Academy of Sciences of the United States of America* 1998, **95**(6):3003-3007.

65. Medina V, Edmonds B, Young GP, James R, Appleton S, Zalewski PD: **Induction of caspase-3 protease activity and apoptosis by butyrate and trichostatin A (inhibitors of histone deacetylase): dependence on protein synthesis and synergy with a mitochondrial/cytochrome c-dependent pathway**. *Cancer Res* 1997, **57**(17):3697-3707.

66. Hughes TR, Marton MJ, Jones AR, Roberts CJ, Stoughton R, Armour CD, Bennett HA, Coffey E, Dai H, He YD *et al*: **Functional discovery via a compendium of expression profiles**. *Cell* 2000, **102**(1):109-126.

67. Mariadason JM, Corner GA, Augenlicht LH: **Genetic reprogramming in pathways of colonic cell maturation induced by short chain fatty acids: comparison with trichostatin A, sulindac, and curcumin and implications for chemoprevention of colon cancer**. *Cancer Res* 2000, **60**(16):4561-4572.

68. Khabele D, Son DS, Parl AK, Goldberg GL, Augenlicht LH, Mariadason JM, Rice VM: **Drug-induced inactivation or gene silencing of class I histone deacetylases suppresses ovarian cancer cell growth: implications for therapy**. *Cancer Biol Ther* 2007, **6**(5):795-801.

69. Weerasinghe SV, Estiu G, Wiest O, Pflum MK: **Residues in the 11 A channel of histone deacetylase 1 promote catalytic activity: implications for designing isoform-selective histone deacetylase inhibitors**. *J Med Chem* 2008, **51**(18):5542-5551.

70. Hassig CA, Tong JK, Fleischer TC, Owa T, Grable PG, Ayer DE, Schreiber SL: **A role for histone deacetylase activity in HDAC1-mediated transcriptional repression**. *Proceedings of the National Academy of Sciences of the United States of America* 1998, **95**(7):3519-3524.

71. Wang DF, Helquist P, Wiech NL, Wiest O: **Toward selective histone deacetylase inhibitor design: homology modeling, docking studies, and molecular dynamics simulations of human class I histone deacetylases**. *Journal of medicinal chemistry* 2005, **48**(22):6936-6947.

72. Witter DJ, Harrington P, Wilson KJ, Chenard M, Fleming JC, Haines B, Kral AM, Secrist JP, Miller TA: **Optimization of biaryl Selective HDAC1&2 Inhibitors (SHI-1:2)**. *Bioorganic & medicinal chemistry letters* 2008, **18**(2):726-731.

73. Alland L, David G, Shen-Li H, Potes J, Muhle R, Lee HC, Hou H, Jr., Chen K, DePinho RA: **Identification of mammalian Sds3 as an integral component of the Sin3/histone deacetylase corepressor complex**. *Mol Cell Biol* 2002, **22**(8):2743-2750.

74. Laherty CD, Yang WM, Sun JM, Davie JR, Seto E, Eisenman RN: **Histone deacetylases associated with the mSin3 corepressor mediate mad transcriptional repression**. *Cell* 1997, **89**(3):349-356.

75. Nicolas E, Morales V, Magnaghi-Jaulin L, Harel-Bellan A, Richard-Foy H, Trouche D: **RbAp48 belongs to the histone deacetylase complex that associates with the retinoblastoma protein**. *J Biol Chem* 2000, **275**(13):9797-9804.

76. Li J, Staver MJ, Curtin ML, Holms JH, Frey RR, Edalji R, Smith R, Michaelides MR, Davidsen SK, Glaser KB: **Expression and functional characterization of recombinant human HDAC1 and HDAC3**. *Life Sci* 2004, **74**(22):2693-2705.

77. Northrop JP, Ullman KS, Crabtree GR: **Characterization of the nuclear and cytoplasmic components of the lymphoid-specific nuclear factor of activated T cells (NF-AT) complex**. *J Biol Chem* 1993, **268**(4):2917-2923.

78. Bishop AC, Shah K, Liu Y, Witucki L, Kung C, Shokat KM: **Design of allele-specific inhibitors to probe protein kinase signaling**. *Curr Biol* 1998, **8**(5):257-266.

79. Bishop AC, Ubersax JA, Petsch DT, Matheos DP, Gray NS, Blethrow J, Shimizu E, Tsien JZ, Schultz PG, Rose MD *et al*: **A chemical switch for inhibitor-sensitive alleles of any protein kinase**. *Nature* 2000, **407**(6802):395-401.

80. Lourido S, Shuman J, Zhang C, Shokat KM, Hui R, Sibley LD: **Calcium-dependent protein kinase 1 is an essential regulator of exocytosis in Toxoplasma**. *Nature* 2010, **465**(7296):359-362.

81. Lourido S, Tang K, Sibley LD: **Distinct signalling pathways control Toxoplasma egress and host-cell invasion**. *The EMBO journal* 2012, **31**(24):4524-4534.

82. Kadosh D, Struhl K: **Histone deacetylase activity of Rpd3 is important for transcriptional repression in vivo**. *Genes & development* 1998, **12**(6):797-805.

83. Weerasinghe SV, Wambua M, Pflum MK: **A histone deacetylase-dependent screen in yeast**. *Bioorganic & medicinal chemistry* 2010, **18**(21):7586-7592.

84. Bieliauskas AV, Weerasinghe SV, Pflum MK: **Structural requirements of HDAC inhibitors: SAHA analogs functionalized adjacent to the hydroxamic acid**. *Bioorganic & medicinal chemistry letters* 2007, **17**(8):2216-2219.

85. Choi SE, Pflum MK: **The structural requirements of histone deacetylase inhibitors: Suberoylanilide hydroxamic acid analogs modified at the C6 position**. *Bioorg Med Chem Lett* 2012, **22**(23):7084-7086.

86. Choi SE, Weerasinghe SV, Pflum MK: **The structural requirements of histone deacetylase inhibitors: Suberoylanilide hydroxamic acid analogs modified at the C3 position display isoform selectivity**. *Bioorganic & medicinal chemistry letters* 2011, **21**(20):6139-6142.

ABSTRACT

HISTONE DEACETYLASE 1: MUTAGENESIS AND SMALL MOLECULES STUDIES

by

MAGDALENE KAMANTHE WAMBUA

August 2013

Advisor: Dr. Mary Kay Pflum

Major: **Chemistry (Biochemistry)**

Degree: **Doctor of Philosophy**

Histone deacetylase 1 (HDAC1) has been linked to cell growth and cell cycle regulation, which makes it a widely recognized target for anticancer drugs. The 14 Å channel of Class 1 HDAC isotypes has long being hypothesized to be the exit cavity for acetate following deacetylation. The amino acids lining this cavity are very similar among the HDAC isoforms, suggesting the role of the cavity is relevant to all HDACs proteins Importantly, HDAC1 selective inhibitors designed to fit the 14Å channel have been designed. To understand the importance of the 14Å channel to HDAC1 activity, we used an alanine scan to determine the influence of residues in the 14 Å channel of the HDAC1. The mutation of eleven channel residues to alanine led to a significant reduction in deacetylase activity. Acetate competition experiment revealed that, charged residues lining the 14Å affect HDAC1 binding to acetate. The combined results reveal 14Å channel residues critical for HDAC1 activity and acetate escape. With no crystallographic information on HDAC1 available, these findings provide important insight HDAC inhibitor design.

Understanding the involvement of HDAC1 in cancer formation is critical in developing selective inhibitors. Towards this goal, we did extensive studies to create a HDAC1 bump-hole inhibitors pair as an alternative to genetic methods which are limited in their usage to characterize HDAC1 function. We developed and validated a histone deacetylase dependent screen in the yeast Rpd3 protein. Using this screen screened a library of Rpd3 mutants with the aim of isolating active mutants for the bump-hole. Of the 15, 000 colonies screened none had a mutation. We focused on testing the active E98A mutant against SAHA inhibitor analogs present in our lab. C-2, C-3 and N-SAHA analogs were screened using a plate based ELISA assay which we developed and validated. All SAHA analogs screened did not qualify for a HDAC1-bump inhibitor system.

AUTOBIOGRAPHICAL STATEMENT

Magdalene Kamanthe Wambua

Wayne State University

Department of Chemistry

5101 Cass Ave, Detroit, MI 48202, USA

Educational Background

- **Ph.D. (*2013)***
  Biochemistry Division, Department of Chemistry, Wayne State University, Detroit, MI, USA.

  Dissertation Title: "Histone Deacetylase 1: Mutagenesis and Small Molecules studies."

- **Bachelor of Science in Chemistry – First Class Honors *(2007)***
  Department of Biochemistry, University of Nairobi, Kenya.

Publications

- Sujith V. W. Weerasinghe, **Magdalene Wambua** and Mary Kay H. Pflum. "An HDAC Dependent Gene Reporter Assay to Screen HDAC Inhibitors and Active Mutants", **2010**.
- Magdalene Wambua and Mary Kay H. Pflum. "Residues in the 14Å channel of HDAC1 are critical for deacetylase activity" *Manuscript in preparation.*